Volume 14 | Number 1 | January-December 2020

DTI | Drug Target Insights

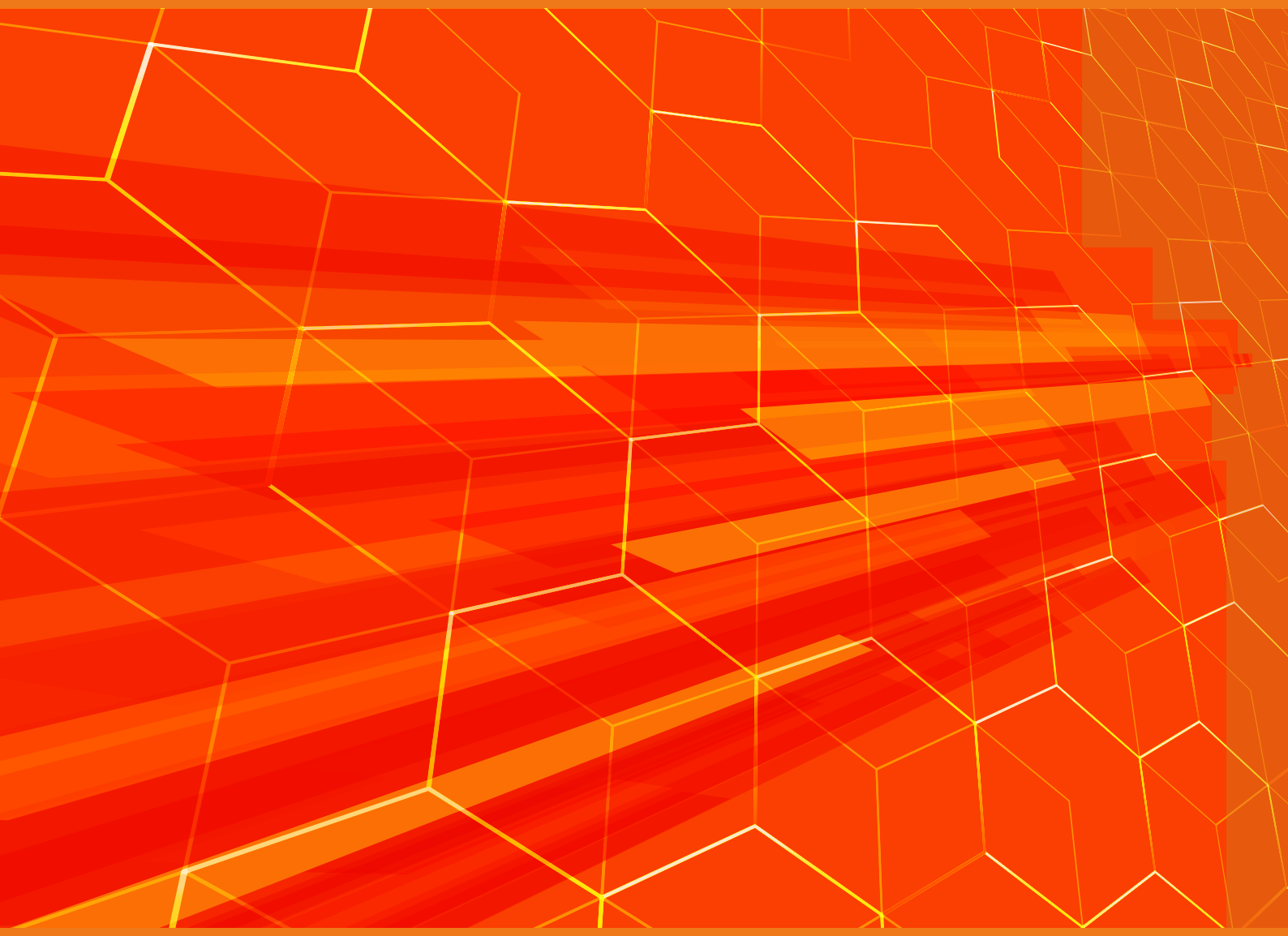

ABOUTSCIENCE

Aims and Scope
Drug Target Insights covers current developments in all areas of the field of clinical therapeutics and focusing on molecular drug targets which include disease-specific proteins, receptors, enzymes, and genes. The journal seeks to elucidate the impact of new therapeutic agents on patient acceptability, preference, satisfaction and quality of life.

Indexing
PubMed Central
Scopus
ESCI | Clarivate Analytics Emerging Sources Citation Index
DOAJ | Directory of Open Access Journals
CrossRef
OCLC WorldCat
ROAD | Directory of Open Access Scholarly Resources
Opac-ACNP| Catalogo Italiano dei periodici
Opac-SBN | Catalogo del servizio bibliotecario nazionale

Publication process
Peer review
Papers submitted to DTI are subject to a rigorous peer review process, to ensure that the research published is valuable for its readership. DTI applies a single-blind review process and does not disclose the identity of its reviewers.

Lead times
Submission to final decision: 6-8 weeks
Acceptance to publication: 2 weeks

Publication fees
All manuscripts are submitted under Open Access terms. Article processing fees cover any other costs, that is no fee will be applied for supplementary material or for colour illustrations. Where applicable, article processing fees are subject to VAT.

Open access and copyright

Author information and manuscript submission
For full author guidelines and online submission visit www.aboutscience.eu

ABOUTSCIENCE

Aboutscience Srl
Piazza Duca d'Aosta, 12 - 20124 Milano (Italy)

Editorial and production enquiries
dti@aboutscience.eu

Supplements, reprints and commercial enquiries
Lucia Steele - email: lucia.steele@aboutscience.eu

Pubblication data
eISSN: 1177-3928
Continuous pubblication
Vol. 14 (January-December 2020) was published on December 28, 2020

1 Identification of the possible therapeutic targets in the insulin-like growth factor 1 receptor pathway in a cohort of Egyptian hepatocellular carcinoma complicating chronic hepatitis C type 4
Nada M.K. Mabrouk, Dalal M. Elkaffash, Mona Abdel-Hadi, Salah-ElDin Abdelmoneim, Sameh Saad ElDeen, Gihan Gewaifel, Khaled A. Elella, Maher Osman, Nahed Baddour

12 Paradoxical bronchoconstriction caused by β2-adrenoceptor agonists
Khadija Ayed, Islam Latifa Hadi Khalifa, Salma Mokaddem, Saloua Ben Khamsa Jameleddine

16 Prevalence of multidrug-resistant and extended-spectrum beta-lactamase (ESBL)-producing gram-negative bacilli: A meta-analysis report in Ethiopia
Mengistu Abayneh, Teshale Worku

26 Targeting Streptococcus pneumoniae UDP-glucose pyrophosphorylase (UGPase): in vitro validation of a putative inhibitor
Monica Sharma, Swati Sharma, Pallab Ray, Anuradha Chakraborti

34 Interaction of drugs with lipid raft membrane domains as a possible target
Hironori Tsuchiya, Maki Mizogami

DTI
ISSN 1177-3928
Drug Target Insights 2020; 14: 1-11
DOI: 10.33393/dti.2020.1548
ORIGINAL RESEARCH ARTICLE
Open Access

Identification of the possible therapeutic targets in the insulin-like growth factor 1 receptor pathway in a cohort of Egyptian hepatocellular carcinoma complicating chronic hepatitis C type 4

Nada M.K. Mabrouk[1], Dalal M. Elkaffash[2,3], Mona Abdel-Hadi[1], Salah-ElDin Abdelmoneim[4], Sameh Saad ElDeen[3], Gihan Gewaifel[6], Khaled A. Elella[5], Maher Osman[5], Nahed Baddour[1]

[1] Department of Pathology, University of Alexandria, Alexandria - Egypt
[2] Alexandria Regional Center for Women's Health and Development, Alexandria - Egypt
[3] Department of Clinical and Chemical Pathology, University of Alexandria, Alexandria - Egypt
[4] Department of Clinical Oncology and Nuclear Medicine, University of Alexandria, Alexandria - Egypt
[5] Department of General Surgery, University of Alexandria, Alexandria - Egypt
[6] Public Health Department, Faculty of Medicine, University of Alexandria, Alexandria - Egypt

ABSTRACT

Background: Molecular targeted drugs are the first line of treatment of advanced hepatocellular carcinoma (HCC) due to its chemo- and radioresistant nature. HCC has several well-documented etiologic factors that drive hepatocarcinogenesis through different molecular pathways. Currently, hepatitis C virus (HCV) is a leading cause of HCC. Therefore, we included a unified cohort of HCV genotype 4-related HCCs to study the expression levels of genes involved in the insulin-like growth factor 1 receptor (IGF1R) pathway, which is known to be involved in all aspects of cancer growth and progression.

Aim: Determine the gene expression patterns of IGF1R pathway genes in a cohort of Egyptian HCV-related HCCs. Correlate them with different patient/tumor characteristics. Determine the activity status of involved pathways.

Methods: Total ribonucleic acid (RNA) was extracted from 32 formalin-fixed paraffin-embedded tissues of human HCV-related HCCs and 6 healthy liver donors as controls. Quantitative reverse transcription polymerase chain reaction (qRT-PCR) using RT^2 Profiler PCR Array for Human Insulin Signaling Pathway was done to determine significantly up- and downregulated genes with identification of most frequently coregulated genes, followed by correlation of gene expression with different patient/tumor characteristics. Finally, canonical pathway analysis was performed using the Ingenuity Pathway Analysis software.

Results: Six genes – AEBP1, AKT2, C-FOS, PIK3R1, PRKCI, SHC1 – were significantly overexpressed. Thirteen genes – ADRB3, CEBPA, DUSP14, ERCC1, FRS3, IGF2, INS, IRS1, JUN, MTOR, PIK3R2, PPP1CA, RPS6KA1 – were significantly underexpressed. Several differentially expressed genes were related to different tumor/patient characteristics. Nitric oxide and reactive oxygen species production pathway was significantly activated in the present cohort, while the growth hormone signaling pathway was inactive.

Conclusions: The gene expression patterns identified in this study may serve as possible therapeutic targets in HCV-related HCCs. The most frequently coregulated genes may serve to guide combined molecular targeted therapies. The IGF1R pathway showed evidence of inactivity in the present cohort of HCV-related HCCs, so targeting this pathway in therapy may not be effective.

Keywords: Gene expression, Hepatitis C virus, Hepatocellular carcinoma, Molecular therapeutic targets

Received: January 8, 2020
Accepted: January 20, 2020
Published online: April 8, 2020

Corresponding author:
Nada M.K. Mabrouk
Department of Pathology
University of Alexandria
Alexandria, Egypt
nada_mabrouk@hotmail.com, nada.mabrouk@alexmed.edu.eg

Introduction

Hepatocellular carcinoma (HCC) has become the fifth most common cancer in men worldwide and the ninth in women and the third leading cause of cancer-related deaths. Distinct geographical variations in the incidence exist. In Egypt, HCC has the highest age-standardized incidence and mortality rates (ASR) from cancer in males and ranks second in females (1). Most of the burden is in developing countries where 83% of cases (and deaths) occur (2). HCC has several

well-documented etiologic factors that drive hepatocarcinogenesis through different molecular pathways. Currently, hepatitis C virus (HCV) is a leading cause of HCC. The multiplicity of etiologies of HCC and the existence of substantial molecular heterogeneity might limit the benefits of targeted approaches to HCC treatment. Therefore, therapeutic vulnerabilities should be studied in homogeneous groups of HCCs sharing similar drivers of the disease (3). In Egypt, the estimated national prevalence of HCV is 14.7%, which is the highest in the world (4), and HCCs attributable to HCV account for around 50% of cases (5). Studies of the HCV genome confirmed that over 90% of Egyptian HCV isolates belong to genotype 4 (6).

The present study was conducted to characterize the molecular alterations in the insulin-like growth factor 1 receptor (IGF1R) pathway in a unified cohort of Egyptian HCCs complicating chronic HCV genotype 4. The IGF1R pathway was chosen as its activation plays an important role in almost every aspect of cancer development, including cell proliferation, neoplastic transformation, cancer cell survival, epithelial to mesenchymal transition (EMT), and metastasis (7) and that IGF1R overexpression correlated with aggressive phenotype in cancer, poor clinical outcome, and therapy resistance (8–10).

Aim

The present work aimed to identify the gene expression of the different subcellular components of the IGF1R pathway in Egyptian HCCs complicating chronic HCV genotype 4, followed by identification of the most frequently coregulated genes, correlation of gene expression with the different clinical and pathological patient and tumor characteristics, and determination of the activity status of involved pathways.

Materials

Two groups were included in the present study; the study group comprised 32 formalin-fixed, paraffin-embedded (FFPE) blocks from 32 Egyptian HCCs complicating chronic HCV genotype 4 etiology (shown as positive by HCV DNA PCR using Inno-LiPA I and II). Twenty-four out of 32 were segmentectomy specimens, while 8 out of 32 were liver explants, and the control group comprised six core biopsies from normal liver donors.

Inclusion criteria were HCV genotype 4 etiology and good quantity and quality of extracted ribonucleic acid (RNA) as measured by NanoDrop spectrophotometer (A260:A280 ratio 1.9:2.0 indicated pure RNA). Exclusion criteria included positive serology for anti-hepatitis B virus surface antibody and any HCC patient who has received previous neoadjuvant chemotherapy (including transarterial chemoembolization).

To accurately define our study population, further identification of other known hepatocarcinogens in the Egyptian environment was performed, including:

1) Hepatitis B core antigen (HBcAg) positivity by immunohistochemistry (IHC) (denoting occult hepatitis B virus [HBV] infection) was found in 7/29 of our HCC cases as evidenced by cytoplasmic positivity to the antibody.
2) Aflatoxin B1-DNA (AFB1-DNA) adduct positivity by IHC was found to be present in 16/29 of our cases as evidenced by nuclear positivity to the antibody.

Methods

The protocol of this study was approved by the Ethics committee of the Faculty of Medicine, University of Alexandria. Paraffin blocks of liver biopsies were obtained from the archives of the Pathology Department at the Faculty of Medicine, Alexandria University.

Clinical data were collected from the patients' files including gender, age, comorbidities (diabetes mellitus and obesity), alfa-fetoprotein (AFP) levels, liver function tests (alanine aminotransferase [ALT], aspartate transaminase [AST], bilirubin, and albumin), hemoglobin concentration, and complete blood picture.

Gross pathologic examination of HCC tumors specifically addressed tumor size, multifocality, gross capsulation, gross necrosis, satellites, and bile production.

Histopathologic study using 5-µm-thick sections assessed pathologic tumor grade (was performed according to the Edmondson and Steiner grading system for HCC), histologic pattern, cell type (including giant cells and clear cells), and vascular invasion. The presence of dysplastic nodules outside HCC and pathological tumor-node-metastasis (pTNM) staging (according to the pTNM staging system of the American Joint Committee on Cancer 8th edition [AJCC]) was also noted.

Real-time quantitative reverse transcription PCR

Preparation of the paraffin blocks and obtaining tissue sections

1) By trimming off the excess paraffin from the edges of the specimen to facilitate deparaffinization.
2) Then two sections, 5 µm thick each, were cut from each block and placed in a 2 mL nuclease-free microfuge tube.

Total RNA was extracted from FFPE tumor sections using the RNeasy® FFPE kit for purification of total RNA from FFPE tissue sections (QIAGEN, Hilden, Germany, cat. no.: 73504) according to the manufacturer's instructions. Its main principle is to remove all the paraffin, reverse formalin-induced cross-linking in the nucleic acid, and prevent any further degradation in the RNA that is known to be induced by formalin and finally to eliminate all genomic DNA. The concentration and purity of extracted RNA were determined using a NanoDrop ND-1000 spectrophotometer. Samples were accepted when the A260/A280 ratio (nucleic acid/protein absorbance) was ≥1.9. Reverse transcription of extracted RNA (0.5 µg [500 ng] of RNA was used for all experimental runs) to complementary DNA (cDNA) was done using RT^2 First Strand Kit (QIAGEN, Hilden, Germany, cat. no.: 330401) according to the manufacturer's instructions. RT^2 SYBR Green ROX qPCR Mastermix (QIAGEN, Hilden, Germany, cat. no.: 330523) was added to the cDNA. The mixture was aliquoted into the 96 wells of the commercially available RT^2 Profiler™ PCR Array Human Insulin Signaling Pathway (PAHS-030ZA) (QIAGEN,

Hilden, Germany, cat. no.: 330231) containing primer assays for 84 genes concerning the human insulin signaling pathway, including genes of the phosphatidylinositol-3-kinase (PI3K) and the mitogen-activated protein kinase (MAPK) signaling pathways that are the two major downstream signaling pathways for IGF1R signaling (11) and also genes involved in carbohydrate, lipid, and protein metabolism; transcription factors and transcription regulators; genes involved in cell proliferation, growth and differentiation (12); and five housekeeping genes (HKGs). In addition, there were one genomic DNA control, three reverse transcription controls, and three positive PCR controls (the full list of genes can be found in the supplementary file). PCR is then performed using the Applied Biosystems® 7500 Real-Time PCR system (ThermoFisher Scientific, Foster City, CA, USA). Finally, relative expression is determined using the ΔΔCT method using the RT2 Profiler PCR Array Data Analysis Webportal (at www.SABiosciences.com/pcrarraydataanalysis.php). Two HKGs with the lowest standard deviations and most stable expression across replicates were selected for data normalization: Beta-2-microglobulin (B2M) (H2) and hypoxanthine phosphoribosyl transferase 1 (HPRT1) (H4).

Fold regulation values for each of the 84 genes in HCC cases was determined by the Qiagen online data analysis Webportal (at www.SABiosciences.com/pcrarraydataanalysis.php). Then for each gene the percentages of cases showing upregulation, normal expression, and downregulation were determined. Determination of the significantly up- and downregulated genes in HCC cases using SPSS statistics software version 20.0 was carried out using nonparametric Mann-Whitney test. The most frequently coregulated genes were identified. Identification of genes significantly correlated with the different patient/tumor characteristics carried out using the Mann-Whitney test. Finally, active and inactive pathways in HCC from the present dataset were identified; an Excel file containing the gene symbols, fold regulation values, and the p values for all 84 tested genes was uploaded to the Ingenuity Pathway Analysis (IPA) software.

Results

The demographic data of the cases included are presented in Table I.

Gross pathological examination of HCC tumors

Tumor size ranged from 1.75 to 16.0 cm, with a median of 4.8 cm and a mean of 5.38 ± 3.46 cm standard deviation (SD; Tab. II).

Microscopic examination of HCC tumors

The most frequently encountered histologic patterns are displayed in Table III.

Twenty-six out of 32 cases showed combined histological patterns in the following frequencies (Tab. IV).

Frequency of different histopathological features of HCC tumors including Edmonson and Steiner tumor grades is shown in Tables V and VI, respectively.

Frequency of pTNM tumor stages is shown in Table VII.

TABLE I - Distribution of the studied cases according to demographic data (n = 32)

	Number	%
Gender		
Male	24	75.0
Female	8	25.0
Age (years)		
≤60	22	68.8
>60	10	31.3
Min.–Max.	47.0–67.0	
Mean ± Standard deviation	56.06 ± 5.49	
Median	56.0	
Comorbidities	17/25	53.1
Alfa-fetoprotein (≥200 ng/mL)	8/25	25.0

TABLE II - The frequency of the gross characteristics of the tumors included in the present study

Gross findings	Number	%
Gross capsulation (n = 32)		
Absent	6	18.8
Present	26	81.3
Gross necrosis (n = 32)		
Absent	21	65.6
Present	11	34.4
Multifocality (n = 32)		
Absent	4	12.5
Present	28	87.5
Satellites (n = 32)		
Absent	6	18.8
Present	26	81.3
Bile production (n = 32)		
Absent	15	46.9
Present	17	53.1

TABLE III - The frequency of the different histologic patterns of the HCC cases included in the present study

Histologic pattern of HCC (n = 32)	Number	%
Trabecular		
Absent	3	9.4
Present	29	90.6
Pseudoglandular		
Absent	12	37.5
Present	20	62.5
Compact		
Absent	20	62.5
Present	12	37.5

HCC = hepatocellular carcinoma.

TABLE IV - The frequency of different combinations of patterns in the tumors included in the present study

HCCs with combined histologic pattern	Number (%)
Trabecular and pseudoglandular	15
Trabecular and compact	6
Trabecular, pseudoglandular, and compact	3
Glandular and compact	2
Total	26

HCC = hepatocellular carcinoma.

TABLE V - The frequency of giant cells, clear cells, vascular invasion, and dysplastic nodules in the HCC cases included in the present study

Histologic feature	Number	%
Giant cells (n = 32)		
Absent	17	53.1
Present	15	46.9
Clear cells (n = 32)		
Absent	17	53.1
Present	15	46.9
Vascular invasion (n = 32)		
Absent	11	34.4
Present	21	65.6
Dysplastic nodules outside HCC (n= 32)		
Absent	13	40.6
Present	19	59.4

HCC = hepatocellular carcinoma.

TABLE VI - Distribution of the studied cases according to Edmondson and Steiner grading system (n = 32)

Grade	Number	%
Low grade (1 + 2)	**14**	**43.8**
Grade I	1	3.1
Grade II	13	40.6
High grade (3 + 4)	**18**	**56.3**
Grade III	3	9.4
Grade IV	15	46.9

TABLE VII - Distribution of the studied cases according to pTNM stage (AJCC 8th Edition) (n = 32)

Stage	Number	%
Early stage (1 and 2)	**12**	**37.5**
Stage I	5	15.6
Stage II	7	21.9
Advanced stage (3)	**20**	**62.5**
Stage III	20	62.5
Stage IV	0	0.0

AJCC = American Joint Committee on Cancer; TNM = tumor-node-metastasis.

TABLE VIII - The six significantly upregulated genes' fold regulation, p values, and percentage of cases showing upregulation of these genes

Position	Gene symbol	Fold regulation	p	Number	%
A04	AEBP1	6.694	0.045*	29	90.6
A06	AKT2	6.0287	0.013*	26	81.3
C01	FOS	3.9608	0.045*	25	78.1
E11	PIK3R1	4.1363	0.020*	25	78.1
F05	PRKCI	7.7467	0.006*	28	87.5
G04	SHC1	11.8326	0.001*	30	93.8

p = p values for Mann-Whitney test for comparing between the two groups.
*Statistically significant at $p \leq 0.05$.

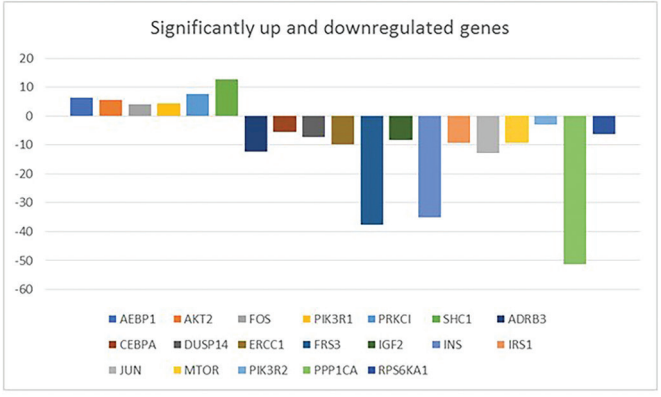

Fig. 1 - Bar chart representing the 6 significantly upregulated and the 13 significantly downregulated genes in the hepatocellular carcinoma group

Significantly up- and downregulated genes

A total of 51 deregulated genes were found in the present cohort of HCCs. Fourteen genes were upregulated while 37 genes were downregulated. Statistically significant upregulation was observed in HCC patients, in comparison to the control group, in six genes, namely AEBP1, AKT2, FOS, PIK3R1, PRKCI, SHC1, where SHC1 was the most significantly overexpressed gene (p value: 0.001) (Tab. VIII, Fig. 1). SHC1, AEBP1, AKT2, and PKCI were the most frequently coregulated genes among the significantly upregulated genes.

On the other hand, the frequency and magnitude of the downregulation events were greater than that of upregulation events (Tabs. VIII and IX). Thirteen genes, namely ADRB3, CEBPA, DUSP14, ERCC1, FRS3, IGF2, INS, IRS1, JUN, MTOR, PIK3R2, PPP1CA, and RPS6KA1, were significantly underexpressed in HCC patients relative to the control group, where PPP1CA and INS were the two most significantly underexpressed genes (p value: 0.002) (Tab. IX, Fig. 1). INS and PPP1CA were the most frequently coregulated genes among the significantly downregulated genes.

TABLE IX - The 13 significantly downregulated genes' fold regulation, p values, and percentage of cases showing downregulation of these genes

Position	Gene symbol	Fold regulation	p	Number	%
A03	ADRB3	−11.3685	0.010*	23	71.9
B02	CEBPA	−5.3981	0.041*	22	68.8
B07	DUSP14	−6.5717	0.016*	23	71.9
B10	ERCC1	−8.7853	0.037*	22	68.8
C03	FRS3	−35.5177	0.006*	27	84.4
D02	IGF2	−8.6788	0.013*	25	78.1
D04	INS	−31.7678	0.002*	30	93.8
D07	IRS1	−8.0248	0.037*	22	68.8
D10	JUN	−13.0027	0.020*	23	71.9
E04	MTOR	−9.0478	0.045*	26	81.3
E12	PIK3R2	−2.8856	0.037*	23	71.9
F03	PPP1CA	−46.4755	0.002*	29	90.6
F12	RPS6KA1	−5.653	0.025*	24	75.0

p = p values for Mann-Whitney test for comparing between the two groups.
*Statistically significant at $p \leq 0.05$.

VEGFA was downregulated (fold regulation of −3.2345) in 71.9% (23/32) of cases in the present study, although this did not reach statistical significance.

A scatter plot and a heat map were generated on the online data analysis web portal representing the distribution of average gene expression levels (Figs. 1 and 2 respectively).

Nonsupervised hierarchical clustering of all cases and controls according to their gene expression profile by the data analysis web portal

The included cases were a homogeneous population with no outstanding clustering as evidenced by the dendrograms. This further supports the study design as it included a specific cohort of HCCs: Egyptian ethnicity and HCV genotype 4 etiology.

Correlations between the gene expression levels and demographic data in HCC patients

Age: There were significant differences in three gene expression levels as regards age; **AEBP1, AKT1, and FBP1** genes were significantly overexpressed in HCC patients ≤60 years of age compared to HCC patients >60 years of age (Tab. X).

Gender: DOK1 was significantly overexpressed in female patients (p = 0.037).

Stage: There were no statistically significant differences detected in the gene expression levels between early **pTNM stage (pT1,2)** and late **stage (pT3,4)** HCC tumors.

Grade: GSK3A was significantly overexpressed in low-grade tumors as compared to high-grade ones where it was normally expressed (p = 0.002)

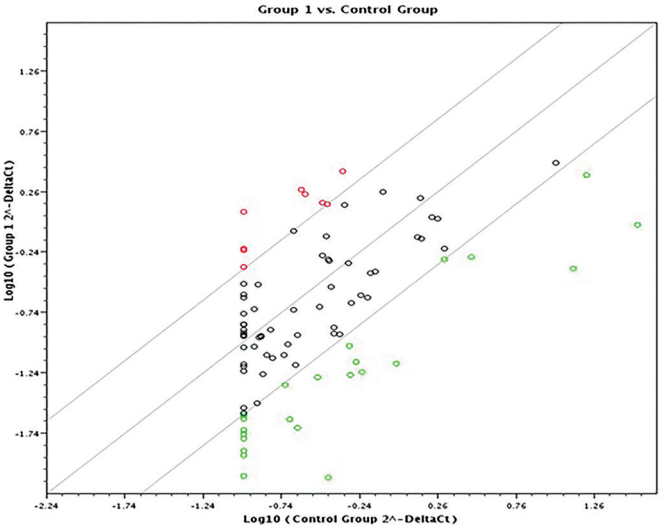

Fig. 2 - Scatter plot representing the normalized expression of each gene on the polymerase chain reaction array between the two groups. Log base 10 of $2^{-\Delta CT}$ value of each gene in the control group is plotted on the x-axis against the corresponding value in the hepatocellular carcinoma (HCC) group, which is plotted on the y-axis to visualize gene expression changes. The central boundary line indicates unchanged gene expression. The upper left section of the scatter plot (above the fold-change boundary lines) contains genes upregulated in the HCC group as compared to the control group. The lower right section of the scatter plot (below the fold-change boundary lines) contains genes downregulated in the HCC group as compared to the control group. It shows the upregulated genes in red and the downregulated genes in green.

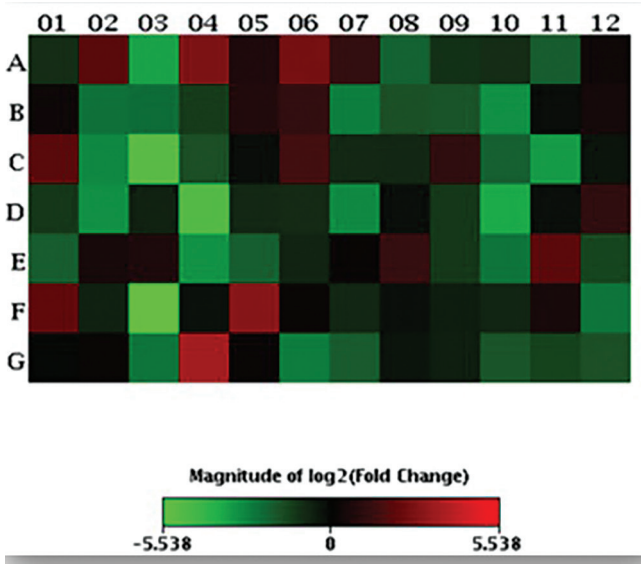

Fig. 3 - Heat map is a color-coded representation of fold regulation expression data between HCC and control groups overlaid onto the polymerase chain reaction array plate layout. The black color represents the average magnitude of gene expression. The brightest green represents the most downregulated genes, the brightest red represents the most upregulated genes in the HCC cases compared to the normal controls.

TABLE X - Differentially expressed genes between HCC cases whose age is ≤60 years and those who are >60 years of age as regards human insulin signaling pathway gene expression levels

Gene symbol	Group 1 Age ≤60 years	Group 1 Age >60 years	p
	Fold regulation	Fold regulation	
AEBP1	9.6655	2.9833	0.040*
AKT1	2.3142	–1.394	0.024*
FBP1	2.1679	–2.1895	0.007*

HCC = hepatocellular carcinoma.
p = p values for Mann-Whitney test for comparing between the two categories.
*Statistically significant at p ≤ 0.05.

TABLE XII - Differentially expressed genes between HCC cases having *multifocal tumor masses* and those with unifocal masses as regards human insulin signaling pathway gene expression levels

	Multifocality		p
	Absent (n = 4)	Present (n = 28)	
AEBP1	26.30	5.51	0.004*
FOS	19.81	3.15	0.003*
LDLR	7.12	1.88	0.035*

HCC = hepatocellular carcinoma.
p = p values for Mann-Whitney test for comparing between the two categories.
*Statistically significant at p ≤ 0.05.

Tumor size: Both **CEBPB** (p = 0.027) and **GPD1** (p = 0.002) were significantly downregulated in tumors >5 cm.

Dysplastic nodules: No statistically significant difference was detected in the gene expression levels of any genes between cases who had dysplastic nodules outside tumor mass and those who did not have any (none were <0.05).

Satellite nodules: AEBP1 and FOS genes were upregulated in the absence of satellite nodules more than double their expression level in the cases which showed satellite nodules. **MAPK1 gene** was overexpressed in the presence of satellite nodules and normally expressed in their absence. **PRKCZ and UCP1 genes** were downregulated in the absence of satellite nodules and normally expressed in their presence (Tab. XI).

Multifocality: AEBP1 and FOS genes were upregulated in the absence of multifocal masses more than double their expression level in the cases which showed multifocal masses.

LDLR gene was overexpressed in the absence of multifocal masses and normally expressed in their presence (Tab. XII).

Gross capsulation: Both INSL**3 (p = 0.043) and IRS1 (p = 0.030) genes** were downregulated in the presence of gross capsulation.

Gross tumor necrosis: CAP1 (p = 0.041), GRB2 (p = 0.047), PRL (p = 0.024), and TG (p = 0.025) were downregulated in the presence of gross necrosis. **PIK3R1** (p = 0.016) was upregulated in the absence of gross tumor necrosis.

Giant cells: Both GSK**3A (p = 0.015) and PCK2** (p = 0.030) were upregulated in the absence of giant cells. **UCP1 (p = 0.033)** was downregulated in tumors that showed giant cells.

Clear cells: CEBPB, HK2, GPD1, IGFBP1 and **PIK3R2 were downregulated in all the studied cases, more so** in tumors that showed clear cells than in tumors which had no clear cells (Tab. XIII).

Vascular invasion: NOS2 showed more significant downregulation in the absence of vascular invasion (p = 0.035).

HBcAg: RPS6KA1 was more significantly underexpressed in the presence of HBcAg (p = 0.034).

AFB1-DNA adduct positivity: AKT1 and MAPK1 were more significantly upregulated in the presence of aflatoxin as compared to negative cases (p = 0.019, 0.017 respectively). **On the other hand, RPS6KA1** was more significantly underexpressed in the presence of AFB1 (p = 0.046).

Correlations between the gene expression levels and the different clinical characteristics of the tumors in HCC patients

Thrombocytopenia: In patients with a low platelet count, **AKT1** was significantly upregulated (p = 0.038) while **BCL2L1**

TABLE XI - Differentially expressed genes between HCC cases having *satellite nodules around the tumor mass* and those without, as regards human insulin signaling pathway gene expression levels

	Satellite nodules		p
	Absent (n = 6)	Present (n = 26)	
AEBP1	17.44	5.37	0.004*
FOS	13.21	3.00	0.007*
MAPK1	–1.97	2.05	0.012*
PRKCZ	–2.63	1.42	0.026*
UCP1	–9.60	–1.98	0.014*

HCC = hepatocellular carcinoma.
p = p values for Mann-Whitney test for comparing between the two categories.
*Statistically significant at p ≤ 0.05.

TABLE XIII - Differentially expressed genes between HCC tumors with *clear cells* and those without as regards human insulin signaling pathway gene expression levels

	Clear cells		p
	Absent (n = 17)	Present (n = 15)	
CEBPB	–2.34	–12.28	0.010*
GPD1	–1.29	–2.64	0.040*
HK2	–6.14	–18.17	0.050*
IGFBP1	1.22	–3.46	0.041*
PIK3R2	–1.41	–6.52	0.021*

HCC = hepatocellular carcinoma.
p = p values for Mann-Whitney test for comparing between the two categories.
*Statistically significant at p ≤ 0.05.

was significantly downregulated (p = 0.045). **VEGFA** was more significantly underexpressed in the presence of normal platelet numbers (p = 0.038).

Comorbidities: There was no statistically significant difference in the gene expression levels between patients who have comorbidities and those who do not have any.

Canonical pathway analysis predicted by IPA database

Nitric oxide and reactive oxygen species production pathway was significantly activated in the present cohort, while the growth hormone signaling pathway was significantly inactivated (Fig. 4).

Discussion

Different etiologic factors result in very diverse HCC molecular profiles between different regions of the world (13,14). Understanding the heterogeneity of HCC is conducive to developing personalized therapy and identifying molecular biomarkers.

Most published work on molecular profiling of HCC was conducted on heterogeneous groups of tumors including different etiologies and ethnic backgrounds (15–19). Once HCC heterogeneity is accepted (20), studies have to be conducted on homogeneous samples to identify characteristic genetic alterations, if personalized management is the target.

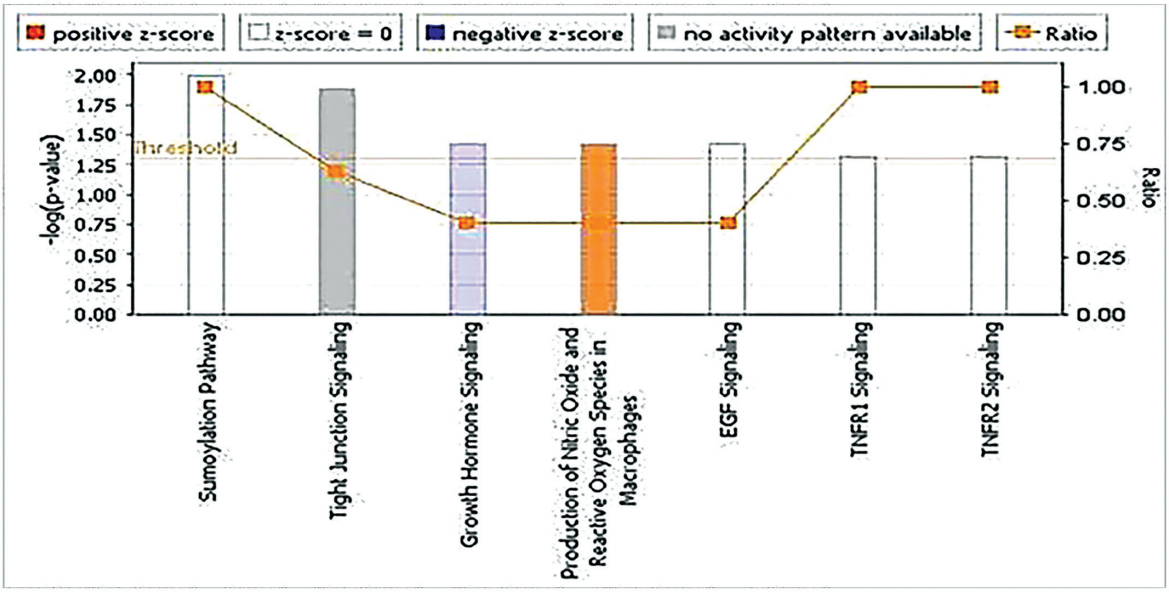

Fig. 4 - Analysis of canonical pathways involved in hepatitis C virus-related hepatocellular carcinoma pathogenesis with the Ingenuity Pathway Analysis (IPA) database using the present dataset (the 84 tested genes). The IGF pathway was found to be inactive. On the other hand, the nitric oxide and reactive oxygen species production pathway were significantly activated. Description: The *white* bars mean that half the molecules suggest an activation and half suggest inhibition, so an overall z-score of 0 (Ingenuity Systems). The *blue* bar indicates that there is evidence that the pathway is inhibited and a negative z-score. The *orange* bar means that there is a positive z-score indicating that there is evidence for activation of this pathway. The horizontal threshold line indicates the threshold for the over-representation analysis and was set at p = 0.05. Only bars that are more significant than p < 0.05 are shown. The ratio line represents the ratio of the number of molecules in the present dataset that map into the pathway relative to the whole size of the pathway (Ingenuity Systems). The pathway analysis was generated through the use of IPA (QIAGEN Inc., https://www.qiagenbioinformatics.com/products/ingenuity-pathway-analysis

HCC is known to be chemo- and radioresistant (21); therefore, identifying therapeutic vulnerabilities for molecular targeted drugs is in dire need. The present study measured levels of messenger RNA (mRNA) expression of 84 insulin signaling-related genes, including genes of the PI3K and the MAPK signaling pathways (11). Also included are genes involved in carbohydrate, lipid and protein metabolism, transcription factors and transcription regulators, genes involved in cell proliferation, growth, and differentiation (12).

Of the 84-cancer pathway-focused genes in this array, upregulation was observed in 14 genes, while 37 genes appeared to be downregulated in the tumor samples, for a total of 51 differentially regulated genes. These upregulated genes may be therapeutic targets for future trials, especially those for which molecularly targeted agents are available.

Among the significantly upregulated genes was c-FOS, a proto-oncogene which is a major nuclear target for signal transduction pathways, including MAPK pathway, and is involved in the regulation of cell growth, differentiation, and transformation (22,23). A novel selective C-FOS/AP-1 inhibitor T-5224 was found to inhibit the invasion and migration of head and neck squamous cell carcinoma cells in vitro and prevented lymph node metastasis in head and neck cancer in an animal model (24).

Most of the significantly upregulated genes found in the present work were also found in common with prior HCC

molecular studies; AKT2, C-FOS, PIK3R1, PRKCι, SHC1 were all found to be similarly significantly upregulated (25–30). AEBP1 is an exception; to the best of our knowledge, this is the first report to find this gene to be significantly and consistently (>90% of HCCs) upregulated in HCC. It is a transcriptional repressor that has been studied in great detail for its role in regulating adipogenesis (31). It has also been found to be a proinflammatory mediator (32). Finally, it has been shown that AEBP1 induces massive obesity in mice with targeted overexpression of AEBP1 in adipose tissue (33). Although its exact role in tumorigenesis is not clear (34), AEBP1 was found to be upregulated in many different cancers such as cervical cancer (35,36), primary glioblastoma multiforme (37), and human breast cancer cell lines (38). Ladha et al found that silencing AEBP1 expression and loss of its function lead to apoptosis in glioma cell lines, meaning that AEBP1 has an antiapoptotic function and is an important survival factor for tumor cells (34).

Two studies found that directly targeting AKT2 by miR-302b in human HCC cells suppresses cell proliferation, invasion, and metastasis in vitro and also inhibited HCC tumor growth in vivo (25,39). A recent preclinical in vitro and in vivo trial using a highly selective allosteric pan-AKT inhibitor in combination with sorafenib found that this combination yielded better outcomes and with minimal toxicity than sorafenib alone. The combination significantly reduced tumor growth, proliferation, and angiogenesis and increased apoptosis (40).

The PKCι blocking agent aurothiomalate (ATM) was found to negatively regulate EMT and invasion of HCC in immortalized murine hepatocytes and was found to inhibit proliferation and induce apoptosis in HepG2 cells (41). Also, a recent patent has been published on a novel drug targeting PKCι. It has been found to be effective at treating colon cancer cells having high level of expression of at least one aPKC (42). These can potentially be tested in preclinical trials as a method for treating HCCs overexpressing atypical PKCs.

Similarly, PKCι was upregulated in HCC in several studies involving different ethnic groups; two Chinese studies (Wang et al (43), Du et al (44)) and an American and Spanish study (Chiang et al (45)). Boyault et al in a French study attempted to classify HCC by unsupervised hierarchical clustering according to the tumors' gene expression profiles by microarray; all three generated subgroups had upregulated PKCι (the HBV and non-HBV-related HCCs) (46).

In line with our findings, PIK3R1 was found to be upregulated in HCV-related HCC subgroups (45) and in HCC patients of Chinese ethnicity as well (47). In a recent study by He et al, PIK3R1 transfection by small interfering RNA significantly inhibited HCC cell migration and invasion (48). There are several PI3K inhibitors including both pan-PI3K and isoform-specific PI3K inhibitors that are still in early phase clinical trials (49).

The strongest associations between upregulated genes in the present study were between AEBP1, SHC1, AKT2, and PRKCi. Possibly, these associations can serve as a guide to molecularly targeted therapy combinations to cotarget the genes that were most frequently coregulated to maximize the benefits in HCC therapy. These potential therapeutic targets and combinations open several pipelines for future preclinical and clinical trials to be conducted for agents targeting those upregulated genes to test their efficacy and their potential use in HCV-related HCC treatment.

The 13 significantly downregulated genes included genes involved in carbohydrate, protein, and lipid metabolism, PI3K signaling target genes, MAPK signaling target genes, insulin receptor-associated proteins, genes involved in cell cycle, cell proliferation, growth factors and receptors, insulin gene and insulin receptor-associated proteins, primary insulin signaling target genes, transcription factors, and transcription regulators (12).

Two of those were tumor suppressor genes. CEBPA has been described as a tumor suppressor, leading to mitotic arrest through activation of p21 and repression of E2Fs and cyclin-dependent kinases (50). Its expression is downregulated in a number of cancers including lung (51), breast cancers (52), head and neck squamous cell carcinoma (53), and HCC. Its downregulation was associated with advanced HCC stages and poor survival (54,55).

Recently, a modified small activating RNA (saRNA) retained activation of CEBPA mRNA and downstream targets and inhibited growth of liver cancer cell lines in vitro (56). This novel drug has been encapsulated in a liposomal formulation for liver delivery in humans and is currently in a phase I clinical trial for patients with liver cancer and represents the first human study of a saRNA therapeutic (57).

FRS3 was significantly downregulated in our patient cohort. This is the first report of its significant downregulation in HCCs. Similar to our findings, FRS3 expression level has been found to be downregulated in brain and lung cancer cell lines. It constitutively binds to EGFR regardless of EGF stimulation and inhibits EGF-induced cell transformation and proliferation (58). It serves as a tumor suppressor in non-small cell lung cancer (NSCLC) (59).

In our work, excision repair cross-complementing rodent repair deficiency, complementation group 1 (ERCC1) was significantly downregulated. It was also found to be downregulated in Chinese (47) and Turkish (60) HCC cohorts as well. Loss of ERCC1 expression in hepatocytes may be one of the leading factors for genetic instability, and thus of tumorigenesis (61). Impaired nucleotide excision repair pathway, in which ERCC1 plays a major role, leads to reduced DNA repair capability and increases DNA adduct levels and genomic instability that in turn could lead to a more malignant phenotype (62). This is not limited to HCCs, but also is a finding in other types of cancer including head and neck squamous cell carcinoma (63).

Gene expression patterns can be used to define the suitable chemotherapeutic agent employed in any given case. ERCC1 overexpression could be associated with resistance to cisplatin-based therapy in HCC, similar to what is observed in NSCLC (64,65).

VEGFA was found to be downregulated in the present study in 71.9% of cases. Several retrospective studies suggested that tumors with a VEGFA amplification respond better to sorafenib, the only approved first-line treatment of advanced HCC (66), suggesting that further studies of currently used molecularly targeted therapies in Egyptian HCV-related HCC patients are needed, and search for molecular biomarkers of response to therapy with prospective

validation of the role of VEGFA expression level to predict response to therapy.

One of the points of strength in our study is that we included HCC samples resulting from a single etiologic agent only (HCV genotype 4-related HCC). Also, the present study unified the controls used in the analysis as we used healthy liver donors as the control group. On the other hand, in the vast majority of studies paired adjacent cirrhotic liver tissues to the HCC tumor masses were used as controls (30,45,67–69). This complicates the interpretation of results since the gene expression patterns in the nontumor cirrhotic liver samples from different patients can vary significantly, affected by the viral infection and degree of fibrosis. Thus, the tumor-specific variation in the expression patterns could not be distinguished from variation due to differences in the corresponding nontumor liver samples (70).

In our cohort, two HKGs – B2M and HPRT1 – were used for data normalization. In a study performed to search for appropriate HKGs to be used for data normalization in HCV-induced HCC specifically. Two of the most commonly used HKGs, which were also included in the standard catalogued 5 HKGs set in the present study's array, namely glyceraldehyde-3-phosphate dehydrogenase (GAPDH) and beta-actin (ACTB), were found to be deregulated in HCV-induced HCC (71). Thus, using them for normalization would have strong effects on the extent of differential expression of genes, leading to misinterpretation of results. This was the exact same case in our study for ACTB and GAPDH, which were found to be unstable and had a wide SD across samples.

A few weaknesses of this study that we recognize are, firstly, the fact that we were studying patients who already had developed disease at a single point in time. Also, as in most studies on HCC, tumor samples have been collected during resection. It could be expected that in a more clinically advanced context with tumor progression, increased crosstalk among pathways and chromosomal instability would contribute to additional signaling deregulation. These samples do not represent the tumors of patients with advanced stage disease, who do not undergo surgery. However, as HCC diagnosis at present is not tissue based, obtaining tissue samples from late cases is not feasible at present.

Conclusions

The significantly up- and downregulated genes identified in the present study can serve as potential therapeutic targets for HCV-related HCCs.

In the present study, the insulin pathway genes including IGF1R, IGF2, INS, INSR, and IRS1 were found to be downregulated and the IGF pathway was found to be significantly inactive, in the present work, which is in concordance with the findings of Zucman-Rossi et al (72). Therefore, drugs targeting the IGF1R pathway may not be suitable for this specific subset of HCV-related HCCs.

Although NOS2 gene expression was unchanged in our cohort, IPA revealed that nitric oxide pathway and reactive oxygen species production in HCV-related HCCs were significantly activated.

The gene expression pattern of each HCC tumor seems to provide a distinctive molecular portrait of that tumor, as no gene was 100% up- or downregulated in the present cohort. Personalized medicine mandates the knowledge of the specific genetic profile of each HCC tumor, which is currently not feasible due to costs associated especially in developing countries where most of the HCC burden lies. Therefore, the present study fills a void in this respect – identifying specific morphologic and clinical patient/tumor characteristics, which significantly correlate with underlying molecular alterations. This may be used as a guide for tailoring molecularly targeted therapies.

We confirm the findings of a previous study that was performed to search for appropriate HKGs to be used for data normalization in HCV-induced HCC specifically. Two of the most commonly used HKGs – ACTB and GAPDH – were found to be unstable and had a wide SD in our study and theirs; therefore these shouldn't be used for normalization. We suggest B2M and HPRT1 to be used instead, as they had more stable levels of expression.

Disclosures

Financial support: The present study was fully funded by a grant from the "Alexandria Regional Center for Women's Health and Development," Alexandria, Egypt (this grant covered all expenses needed for provision of all experimental kits).
Conflict of interest: All the authors declare no conflict of interest.

References

1. International Agency for Research on Cancer (IARC). Globocan 2012: Estimated cancer incidence, mortality and prevalence worldwide in 2012. France: IARC; 2012.
2. Shi J, Zhu L, Liu S, Xie WF. A meta-analysis of case-control studies on the combined effect of hepatitis B and C virus infections in causing hepatocellular carcinoma in China. Br J Cancer. 2005;92(3):607–612.
3. Llovet JM, Villanueva A, Lachenmayer A, Finn RS. Advances in targeted therapies for hepatocellular carcinoma in the genomic era. Nat Rev Clin Oncol. 2015;12(7):408–424.
4. El-zanaty F, Way A. Egypt Demographic and Health Survey 2008. Cairo, Egypt: Ministry of Health, El-Zanaty and Associates, and Macro International; 2009.
5. Maucort-Boulch D, de Martel C, Franceschi S, Plummer M. Fraction and incidence of liver cancer attributable to hepatitis B and C viruses worldwide. Int J Cancer. 2018;142(12):2471-7.
6. Ray SC, Arthur RR, Carella A, Bukh J, Thomas DL. Genetic epidemiology of hepatitis C virus throughout Egypt. J Infect Dis. 2000;182(3):698–707.
7. Wang Y, Sun Y. Insulin-like growth factor receptor-1 as an anticancer target: blocking transformation and inducing apoptosis. Curr Cancer Drug Targets. 2002;2(3):191–207.
8. Christopoulos PF, Msaouel P, Koutsilieris M. The role of the insulin-like growth factor-1 system in breast cancer. Mol Cancer. 2015;14(1):43.
9. Papa V, Gliozzo B, Clark GM, et al. Insulin-like growth factor-I receptors are overexpressed and predict a low risk in human breast cancer. Cancer Res. 1993;53(16):3736–3740.
10. Jones R, Campbell C, Gunther E, et al. Transgenic overexpression of IGF-IR disrupts mammary ductal morphogenesis and induces tumor formation. Oncogene. 2007;26(11):1636–1644.
11. Samani AA, Yakar S, LeRoith D, Brodt P. The role of the IGF system in cancer growth and metastasis: overview and recent insights. Endocr Rev. 2007;28(1):20–47.

12. Vescovo T, Refolo G, Vitagliano G, Fimia GM, Piacentini M. Molecular mechanisms of hepatitis c virus–induced hepatocellular carcinoma. Clin Microbiol Infect. 2016;22(10):853–861.
13. Patel A, Sun W. Molecular targeted therapy in hepatocellular carcinoma: from biology to clinical practice and future. Curr Treat Opt Oncol. 2014;15(3):380–394.
14. Lu L-C, Hsu C-H, Hsu C, Cheng A-L. Tumor heterogeneity in hepatocellular carcinoma: facing the challenges. Liver Cancer. 2016;5(2):128–138.
15. Luo JH, Ren B, Keryanov S, et al. Transcriptomic and genomic analysis of human hepatocellular carcinomas and hepatoblastomas. Hepatology. 2006;44(4):1012–1024.
16. Lee JS, Chu IS, Heo J, et al. Classification and prediction of survival in hepatocellular carcinoma by gene expression profiling. Hepatology. 2004;40(3):667–676.
17. Shirota Y, Kaneko S, Honda M, Kawai HF, Kobayashi K. Identification of differentially expressed genes in hepatocellular carcinoma with cDNA microarrays. Hepatology. 2001;33(4): 832–840.
18. Tackels-Horne D, Goodman MD, Williams AJ, et al. Identification of differentially expressed genes in hepatocellular carcinoma and metastatic liver tumors by oligonucleotide expression profiling. Cancer. 2001;92(2):395–405.
19. Patil MA, Chua M-S, Pan K-H, et al. An integrated data analysis approach to characterize genes highly expressed in hepatocellular carcinoma. Oncogene. 2005;24(23):3737–3747.
20. Guimei M, Baddour N, ElKaffash D, Abdou L, Taher Y. Gremlin in the pathogenesis of hepatocellular carcinoma complicating chronic hepatitis C: an immunohistochemical and PCR study of human liver biopsies. BMC Res Notes. 2012;5(1):390.
21. Huynh H. Molecularly targeted therapy in hepatocellular carcinoma. Biochem Pharmacol. 2010;80(5):550–560.
22. Saez E, Rutberg SE, Mueller E, et al. C-fos is required for malignant progression of skin tumors. Cell. 1995;82(5):721–732.
23. Yuen MF, Wu PC, Lai VCH, Lau JYN, Lai CL. Expression of c-Myc, c-Fos, and c-Jun in hepatocellular carcinoma. Cancer. 2001; 91(1):106–112.
24. Kamide D, Yamashita T, Araki K, et al. Selective activator protein-1 inhibitor t-5224 prevents lymph node metastasis in an oral cancer model. Cancer Sci. 2016;107(5):666–673.
25. Wang L, Yao J, Zhang X, et al. Mirna-302b suppresses human hepatocellular carcinoma by targeting Akt2. Mol Cancer Res. 2014;12(2):190–202.
26. Zhang Y, Guo X, Yang M, Yu L, Li Z, Lin N. Identification of AKT kinases as unfavorable prognostic factors for hepatocellular carcinoma by a combination of expression profile, interaction network analysis and clinical validation. Mol BioSyst. 2014;10(2):215–222.
27. Kurokawa Y, Matoba R, Takemasa I, et al. Molecular features of non-B, non-C hepatocellular carcinoma: a PCR-array gene expression profiling study. J Hepatol. 2003;39(6):1004–1012.
28. Huang C-Y, Huang X-P, Zhu J-Y, et al. miR-128-3p suppresses hepatocellular carcinoma proliferation by regulating PIK3R1 and is correlated with the prognosis of HCC patients. Oncol Rep. 2015;33(6):2889–2898.
29. Wang JM, Li Q, Du GS, Lu JX, Zou SQ. Significance and expression of atypical protein kinase C-iota in human hepatocellular carcinoma. J Surg Res. 2009;154(1):143–149.
30. Chen X, Cheung ST, So S, et al. Gene expression patterns in human liver cancers. Mol Biol Cell. 2002;13(6):1929–1939.
31. Ro H-S, Roncari D. The C/EBP-binding region and adjacent sites regulate expression of the adipose p2 gene in human preadipocytes. Mol Cell Biol. 1991;11(4):2303–2306.
32. Majdalawieh A, Ro HS. Regulation of IkappaBalpha function and NF-kappaB signaling: AEBP1 is a novel proinflammatory mediator in macrophages. Mediators Inflamm. 2010;2010:823–821.
33. Zhang L, Reidy SP, Nicholson TE, et al. The role of AEBP1 in sex-specific diet-induced obesity. Mol Med. 2005;11(1–12):39.
34. Ladha J, Sinha S, Bhat V, Donakonda S, Rao SM. Identification of genomic targets of transcription factor AEBP1 and its role in survival of glioma cells. Mol Cancer Res. 2012;10(8): 1039–1051.
35. Han S-J, Cho YL, Nam GH, Kim CK, Seo J-S, Ahn WS. CDNA microarray analysis of gene expression profiles associated with cervical cancer. Cancer Res Treat. 2003;35(5):451–459.
36. Ahn WS, Bae SM, Lee JM, et al. Searching for pathogenic gene functions to cervical cancer. Gynecol Oncol. 2004;93(1):41–48.
37. Reddy SP, Britto R, Vinnakota K, et al. Novel glioblastoma markers with diagnostic and prognostic value identified through transcriptome analysis. Clin Cancer Res. 2008;14(10):2978–2987.
38. Grigoriadis A, Mackay A, Reis-Filho JS, et al. Establishment of the epithelial-specific transcriptome of normal and malignant human breast cells based on MPSS and array expression data. Breast Cancer Res. 2006;8(5):R56.
39. Wang L, Yao J, Sun H, et al. miR-302b suppresses cell invasion and metastasis by directly targeting AKT2 in human hepatocellular carcinoma cells. Tumor Biol. 2016;37(1):847–855.
40. Jilkova ZM, Kuyucu AZ, Kurma K, et al. Combination of AKT inhibitor ARQ 092 and sorafenib potentiates inhibition of tumor progression in cirrhotic rat model of hepatocellular carcinoma. Oncotarget. 2018;9(13):11145–11158.
41. Ma C, Yang Y, Wang J, et al. The aPKCι blocking agent atm negatively regulates EMT and invasion of hepatocellular carcinoma. Cell Death Dis. 2014;5(3):e1129.
42. Acevedo-Duncan M. Method of treating colorectal cancers using a PKC inhibitor. In: Google Patents; 2018.
43. Wang J-M, Li Q, Du G-S, Lu J-X, Zou S-Q. Significance and expression of atypical protein kinase c-ι in human hepatocellular carcinoma. J Surg Res. 2009;154(1):143–149.
44. Du G-S, Wang J-M, Lu J-X, et al. Expression of P-aPKC-ι, E-cadherin, and β-catenin related to invasion and metastasis in hepatocellular carcinoma. Ann Surg Oncol. 2009;16(6):1578–1586.
45. Chiang DY, Villanueva A, Hoshida Y, et al. Focal gains of VEGFA and molecular classification of hepatocellular carcinoma. Cancer Res. 2008;68(16):6779–6788.
46. Boyault S, Rickman DS, De Reyniès A, et al. Transcriptome classification of HCC is related to gene alterations and to new therapeutic targets. Hepatology. 2007;45(1):42–52.
47. De Yun F, Hui Z, Tan Y, Cheng RX. Effect of phosphorylation of MAPK and Stat3 and expression of c-fos and c-jun proteins on hepatocarcinogenesis and their clinical significance. World J Gastroenterol. 2001;7(1):33–36.
48. He S, Zhang J, Zhang W, Chen F, Luo R. Foxa1 inhibits hepatocellular carcinoma progression by suppressing PIK3R1 expression in male patients. J Exp Clin Cancer Res. 2017;36(1):175.
49. Rodon J, Tabernero J. Improving the armamentarium of PI3K inhibitors with isoform-selective agents: a new light in the darkness. Cancer Discov. 2017;7(7):666–669.
50. Schuster MB, Porse BT. C/EBPalpha: a tumour suppressor in multiple tissues? Biochim Biophys Acta. 2006;1766(1):88–103.
51. Costa DB, Li S, Kocher O, et al. Immunohistochemical analysis of C/EBPalpha in non-small cell lung cancer reveals frequent down-regulation in stage II and IIIA tumors: a correlative study of e3590. Lung Cancer (Amsterdam, Netherlands). 2007; 56(1):97–103.
52. Gery S, Tanosaki S, Bose S, Bose N, Vadgama J, Koeffler HP. Down-regulation and growth inhibitory role of C/EBPalpha in breast cancer. Clin Cancer Res. 2005;11(9):3184–3190.
53. Bennett KL, Hackanson B, Smith LT, et al. Tumor suppressor activity of CCAAT/enhancer binding protein alpha is epigenetically down-regulated in head and neck squamous cell carcinoma. Cancer Res. 2007;67(10):4657–4664.

54. Tseng HH, Hwang YH, Yeh KT, Chang JG, Chen YL, Yu HS. Reduced expression of C/EBPalpha protein in hepatocellular carcinoma is associated with advanced tumor stage and shortened patient survival. J Cancer Res Clin Oncol. 2009;135(2): 241–247.
55. Tomizawa M, Watanabe K, Saisho H, Nakagawara A, Tagawa M. Down-regulated expression of the CCAAT/enhancer binding protein alpha and beta genes in human hepatocellular carcinoma: a possible prognostic marker. Anticancer Res. 2003;23(1a):351–354.
56. Voutila J, Reebye V, Roberts TC, et al. Development and mechanism of small activating RNA targeting CEBPA, a novel therapeutic in clinical trials for liver cancer. Mol Ther. 2017;25(12): 2705–2714.
57. Reebye V, Huang KW. Gene activation of CEBPA using saRNA: preclinical studies of the first in human saRNA drug candidate for liver cancer. 2018;37(24):3216-28.
58. Huang L, Watanabe M, Chikamori M, et al. Unique role of SNT-2/FRS2β/FRS3 docking/adaptor protein for negative regulation in EGF receptor tyrosine kinase signaling pathways. Oncogene. 2006;25(49):6457.
59. Iejima D, Minegishi Y, Takenaka K, et al. FRS2β, a potential prognostic gene for non-small cell lung cancer, encodes a feedback inhibitor of EGF receptor family members by ERK binding. Oncogene. 2010;29(21):3087.
60. Turhal N, Bas E, Er O, et al. ERCC1 is not expressed in hepatocellular cancer: a Turkish oncology group, gastrointestinal oncology subgroup study. J Buon. 2010;15(4):794–796.
61. Cheng L, Spitz MR, Hong WK, Wei Q. Reduced expression levels of nucleotide excision repair genes in lung cancer: a case-control analysis. Carcinogenesis. 2000;21(8):1527–1530.
62. Simon GR, Sharma S, Cantor A, Smith P, Bepler G. ERCC1 expression is a predictor of survival in resected patients with non-small cell lung cancer. Chest. 2005;127(3):978–983.
63. Cheng L, Sturgis EM, Eicher SA, Spitz MR, Wei Q. Expression of nucleotide excision repair genes and the risk for squamous cell carcinoma of the head and neck. Cancer. 2002;94(2):393–397.
64. Ueda S, Shirabe K, Morita K, et al. Evaluation of ERCC1 expression for cisplatin sensitivity in human hepatocellular carcinoma. Ann Surg Oncol. 2011;18(4):1204–1211.
65. Fautrel A, Andrieux L, Musso O, Boudjema K, Guillouzo A, Langouët S: Overexpression of the two nucleotide excision repair genes ERCC1 and XPC in human hepatocellular carcinoma. J Hepatol. 2005;43(2):288–293.
66. Lopez PM, Patel P, Uva P, Villanueva A, Llovet JM. Current management of liver cancer. Eur J Cancer Suppl. 2007;5(5):444–446.
67. Xu XR, Huang J, Xu ZG, Qian BZ, et al. Insight into hepatocellular carcinogenesis at transcriptome level by comparing gene expression profiles of hepatocellular carcinoma with those of corresponding noncancerous liver. Proc Natl Acad Sci USA. 2001;98(26):15089–15094.
68. Boyault S, Rickman DS, de Reynies A, et al. Transcriptome classification of HCC is related to gene alterations and to new therapeutic targets. Hepatology. 2007;45(1):42–52.
69. Chuma M, Sakamoto M, Yamazaki K, et al. Expression profiling in multistage hepatocarcinogenesis: identification of HSP70 as a molecular marker of early hepatocellular carcinoma. Hepatology. 2003;37(1):198–207.
70. Makowska Z, Boldanova T, Adametz D, et al. Gene expression analysis of biopsy samples reveals critical limitations of transcriptome-based molecular classifications of hepatocellular carcinoma. J Pathol Clin Res. 2016;2(2):80–92.
71. Waxman S, Wurmbach E. De-regulation of common housekeeping genes in hepatocellular carcinoma. BMC Genomics. 2007;8:243.
72. Zucman-Rossi J, Villanueva A, Nault J-C, Llovet JM. Genetic landscape and biomarkers of hepatocellular carcinoma. Gastroenterology. 2015;149(5):1226–1239. e1224.

DTI
ISSN 1177-3928
Drug Target Insights 2020; 14: 12-15
DOI: 10.33393/dti.2020.2188
SHORT COMMUNICATION
Open Access

Paradoxical bronchoconstriction caused by β_2-adrenoceptor agonists

Khadija Ayed, Islam Latifa Hadj Khalifa, Salma Mokaddem, Saloua Ben Khamsa Jameleddine

Department of Physiology, Faculty of Medicine of Tunis, University of Tunis el Manar, Tunis - Tunisia

ABSTRACT

Introduction: Salbutamol and terbutaline are short-acting β_2 adrenergic agonists that produce bronchial smooth muscle relaxation and are widely used in obstructive pulmonary diseases. Nevertheless, their use has been the cause of a paradoxical bronchoconstriction, which is a rare and potentially serious adverse reaction. The aim of this study is to report a case of paradoxical bronchoconstriction caused by β_2 adrenergic agonists.

Methods: This case is about a 50-year-old asthmatic patient who describes a history of repeated acute asthma attacks after salbutamol inhalation or terbutaline nebulization. A double-blind crossover study was performed over 3 days, in order to compare the effects of each bronchodilator. Forced expiratory volume in 1 second (FEV_1), forced vital capacity (FVC), and maximal expiratory flow 25-75 (MEF25-75) were measured.

Results: On the first day, a bronchoconstriction caused by deep and repeated inhalations was eliminated. On the second day, an airway obstruction was confirmed by a decrease in FEV_1 at 40% from baseline values after nebulization of a standard dose of terbutaline. On the third day, a spirometry was performed before and after nebulization of a standard dose of ipratropium bromide, and there were no significant changes in the spirometric parameters. Finally the patient was discharged with a written warning mentioning the danger of salbutamol and terbutaline use.

Conclusion: Salbutamol and terbutaline are generally well-tolerated β_2 adrenergic agonists. Nevertheless, in rare cases, these substances can cause a paradoxical bronchoconstriction. Doctors must therefore remain vigilant about its side effect and possibly investigate each case.

Keywords: Asthma, Bronchoconstriction, Bronchodilators, β_2 adrenergic agonists, Spirometry

Background

Salbutamol and terbutaline are both short-acting β_2-adrenoceptor agonists that are believed to exert their maximal therapeutic effect through bronchodilation. Activated β_2-adrenergic receptors promote their binding to a stimulating G protein called Gs. This binding stimulates adenylyl cyclase, which in turn activates the intracellular cyclic adenosine monophosphate (cAMP) that phosphorylates several relaxation proteins. In bronchial smooth muscle, activated protein kinase inhibits both myosin and phosphoinositide light chain kinase hydrolysis. In addition, it promotes the exchange of calcium/sodium, which results in a decrease in intracellular calcium concentration, and stimulates the Na+/K+ adenosine triphosphatase (ATPase) pump.

This discovery justifies the use of these substances as a pillar of the treatment of bronchial obstruction in addition to their safety and efficiency (1-5).

Nevertheless, use of salbutamol and terbutaline has been the cause of paradoxical bronchoconstriction, which is a rare and potentially serious adverse event requiring vigilance by treating physicians (6,7).

We describe a case of paradoxical bronchoconstriction in an asthmatic patient caused by β_2-adrenoceptor agonists objectively demonstrated with an appreciable decrease of forced expiratory volume in one second (FEV_1) in a double-blind crossover study.

Methods and Results

This case is about a 50-year-old asthmatic patient with no other past medical history and whose body mass index was 20.7 kg/m^2. He described a history of repetitive acute attacks of asthma after inhalation of salbutamol. Asthma was

Received: September 21, 2020
Accepted: September 28, 2020
Published online: October 5, 2020

Corresponding author:
Khadija Ayed
12 Avenue Farhat Hachèd
Soliman
8020 Nabeul - Tunisia
ayed_khadija@yahoo.fr

TABLE I - Spirometric parameters before and after salbutamol inhalation

Spirometric parameters	Baseline spirometry		After salbutamol		
	Measured	% Predicted	Measured	% Predicted	% Changing
FEV_1	2.36 L	74	1.76 L	55	–25
FVC	3.57 L	91	3.36 L	86	–6
FEV_1/FVC	66%	–	52%	–	–21
FEF25-75	1.34 L	36	0.68 L	18	–49

FEF25-75 **=** FEF between 25% and 75% of the FVC; FEV_1 = forced expiratory volume in 1 second; FVC = forced vital capacity.

diagnosed 5 years earlier, based on clinical arguments without neither atopy nor spirometric confirmation. The patient was then treated with inhaled corticosteroids and salbutamol for 3 years. During this period, the patient continued to have respiratory symptoms such as wheezing and dry cough after taking medication. In April 2016, the patient presented dramatic symptoms after taking a standard dose of terbutaline via nebulizer and developed a respiratory failure requiring intubation and hospitalization in an intensive care unit.

As part of the follow-up of his disease, the patient was sent to our pulmonary function department in August 2017. Spirometry and bronchodilator reversibility test were carried out by a "CareFusion MicroLab" spirometer, and spirometry was performed by experts in respiratory functional exploration according to the latest American Thoracic Society (ATS)/ European Respiratory Society (ERS) recommendations. Predicted values were obtained according to reference equations from the work of Stocks and Quanjer (8).

Baseline spirometry revealed a small airways obstruction, which is defined by a normal forced vital capacity (FVC), a normal FEV_1/FVC ratio, and a decrease of at least one forced expiratory flow (FEF): FEF50%, FEF25%, or FEF between 25% and 75% of the FVC (FEF25-75). During bronchodilator reversibility test, the patient developed an explosive cough and dyspnea just after salbutamol inhalation (400 µg) by metered dose inhaler (MDI). A decrease in FEV_1 at 25% from baseline was noticed (Tab. I). An administration of ipratropium bromide via nebulizer restored basic spirometric values.

In the light of this ascertainment, we studied the influence of terbutaline and ipratropium bromide on bronchial reactivity. A double-blind crossover study was performed, over 3 days; neither the patient nor the technician knew the composition of the nebulization in order to compare the effects of each bronchodilator on bronchial reactivity. An informal consent was obtained and the patient was asked to avoid using bronchodilators for at least 12 hours prior to the study. FEV_1, FVC, and FEF25-75 were measured and the patient was monitored by blood oxygen saturation.

On the first day, a basic spirometry was performed with eight measurements in order to eliminate bronchoconstriction due to deep inhalation during spirometry testing. No significant changes compared to baseline spirometry were found (Tab. II).

On the second day, a spirometry was planned before and 15 minutes after a nebulization of a standard dose of terbutaline made up to a total volume of 5 mL with 0.9% saline solution (5 mg/unit). The patient was initially asymptomatic, but nebulization was interrupted because of important dyspnea, coughing, wheezing, and discrete cyanosis. Physical examination revealed a wheezing, sinusal tachycardia at 110 per minute, and blood oxygen saturation at 85%. There was no urticaria, pruritus, or macular rash. The spirometry was performed earlier because of the reaction and revealed an airway obstruction confirmed by a decrease in FEV_1 at 40% from baseline spirometry (Tab. III).

TABLE II - Spirometric parameters during repeated spirometry testing

	FEV_1	FVC	FEV_1/FVC (%)
Baseline or 1st spirometry	2.41 L (75%)	3.27 L (83%)	73
2nd spirometry	2.36 L (74%)	3.11 L (79%)	75
3rd spirometry	2.29 L (71%)	3.15 L (80%)	73
4th spirometry	2.35 L (73%)	3.19 L (81%)	73
5th spirometry	2.30 L (71%)	3.11 L (79%)	73
6th spirometry	2.42 L (75%)	3.22 L (82%)	75
7th spirometry	2.31 L (71%)	3.20 L (81%)	72
8th spirometry	2.35 L (73%)	3.22 L (82%)	72

FEV_1 = forced expiratory volume in 1 second; FVC = forced vital capacity.

On the third day, a spirometry was performed before and 30 minutes after a nebulization of a standard dose of ipratropium bromide made up to a total volume of 5 mL with 0.9% saline solution (0.5 mg/unit). There were no significant clinical or spirometric changes (Tab. IV). Finally, the patient was discharged with a written warning mentioning the danger of salbutamol and terbutaline use via MDI or nebulizer solutions.

Discussion

Currently, inhaled β_2-adrenoceptor agonists are generally used in the treatment of acute asthma attacks, based on their effectiveness and relative safety. However, in rare cases, they may cause unexpected adverse effects such as paradoxical bronchoconstriction.

Paradoxical bronchoconstriction was recorded in this patient each time he used β_2-adrenoceptor agonists, whether with salbutamol via MDI or terbutaline via nebulizer. Many

TABLE III - Spirometric parameters before and after terbutaline nebulization

Spirometric parameters	Baseline spirometry		After terbutaline		
	Measured	% Predicted	Measured	% Predicted	% Changing
FEV_1	2.36 L	74	1.41 L	44	−40
FVC	3.11 L	79	2.82 L	72	−9
FEV_1/FVC	75%	–	40%	–	−35
FEF25-75	2.22 L/s	51	0.79 L/s	18	−64

FEF25-75 = FEF between 25% and 75% of the FVC; FEV_1 = forced expiratory volume in 1 second; FVC = forced vital capacity.

TABLE IV - Spirometric parameters before and after nebulization of ipratropium bromide

Spirometric parameters	Baseline spirometry		After ipratropium bromide		
	Measured	% Predicted	Measured	% Predicted	% Changing
FEV_1	2.54 L	79	2.59 L	80	+2
FVC	3.78 L	76	3.85 L	79	+2
FEV_1/FVC	64%	–	67%	–	+3
FEF25-75	1.89 L	43	1.97 L/s	45	+4

FEF25-75 = FEF between 25% and 75% of the FVC; FEV_1 = forced expiratory volume in 1 second; FVC = forced vital capacity.

factors have been excluded before reaching the conclusion of paradoxical bronchoconstriction.

First, in some asthma patients, deep inhalation can produce paradoxical bronchoconstriction during spirometry testing (9). This is why we performed the test on the first day with more than three measurements, but no spirometric changes were found. Second, double-blind crossover study was performed to avoid psychological response to spirometry testing. In fact, psychological stress can exacerbate clinical symptoms in patients with asthma (10). Third, several studies suggested that excipients (as chlorofluorocarbon propellants and surfactants) or preservatives (as benzalkonium chloride) in MDIs have been incriminated in paradoxical bronchoconstriction due to a bronchial irritation (11,12).

In our case, this possibility was rejected because the same response was seen after nebulization of terbutaline solution, which did not contain foreign substances as preservatives or stabilizers. In fact, excipients of our terbutaline solution were sodium chloride, sodium edetate, and hydrochloric acid.

In addition, osmolarity of liquids of nebulization may induce bronchoconstriction. Hyperosmolar buffers have been shown to cause histamine release from normal human basophils and mast lung cells (13,14). Saline solutions that are hypotonic or hypertonic are both able to induce bronchoconstriction (15). For these reasons, we used isotonic saline in all nebulizer solutions.

This bronchoconstriction was most likely related to an adverse reaction to β_2-adrenoceptor agonists. It is, however, difficult to specify their exact action mechanism on bronchi during this paradoxical reaction. A number of questions remain to be answered with a biocellular study.

All possibilities should be taken into account. It is dangerous to reject a possible cause of asthma mortality. Doctors and patients should be aware that although β_2-adrenoceptor agonists do not generally produce adverse effects, it may aggravate symptoms. This adverse reaction needs to be considered as one of the possible causes of sudden death or acute asthma attack.

Finally, some precautions should be taken with the use of β_2-adrenoceptor agonists. Since short-acting β_2-adrenoceptor agonists represent the first-line treatment of acute asthma (2,3), any discrepancy between a good adherence to treatment and refractory symptoms should lead the physician to suspect paradoxical bronchoconstriction. In this case, the patient should be treated with other bronchodilators such as anticholinergics.

Similar reactions should lead to a new assessment including a full spirometric study with bronchial reversibility tests as well as the above-cited protocol, in order to define the causative agent.

Conclusion

β_2-adrenoceptor agonists are an important and well-tolerated pharmacological class in the management of asthma. In rare cases, salbutamol and terbutaline may cause unusual paradoxical bronchoconstriction, whose mechanism remains unknown. Therefore, physicians must be vigilant about this potentially serious side effect and investigate each case.

Disclosures

Conflict of interest: The authors declare that there is no conflict of interest.
Financial support: This research received no specific grant from any funding agency in the public, commercial, or not-for-profit sectors.

References

1. Spooner LM, Olin JL. Paradoxical bronchoconstriction with albuterol administered by metered-dose inhaler and nebulizer solution. Ann Pharmacother. Nov 2005;39(11):1924-1927.
2. Johnson M. Beta2-adrenoceptors: mechanisms of action of beta2-agonists. Paediatr Respir Rev. Mar 2001;2(1):57-62.
3. Jacobson GA, Hostrup M. Terbutaline: level the playing field for inhaled β_2-agonists by introducing a dosing and urine threshold. Br J Sports Med. 26 Jul 2016;bjsports-2016-096453.
4. Matthew N, Octavio A, Ricardo MF, Ian S. Salbutamol or aminophylline for acute severe asthma: how to choose which one, when and why? Arch Dis Child Educ Pract. Dec 2014;2015(100):215-222.
5. Barisione G, Baroffio M, Crimi E, Brusasco V. Beta-adrenergic agonists. Pharmaceuticals. 30 Mar 2010;3(4):1016-1044.
6. Williams C, Crossland L, Finnerty J, et al. Case-control study of salmeterol and near-fatal attacks of asthma. Thorax. 1998;53(1):7-13.
7. Gallelli L. Retrospective analysis of adverse drug reactions to bronchodilators observed in two pulmonary divisions of Catanzaro, Italy. Pharmacol Res. June 2003;47(6):493-499.
8. Stocks J, Quanjer PH. Reference values for residual volume, functional residual capacity and total lung capacity. ATS Workshop on Lung Volume Measurements. Official Statement of The European Respiratory Society. Eur Respir J. 1995;8:492-506.
9. Haynes JM. Bronchoconstriction in response to deep inhalation during spirometry testing. Respir Care. 1 May 2015;60(5):e105-e109.
10. Chen E, Miller GE. Stress and inflammation in exacerbations of asthma. Brain Behav Immun. 2007;21(8):993-999.
11. Beasley CR, Rafferty P, Holgate ST. Bronchoconstrictor properties of preservatives in ipratropium bromide (Atrovent) nebuliser solution. Br Med J Clin Res Ed. 1987;294(6581):1197.
12. George M, Joshi SV, Concepcion E, Lee H. Paradoxical bronchospasm from benzalkonium chloride (BAC) preservative in albuterol nebulizer solution in a patient with acute severe asthma. A case report and literature review of airway effects of BAC. Respir Med Case Rep. 2017;21:39-41.
13. Findlay SR, Dvorak AM, Kagey-Sobotka A, Lichtenstein LM. Hyperosmolar triggering of histamine release from human basophils. J Clin Invest. 1981;67(6):1604.
14. Stellato C, de Crescenzo G, Patella V, Mastronardi P, Mazzarella B, Marone G. Human basophil/mast cell releasability. XI. Heterogeneity of the effects of contrast media on mediator release. J Allergy Clin Immunol. 1996;97(3):838-850.
15. Schoeffel RE, Anderson SD, Altounyan RE. Bronchial hyperreactivity in response to inhalation of ultrasonically nebulised solutions of distilled water and saline. Br Med J Clin Res Ed. 1981;283(6302):1285-1287.

DTI
ISSN 1177-3928
Drug Target Insights 2020; 14: 16-25
DOI: 10.33393/dti.2020.2170
REVIEW
Open Access

Prevalence of multidrug-resistant and extended-spectrum beta-lactamase (ESBL)-producing gram-negative bacilli: A meta-analysis report in Ethiopia

Mengistu Abayneh and Teshale Worku

School of Medical Laboratory Sciences, Mizan-Tepi University, Mizan-Aman - Ethiopia

ABSTRACT

Multidrug-resistant (MDR) extended-spectrum beta-lactamase (ESBL)-producing bacterial isolates have emerged as a global threat to human health. Little is known about the overall prevalence of multidrug resistance profile and ESBL-producing gram-negative bacilli (GNB) in Ethiopia. Therefore, this meta-analysis was performed to produce proportional estimates of multidrug resistance and ESBL-producing GNB in Ethiopia.

A web-based search was conducted in PubMed, Google Scholar, Research Gate, Scopus and other databases. Articles published till 2019 on the prevalence and antimicrobial resistance profiles of ESBL-producing GNB in Ethiopia were included in the study. Relevant data were extracted and statistical analysis was performed using comprehensive meta-analysis version 3.3.0 software. Publication bias was analyzed and presented with funnel plots.

In this meta-analysis, the overall proportional estimate of ESBL-producing GNB was 48.9% (95% confidence interval [CI]: 0.402, 0.577). The pooled proportional estimates of ESBL-producing *Klebsiella pneumoniae*, *Escherichia coli* and other GNB were 61.8%, 41.2% and 42.9%, respectively. Regarding antimicrobial resistance profiles against selected drugs, the pooled proportional estimates of resistance against amoxicillin-clavulanic acid, trimethoprim-sulfamethoxazole, cefotaxime, ceftazidime, tetracycline, gentamicin and ciprofloxacin was 79.0%, 78.4%, 78.0%, 72.4%, 72.7%, 58.9% and 43.8%, respectively. The pooled proportional estimates of MDR isolates were found to be 82.7% (95% CI: 0.726, 0.896), which are relatively high as compared to other countries. This highlights a need for active surveillance systems which can help understand the actual epidemiology of ESBL, aid in formulating national guidelines for proper screening of ESBL and support developing standardized approaches for managing patients colonized with ESBL.

Keywords: Ethiopia, Extended-spectrum beta-lactamase, Gram negative, Multidrug resistance

Introduction

The production of extended-spectrum beta-lactamase (ESBL) enzymes is the main bacterial mechanism to acquire resistance to currently used broad-spectrum beta-lactam antibiotics. The infections caused by such enzyme-producing bacteria have significant potential impacts on antibiotic use and patient outcomes. Especially in resource-limited countries, limited availability of drugs coupled with inappropriate use could worsen the condition, increasing infections caused by such resistant strains, its emergency and transmission (1,2). For instance, in Ethiopia studies show that about 36.8% of the population got antibiotics from community drug retail outlets without a prescription and 67.9% of people had discontinued the use of antibiotics once their symptoms subside (3). Low educational status, dissatisfaction with healthcare services provided, pharmacy owners' influence to maximize revenue, customer's pressure, weak regulatory mechanism and professional conflicts of interest were found to be strong predictors of inappropriate use of antibiotic use among the community (3,4).

Enterobacteriaceae that produce ESBL carry plasmid-encoded enzymes that can efficiently hydrolyze and confer resistance to a variety of beta-lactam antibiotics, but not to carbapenems or cephamycins. Besides beta-lactam class of antibiotic, ESBL producers are commonly resistant to different families of antibiotics including fluoroquinolones, aminoglycosides and trimethoprim-sulfamethoxazole (SXT), which contribute to the selection and persistence of

Received: June 29, 2020
Accepted: September 14, 2020
Published online: October 5, 2020

Corresponding author:
Mengistu Abayneh
School of Medical Laboratory Sciences
Mizan-Tepi University
Mizan-Aman- Ethiopia
mengeabayneh@mtu.edu.et

multidrug-resistant (MDR) ESBL strains and plasmids in both clinical and community settings. These enzymes are predominantly found in *Escherichia coli* and *Klebsiella pneumoniae*, although they are also present in other members of the gram-negative bacilli (GNB) (5-7).

ESBL-producing organisms play an important role in healthcare infections, increasing hospitalization time and morbidity and mortality rates (8). The presence of ESBL complicates antibiotic selection, especially in patients with serious infections, such as bacteremia. The reason for this is that ESBL-producing bacteria are often multiresistant to various antibiotics, an interesting feature of CTX-M (CTX stands for cefotaxime and M for Munich)-producing isolates is the coresistance to various classes of antibiotics such as fluoroquinolones, aminoglycosides and co-trimoxazole due to associated resistance mechanisms, which may be either chromosomally or plasmid-encoded (8-11).

The spread and the burden of ESBL-producing bacteria are greater in developing countries. For instance, the major epicenters of ESBL-expressing bacteria are located in Asia, Africa and the Middle East (12-14). Findings of a recent review showed that pooled prevalence of healthcare-associated infections in resource-limited settings (15.5%) was twice the average prevalence in Europe (7.1%) (15). Some plausible reasons for this difference include the following conditions that are prevalent in low-income countries: crowded hospitals, more extensive self-treatment and use of nonprescription antimicrobials, poorer hygiene in general and particularly in hospitals as well as less effective infection control.

Comprehensive data regarding ESBL-producing bacteria are generally lacking in African countries, compared with the developed world. In Ethiopia also, it is difficult to evaluate the spread and the burden of ESBL-producing organisms, because of the limited scope of studies and lack of coordinated epidemiological surveillance systems. By combining information from all relevant studies, meta-analyses can provide more precise estimates of the effects of healthcare than those derived from the individual studies included within a review. Therefore, to gain a better insight into the proportional estimates of MDR profiles and ESBL-producing GNB in Ethiopia, we retrieved available articles and collated the information in this study article.

Methods

Study design

A descriptive meta-analysis study comprising different studies on the prevalence and antimicrobial resistance profile of ESBL-producing GNB in Ethiopia was conducted.

Data sources and search strategies

A systematic and comprehensive search on available records up to December 2019 was carried out in PubMed, Google Scholar, Research Gate, Scopus and other databases. The following medical subject headings (MESH) in the title or abstract, such as "clinical specimen," "ESBL," OR "extended spectrum β-lactamase" "*Enterobacteriaceae*" OR "extended-spectrum-beta-lactamase," "gram negatives" OR "antibacterial resistance," "gram negatives" OR "antimicrobial susceptibility" AND "gram negatives" and "Ethiopia," were searched. In addition, bibliographies of eligible studies and other meta-analyses were manually searched carefully to identify additional relevant articles.

Study selection and eligibility criteria

All articles related to the detection of ESBL-producing GNB from clinical specimens and hospital environment samples, written in English language, possessing approved microbiological methods for pathogen detection and containing sufficient and extractable data were included in the meta-analysis. Having assessed all the information from the recovered publications, online records that were available up to 2019 were considered as appropriate for eligibility assessment. All review articles and original articles conducted outside Ethiopia, articles with irretrievable full texts and records with unrelated outcomes of interest were excluded during screening and eligibility assessment.

Screening and eligibility criteria

There were no limits with regard to study type except that the study had to be a primary study. However, the analysis was made to those studies which reported sufficient information to meet outcomes of interests. Some duplicates records were addressed manually due to variation in reference styles across sources. Thereafter, the authors (MA and TW) independently inspected all the titles and abstracts of articles related to the study question and these were included in a group of eligible articles with their own code and with irrelevant articles being excluded. All articles in the initially selected group were further screened in a second step by reviewing the full texts and evaluated for eligibility for final inclusion (Fig. 1).

Data extraction

Studies were identified by the main study name/identifier, followed by the year of publication. Using a predetermined, standardized and piloted data extraction form, the authors (MA and TW) independently extracted important data related to study characteristics from each article. Data extraction sheets were individually designed and pilot-tested using Microsoft Excel 2007. For each study meeting the review inclusion criteria, the following data, such as first author, study area, year of publication, study design, sample type, sample size, target population, isolate sources and outcomes of interests, number and common species isolated, proportion of ESBL-positive strains and proportion and/or number of drug and MDR isolate and the methods used to test for ESBL producers, were recorded. Data were extracted and analyzed at least twice to remove any discordance. Whenever there was discordance in the data extracted, a third person, a trained MSc laboratory professional, played a role in checking the data and a consensus was reached by double-checking of the articles with the two authors.

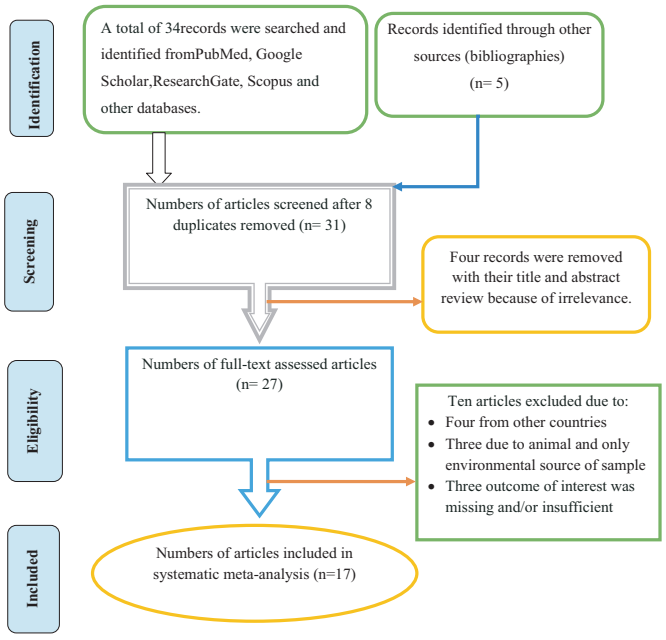

Fig. 1 - Flow chart showing the selection process of articles.

Quality assessment of included studies

The qualities of eligible studies were checked against items included in strengthening the reporting of observational studies in epidemiology (STROBE) Statement checklist (16). The quality scores (proportion) for each study were calculated against items of the STROBE checklist adequately. There were no limits with regard to study type except that the study had to be a primary study and we did not exclude any studies based on quality.

Outcome measurements

The first outcome measure is the proportion of ESBL-producing GNB from clinical specimens in Ethiopia. The pooled proportion of ESBL-producing GNB was calculated per bacterium isolate. The second outcome measure is the antimicrobial and MDR profiles of ESBL-producing and non-ESBL-producing GNB against selected antimicrobials of different categories.

Data processing and analysis

The relevant data were analyzed using comprehensive meta-analysis version 3.3.0 software (www.Meta-analysis.com). Both random and fixed effects models were used to calculate the pooled proportional estimates of ESBL-positive and MDR isolates. The I^2 statistics was used to expresses the percentage of total variation across studies and significant heterogeneity was considered at $p < 0.05$ and $I^2 > 50\%$. Publication bias was evaluated by using Begg's and Egger's tests and presented with funnel plots of standard error of Logit event rate, and a statistical significant publication bias was considered at $p < 0.05$.

Results

Search and screening results and distribution of included articles

A total of 39 studies were identified from several sources including PubMed, Google Scholar, Research Gate, Scopus and other databases. After removing eight duplicated articles, 31 were screened and four records were removed with their title and abstract review because of irrelevance. After full-text assessment, ten articles excluded: four from other countries, three due to animal and only nonhospital environment source of sample and three outcome of interest was missing and/or insufficient. Seventeen articles fulfilling the eligibility criteria were included for systematic meta-analysis (Fig. 1). The eligible studies were published in the year up to 2019. The study design of all included articles was cross-sectional studies. Most of the studies indicated that various specimens had been utilized for screening of GNB; particularly biological fluids like blood, urine, pus, stool and cerebrospinal fluid (CSF) were taken for test. Hospital environment samples such as wastewater and different swab samples from hospital contact surfaces were also taken for test. With regard to sources of biological samples, most of the studies included inpatients and outpatients as their sources of samples. With regard to study areas, six (35.3%) were conducted in the southwestern parts of Ethiopia, six (35.3%) in central Ethiopia, four (23.5%) in northern parts of Ethiopia and one (5.9%) in eastern parts of Ethiopia. Based on the available evidence, the maximum number of articles on this subject was published in the year 2014, which means only three articles were published in 2005, 2011 and 2012 (Tab. I). The median score of published studies against STROBE items was 72.2% (with a range of [50.7-79.7]).

Proportional estimates of ESBL-positive GNB

This study indicates that although different bacterial pathogens have the probability of producing ESBL as their resistance mechanisms, studies on the proportion of ESBL-producing bacteria have not been carried out properly in all parts of Ethiopia. Based on the available data, the pooled proportional estimate of ESBL-producing GNB in Ethiopia was 0.489 (95% confidence interval [CI]: 0.402, 0.577). Proportional estimates of ESBL-producing *K. pneumoniae* were 0.618 (95% CI: 0.487, 0.734), whereas proportional estimates of ESBL-producing *E. coli* were 0.412 (95% CI: 0.326, 0.504). The proportional estimate of other ESBL-producing GNB was 0.429 (95% CI: 0.352, 0.509). Overall heterogeneity was significant [$I^2 = 93.41\%$; $p = 0.000$] (Tab. II and Fig. 2).

Proportional estimates of MDR profiles of bacterial isolates

The bacterial isolates that showed different antimicrobial resistance profile against selected agents were extracted. Accordingly, the pooled estimate indicated that 0.720 (95%

TABLE I - Distribution of articles reviewed on ESBL-producing clinical isolates from different regions of Ethiopia

First author, publication year	Study design	Study area	Sample types	Sample sources	Sample size	Total isolates	Total ESBL positives	Common ESBL producers			ESBL confirmation method
								E. coli	K. pneumoniae	Other gram-negatives	
Desta et al, 2016 (17)	CS	AA	Fecal sample/swab	IP	267	295	151/295	106/235	44/58	1/2	CDT + Vitek2
Teklu et al, 2019 (18)	CS	AA	Urine, blood, sputum, CSF, body fluid, pus and discharge	IP and OP	426	426	246/426	119/228	81/103	46/95	CDT
Moges et al, 2019 (19)	CS	Bahir Dar	Urine, blood, stool, pus, sputum, CSF, body fluid, ear, nasal, cervical discharge	IP and OP	532	263	127/148	14/23	79/97	34/76	CDT
Legese et al, 2017 (20)	CS	AA	Blood and urine	IP and OP	322	33	22/28	5/6	16/19	1/8	CDT
Engda et al, 2018 (21)	CS	Gondar	Swabs of sinks, bed, door handles, wastewater	Hospital env't	384	57	57/57	20/57	24/57	13/57	Hicrome ESBL agar
Gashaw et al, 2018 (22)	CS	Jimma	Urine, blood, sputum, wound/pus swab	IP	118	126	51/100	19/31	16/30	18/39	DDST
Mulualem et al, 2012 (23)	CS	Jimma	Urine, stool, sputum, wound/pus swab	IP and OP	359	67	24/67	24/67	NA	NA	CDT
Zeynudin et al, 2018 (24)	CS	Jimma	Wound swabs, urine, biopsies, sputum	IP and OP	224	224	71/112	13/13	30/31	28/68	Check-MDR Microarray Kits
Eshetie et al, 2015 (25)	CS	Gondar	Urine	IP and OP	442	183	5/160	2/104	3/28	42 (NA)	CHROMagar
Beyene et al, 2011 (26)	CS	Jimma	Stool, blood	IP and OP	1,225	113	71/113	NA	NA	71/113	E-test
Abera et al, 2016 (27)	CS	Bahir Dar	Blood, urine, pus, CSF, ear discharges, wound swab, water	IP and OP	757	274	127/274	73/170	36/55	17/49	DDST
Seid et al, 2005 (28)	CS	Harrar	Sputum, urine and pus	IP and OP	384	57	19/57	NA	19/57	NA	CDT
Abayneh et al., 2018 (29)	CS	Jimma	Urine	OP	342	74	17/74	13/63	4/11	NA	DDST
Siraj et al, 2014 (30)	CS	Jimma	Urine, sputum, blood, vaginal swabs, wound/pus swab, eye discharge	IP and OP	471	112	43/112	24/85	19/27	NA	DDST
Mulisa et al, 2016 (31)	CS	Adama	Urine, wound, nasal, stool, pleural fluids, ear discharge	IP and OP	384	133	17/68	10/35	2/8	5/25	DDST
Bitew (2019) (32)	CS	AA	Urine, wound, blood, CSF, ear, nasal	IP and OP	996	153	66/135	NA	NA	66/135	CDT
Beyene (2019) (33)	CS	AA	Urine, sputum, blood, vaginal, wound/pus, eye discharge	IP	947	238	159/238	91/144	55/72	13/21	CDT

AA = Addis Ababa; CDT = Combination Disc Test; CS = cross-sectional; CSF = cerebrospinal fluid; DDST = Double Disc Synergy Test; ESBL = extended-spectrum beta-lactamase; E-Test = Epsilometric Test; IP = inpatient; MDR = multidrug resistance; NA = not analyzed; OP = outpatient.

TABLE II - Proportional estimates of ESBL-producing gram-negative bacteria in different regions of Ethiopia

Studies	Total proportions of ESBL		Proportions of ESBL-producing *E. coli*		Proportions of ESBL-producing *K. pneumoniae*		Proportions of ESBL-producing other GNs	
	ES [95% CI]	Weight	ES [95% CI]	Weight	ES [95% CI]	Weight	ES [95% CI]	Weight
Desta et al (2016)	0.51 [0.455, 0.569]	1.80	0.451 [0.389, 0.515]	2.91	0.759 [0.633, 0.852]	1.00	0.500 [0.059, 0.941]	0.45
Teklu et al (2019)	0.58 [0.530, 0.624]	1.81	0.522 [0.457, 0.586]	2.91	0.786 [0.697, 0.855]	1.04	0.484 [0.386, 0.584]	3.53
Moges et al (2019)	0.858 [0.792, 0.906]	1.67	0.609 [0.402, 0.782]	1.96	0.814 [0.725, 0.880]	1.03	0.447 [0.340, 0.560]	3.40
Legese et al (2017)	0.786 [0.598, 0.900]	1.32	0.833 [0.369, 0.977]	0.66	0.842 [0.608, 0.948]	0.77	0.125 [0.017, 0.537]	0.72
Engda et al (2018)	0.991 [0.877, 0.999]	0.39	0.351 [0.239, 0.482]	2.48	0.421 [0.301, 0.552]	1.02	0.228 [0.137, 0.354]	2.93
Gashaw et al (2018)	0.510 [0.413, 0.606]	1.71	0.613 [0.435, 0.765]	2.16	0.533 [0.358, 0.701]	0.96	0.462 [0.317, 0.617]	2.90
Mulualem et al (2012)	0.358 [0.253, 0.479]	1.64	0.358 [0.253, 0.479]	2.55	NA		NA	NA
Zeynudin et al (2018)	0.634 [0.541, 0.718]	1.72	0.964 [0.616, 0.998]	0.42	0.968 [0.804, 0.995]	0.52	0.412 [0.302, 0.532]	3.31
Eshetie et al (2015)	0.027 [0.011, 0.064]	1.34	0.018 [0.004, 0.069]	1.20	0.103 [0.034, 0.276]	0.78	42 (NA)	NA
Beyene et al (2011)	0.628 [0.536, 0.712]	1.72	NA	NA	NA		0.628 [0.536, 0.712]	3.58
Abera et al (2016)	0.464 [0.405, 0.523]	1.79	0.429 [0.357, 0.505]	2.85	0.655 [0.521, 0.768]	1.01	0.415 [0.276, 0.569]	2.93
Seid et al (2005)	0.333 [0.224, 0.464]	1.61	NA	NA	0.333 [0.224, 0.464]	1.02	NA	NA
Abayneh et al (2018)	0.230 [0.148, 0.339]	1.61	0.206 [0.124, 0.324]	2.36	0.364 [0.143, 0.661]	0.77	NA	NA
Siraj et al (2014)	0.384 [0.299, 0.477]	1.72	0.282 [0.197, 0.387]	2.60	0.704 [0.510, 0.844]	0.92	NA	NA
Mulisa et al (2016)	0.250 [0.161, 0.366]	1.61	0.286 [0.161, 0.454]	2.14	0.250 [0.063, 0.623]	0.64	0.200 [0.086, 0.400]	2.04
Bitew (2019)	0.489 [0.406, 0.573]	2.00	NA	NA		NA	0.489 [0.406, 0.573]	4.42
Beyene (2019)	0.668 [0.606, 0.725]	20.5	0.632 [0.550, 0.707]	2.57	0.764 [0.653, 0.848]	1.11	0.619 [0.402, 0.797]	2.51
Overall R ES [95% CI]	**0.489 [0.402, 0.577]**		**0.412 [0.326, 0.504]**		**0.618 [0.487, 0.734]**		**0.429 [0.352, 0.509]**	
Overall F ES [95% CI]	**0.526 [0.505, 0.548]**		**0.451 [0.422, 0.481]**		**0.646 [0.604, 0.686]**		**0.461 [0.424, 0.500]**	

CI = confidence interval; ESBL = extended-spectrum beta-lactamase; F = fixed; GN = gram negatives; NA = not analyzed; R = random; ES = event rate.

CI: 0.586, 0.820) and 0.780 (95% CI: 0.615, 0.891) of the ESBL-producing and non-ESBL-producing GNB were found resistant to third-generation cephalosporin (ceftazidime and cefotaxime), respectively. The pooled estimate indicated that 0.589 (95% CI: 0.482, 0.688), 0.438 (95% CI: 0.347, 0.534) and 0.790 (95% CI: 0.713, 0.850) of ESBL-producing and non-ESBL-producing GNB isolates were resistant to gentamicin, ciprofloxacin and amoxicillin-clavulanic acid, respectively. Besides, 0.784 (95% CI: 0.726, 0.832) and 0.727 (95% CI: 0.605, 0.823) of ESBL-producing and non-ESBL-producing GNB isolates were resistant to SXT and tetracycline (TET), respectively. The pooled proportional estimates of MDR isolates were found to be 0.827 (95% CI: 0.726, 0.896) (Tab. III).

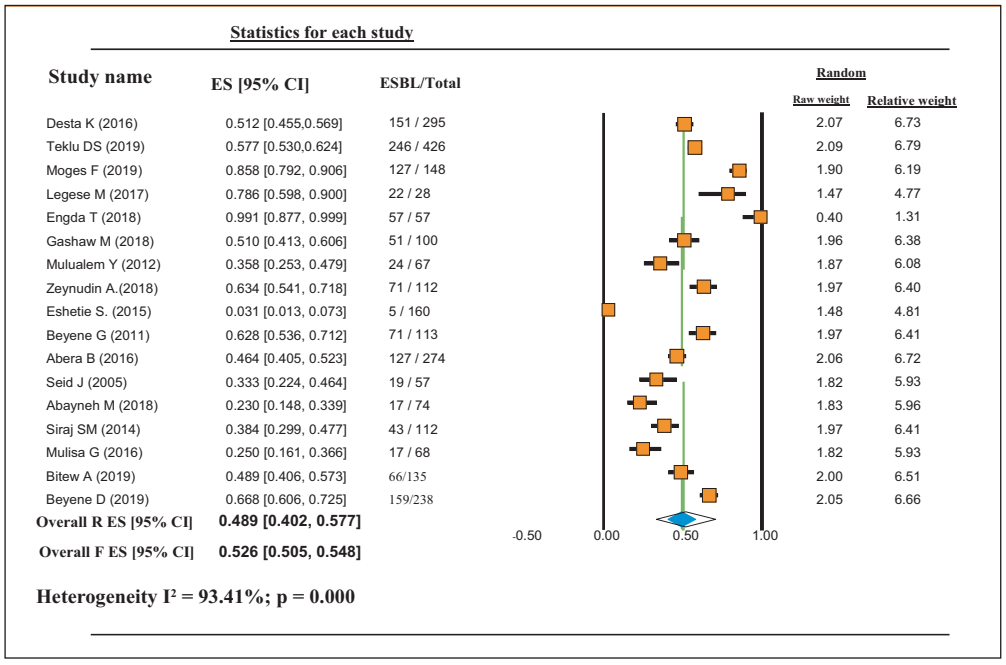

Fig. 2 - Proportional estimates of ESBL-producing GNB in different clinical samples in Ethiopia. CI = confidence interval; ESBL = extended-spectrum beta-lactamase; ES = event rate.

TABLE III - Antimicrobial and multidrug resistance profile of bacterial isolates obtained from different samples in Ethiopia

Authors	Total isolates	Total ESBL-producer	Antimicrobial resistance profiles							
			CAZ	CTX	GNT	CIP	SXT	TET	AMC	MDR
Desta et al. (2016)	295	151/295	137/150	146/150	105/150	94/150	136/150	NA	134/150	150/150
Teklu et al. (2019)	426	246/426	257/426	265/426	185/426	240/426	324/426	NA	305/426	237/246 or 291/426*
Moges et al. (2019)	185	127/148	143/148	129/148	116/148	52/148	138/148	127/148	117/148	127/148 or 148/185*
Legese et al. (2017)	33	22/28	NA	29/33	26/33	NA	29/33	25/33	28/33	NA
Engda et al. (2018)	57	57/57	57/57	57/57	11/57	25/57	37/57	NA	57/57	32/57
Gashaw et al. (2018)	100	51/100	63/100	60/100	68/100	48/100	79/100	90/100	94/100	28/100*
Mulualem et al. (2012)	67	24/67	4/67	6/67	2/67	14/67	38/67	49/67	47/67	67/67*
Zeynudin et al. (2018)	224	71/112	63/68	66/68	60/68	41/68	62/68	NA	NA	67/68*
Eshetie et al. (2015)	183	5/183	90/160	40/160	94/160	4/160	103/160	79/160	81/160	160/183*
Beyene et al. (2011)	113	71/113	NA	NA	84	1	91	45	NA	78/113*
Abera et al. (2016)	274	127/274	NA	NA	NA	106/274	174/274	NA	NA	NA
Seid et al. (2005)	57	19/57	23/57	22/57	35/57	NA	37/57	NA	NA	41/57*
Abayneh et al. (2018)	74	17/74	12/17	17/17	11/17	13/17	14/17	14/17	14/17	14/17

(*Continued*)

TABLE III - Continued

Authors	Total isolates	Total ESBL-producer	Antimicrobial resistance profiles							
			CAZ	CTX	GNT	CIP	SXT	TET	AMC	MDR
Siraj et al. (2014)	112	43/112	42/43	43/43	36/43	33/43	41/43	39/43	38/43	38/43
Mulisa et al. (2016)	68	17/68	NA	NA	12/17	14/17	14/17	6/17	NA	17/17
Bitew (2019)	135	66/135	45/135	NA	32/135	47/135	86/135	92/135	100/135	110/135*
Beyene (2019)	238	159/238	176/238	NA	117/238	137/238	195/238	191/238	148/238	225/238*
Overall R, ES [95% CI]		**1273/2487**	**0.72 [0.586, 0.820]**	**0.78 [0.615, 0.891]**	**0.589 [0.482, 0.688]**	**0.438 [0.347, 0.534]**	**0.784 [0.726, 0.832]**	**0.727 [0.605, 0.823]**	**0.790 [0.713, 0.850]**	**0.827 [0.726, 0.896]**

AMC = ampicillin-clavulanic acid; CAZ = ceftazidime; CI = confidence interval; CIP = ciprofloxacin; CTX = cefotaxime; GNT = gentamicin; ESBL = extended-spectrum beta-lactamase; MDR = multi-drug resistance; NA = not analyzed; R = resistance; SXT = trimethoprim-sulfamethoxazole; TET = tetracycline; ES = event rate.
*From overall isolates.

Laboratory methods used to estimate the proportion of ESBL-producing strains

According to this review, 8/17 (47.1%) of the articles reviewed used combination disk test (CDT) and 5/17 (29.4%) articles used double disk synergy test (DDST) methods alone. Two (11.8%) articles used CHROMagar and one article used E-test to estimate ESBL proportions. Only one article used Check-MDR CT103 Microarray Kits for detection and molecular characterization of the ESBL genes (Tab. I).

Publication bias

Funnel plots of standard error with Logit event rate confirmed that there is no statistically significant evidence of publication bias on studies reporting the prevalence of ESBL-producing bacterial isolates from different clinical samples in Ethiopia (Begg's test, p = 0.217; Egger's test, p = 0.231) (Fig. 3). However, Begg suggested that a nonsignificant correlation may be due to low statistical power and cannot be taken as evidence that bias is absent.

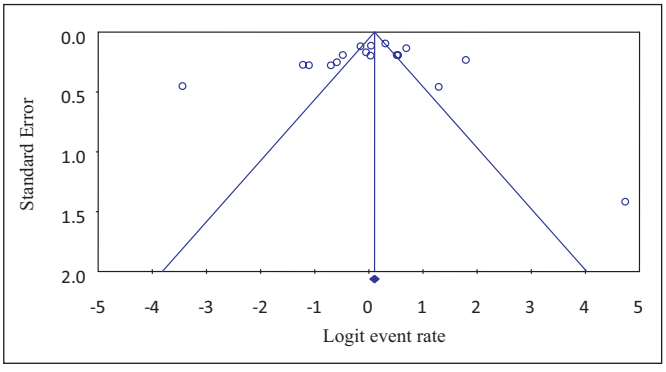

Fig. 3 - Funnel plot depicting publication bias of studies reporting the prevalence of extended-spectrum beta-lactamase (ESBL)-producing gram-negative bacilli in different clinical samples in Ethiopia.

Discussion

This is the first meta-analysis study relating the extent of the ESBL-producing GNB in Ethiopia. Accordingly, the pooled proportional estimates of ESBL-producing GNB were 48.9%, which is higher than previous estimates of meta-analysis in East Africa (34) and Pakistan (35), in which overall pooled proportion of ESBL-producers was 42% and 40%, respectively. As compared to each country in East Africa, this finding is higher than the pooled proportion of ESBL-producing Enterobacteriaceae in Tanzania (39%) and Kenya (47%) (34). The result is also higher than estimates of meta-analysis in African countries, in which the total proportion of ESBL-producing isolates was 15% in 16 out of 26 studies (36).

As compared to resource-rich countries, the pooled proportion of ESBL-producing isolates was thus considerably higher in resource-limited countries, including our setting. For instance, the pooled global prevalence of ESBL-producing Enterobacteriaceae among pregnant women diagnosed with urinary tract infections (UTIs) is 25%, with the highest rates in Africa (45%) and India (33%), followed by 15% in other Asian countries, 5% (2.8%) in Europe and the lowest one of 4% in South America and 3% in North America (37). This study finding is also close to data reported for China, where a nationwide survey that included 30 hospitals reported over 46% resistance due to ESBL (38). However, our estimate is slightly lower than for Uganda (62%) (34), Ghana (49%) (39), Cameroon (54%) (40) and Morocco (43%) (41).

With regard to the frequency of isolates, in this study, the pooled proportional estimates of ESBL-producing *K. pneumoniae*, *E. coli* and other GNB were 60.3%, 39.0% and 40.9%, respectively. This is much higher than a SMART study between 2009 and 2010, in which ESBL prevalence among *K. pneumoniae* and *E. coli* was 38.9% and 17.6%, respectively, in Europe, and 8.8% and 8.5, respectively, in

North America (42). Moreover, our meta-analysis result is also higher than a report of in vitro activity of tigecycline and comparators against gram-negative and gram-positive organisms collected from Asia-Pacific during 2004-2010 and 2015, in which 24.6% and 15.8% of *E. coli* and *K. pneumoniae* were ESBL producers in 2015, respectively[A: Please check the clarity of this sentence.] (43). In addition, among GNB collected from intra-abdominal infections in the Asia-Pacific region during 2007, 42.2% and 35.8% of *E. coli* and *Klebsiella* spp., respectively, were ESBL positive (44). However, higher proportions of ESBL-producing *E. coli* and *K. pneumoniae* were reported from India, Vietnam and China (44,45).

In this study, inter-study results showed a wide and statistically significant degree of variation in proportion estimates of ESBL proportions ($p < 0.05$). There are several possible factors that may account for the variations seen in this review. The first factor is the difference in sensitivity and specificity between methods used in estimating ESBL proportions. Some studies reviewed estimated ESBL proportions using purely phenotypic methods, while others used both phenotypic and molecular-based methods. For instance, in this study, most of the reviewed articles used CDT (17-20,23,28,32,33) and DDST (22, 27,29-31) methods alone for the detection of ESBL-producing isolates, and only one study used molecular technique for investigations and characterizations of the gene encoding ESBL (24).

The other factor contributing to the variation in proportion estimates of ESBL proportions is type of wards or units, type of specimen collected and whether patients were attending outpatient or inpatient departments. In this meta-analysis, many reviewed studies showed that ESBL-producing isolates were more among inpatients than outpatients (20,24,30). In contrast, two reviewed studies showed the reverse finding (23,27). A meta-analysis study in areas of sub-Saharan Africa showed that pooled ESBL-producing Enterobacteriaceae colonization was 18%, 32% and 55% in community studies, at hospital admission and for inpatient studies, respectively (46). Many reports have documented the difference in ESBL proportion estimates between hospitals versus community-based surveys (23,25,27,30). However, the lack of any estimates for community-based ESBL carriage in Ethiopia underscores an urgent need for surveillance in the region. Infection control in hospitals including hand hygiene and rational antibiotic use can be effective measures to stop further spread of the ESBL-producing and MDR strains in both hospitals and communities.

MDR GNB are now globally widespread and present a major challenge to modern medical practice. To date, the overall epidemiology and burden of MDR bacteria and their mechanisms of resistance have not been fully understood, especially in resource-limited countries, including Ethiopia. This is the first meta-analysis study conducted to determine the pooled proportional estimates of ESBL-producing GNB and MDR isolates in Ethiopia. Accordingly, the pooled proportional estimates of MDR isolates were found to be 82.7% (Tab. III). This finding is higher than a finding of previous meta-analysis in Ethiopia, in which the pooled proportional estimates of MDR isolates were 59.7% (47); however, it was lower than a single study finding in Ethiopia (33) and Chile (48), in which 94.5% and 100% isolates exhibited MDR profiles. Lower study finding was also reported in Ethiopia, in which the overall prevalence of MDR was 69.9%, of which 81.5% was in the hospital environment, while 54.2% was in non-hospital environment samples (49). The occurrence of MDR may be linked with indiscriminate utilization of antimicrobial agents such as wrong indication, wrong duration, improper route of administration, use of leftover antibiotics from a family member and improper discontinuation of antibiotics or genetic mutation (47,50,51). A meta-analysis finding in Ethiopia indicated that the pooled estimate of inappropriate antibiotic use was 49.2% and the pooled proportion of self-antibiotic prescription was 43.3% (47). Thus, the frequent and inappropriate use of antibiotics in humans and animals may contribute to the recent emergence of ESBL producers and MDR strains both in healthcare institutions and communities.

Moreover, medication required to treat ESBL-producing isolates is expensive and unaffordable for the majority of the population in these settings, making these bacteria difficult to treat. A study in Ethiopia concluded that mortality was significantly associated with antimicrobial resistance (52). For instance, all 11 patients with Enterobacteriaceae resistant to third-generation cephalosporins died. Another systematic review and meta-analysis estimated that the mortality in neonates with bloodstream infections (BSIs) due to ESBL-producing Enterobacteriaceae was 36%, as compared to 18% among all other neonates with BSI (53). It is therefore of the utmost importance to make reliable data available to guide strategies devoted to limiting the spread of particularly ESBL-producing pathogens and MDR strains in Ethiopia.

In this study, significant numbers of bacterial isolates showed different resistance profile against selected antimicrobial agents. The pooled proportional estimate of resistance against third-generation cephalosporins (cefotaxime and ceftazidime), amoxicillin-clavulanic acid, gentamicin, ciprofloxacin, SXT and TET ranges from 43.8% to 79.0%. Almost similar findings were reported in Ethiopia and Chile, in which 45.4% to >88% isolates exhibit resistance against beta-lactams and non-lactam drugs (33,48). This high resistance rate might be associated with an interesting feature of ESBL-producing isolates as resistance mechanisms, which may be either chromosomally or plasmid-encoded, especially CTX-M that often showed feature of coresistance to various classes of antibiotics such as fluoroquinolones, aminoglycosides, and co-trimoxazole. Therefore, interventions including infection control measures and restriction of low-quality and inappropriate use of antibiotics may aid in controlling the emergency and spread of ESBL-producing pathogens and may actually prove cost-beneficial. As a limitation, in this study, due to the lack of sufficient records on the prevalence of ESBL producers from different clinical samples in Ethiopia, all primary studies, including those with very small datasets (<10 ESBL-producing strains) were included.

Conclusion

The problems related to antibiotic resistance, including MDR due to ESBL, are significant in Ethiopia. The scarcity of data on predictors, clinical outcomes, magnitudes and gene variants encoding resistance due to ESBL-producing GNB

calls for active surveillance systems, which can help understand the current epidemiology of ESBL within the country. Furthermore, this can aid in developing national guidelines for proper screening of ESBL as well as developing standardized approaches for managing patients colonized with ESBL-producing GNB.

Disclosures

Conflict of interest: The authors declare that they have no competing interest.
Financial support: No funding was allocated for this study.
Availability of data and materials: All the data supporting our findings were incorporated within the manuscript, but are available from the corresponding author on reasonable request.
Authors' contributions: MA and TW participated in the study design, study searching and screening and data extractions. MA analyzed the data and drafted the manuscript. TW support data analysis, read, revised and approved the final version of the manuscript.

References

1. Dhillon RH, Clark J. ESBLs: a clear and present danger? *Hindawi Publ Corp*. 2012;11.
2. Byarugaba DK. Antimicrobial resistance in developing countries Springer, 2009;15-27.
3. Erku DA, Mekuria AB, Belachew SA. Inappropriate use of antibiotics among communities of Gondar town, Ethiopia: a threat to the development of antimicrobial resistance. Antimicrob Resist Infect Control. 2017;6:112. Crossref
4. Gebretekle GB, Serbessa MK. Exploration of over the counter sales of antibiotics in community pharmacies of Addis Ababa, Ethiopia: pharmacy professionals' perspective. Antimicrob Resist Infect Control. 2016;5:2. Crossref
5. European Centre for Disease Prevention and Control. Systematic review of the effectiveness of infection control measures to prevent the transmission of extended-spectrum beta-lactamase-producing *Enterobacteriaceae* through cross-border transfer of patients. Stockholm: ECDC 2014. Crossref
6. Morosini MI, García-Castillo M, Coque TM, et al. Antibiotic co-resistance in ESBL-producing *Enterobacteriaceae* and in vitro activity of tigecycline. Antimicrob Agents Chemother. 2006;50(8):2695-2699.
7. Cantón R, Novais A, Valverde A, et al. Prevalence and spread of extended-spectrum beta-lactamase-producing Enterobacteriaceae in Europe. Clin Microbiol Infect. 2008;14 Suppl 1: 144-153.
8. Shamsrizi P, Gladstone BP, Carrara E, et al. Variation of effect estimates in the analysis of mortality and length of hospital stay in patients with infections caused by bacteria-producing extended-spectrum beta-lactamases: a systematic review and meta-analysis. *BMJ Open.* 2020;10:e030266. Crossref
9. Paterson DL, Bonomo RA. Extended-spectrum β-lactamases: a clinical update. Clin Microbiol Rev. 2005;18(4):657-686.
10. Giske CG, Monnet DL, Cars O, Carmeli Y, ReAct-Action on Antibiotic Resistance. Clinical and economic impact of common multidrug-resistant gram-negative bacilli. Antimicrob Agents Chemother. 2008;52(3):813-821
11. Bonnet R. Growing group of extended-spectrum beta-lactamases: the CTX-M enzymes. *Antimicrob Agents Chemother*. 2004;48(1):1-14.
12. Villegas M V, Kattan JN, Quinteros MG, Casellas JM. Prevalence of extended-spectrum b-lactamases in South America. Clin Microbiol Infect. European Society of Clinical Microbiology and Infectious Diseases; 2008;14:154-158.
13. Hawkey PM. Prevalence and clonality of extended-spectrum beta-lactamases in Asia. Clin Microbiol Infect. 2008;14:159-165.
14. Bradford PA. Extended-spectrum beta-lactamases in the 21st century: characterization, epidemiology, and detection of this important resistance threat. Am Soc Microbiol. 2001;14(4):933-951.
15. Tham J, Melander E, Walder M, Edquist PJ, Odenholt I. Prevalence of faecal ESBL carriage in the community and in a hospital setting in a county of Southern Sweden. Eur J Clin Microbiol Infect Dis. 2011;10:1159-1162
16. Malta M, Cardoso LO, Bastos FI, Magnanini MM, Silva CM. STROBE initiative: guidelines on reporting observational studies. Saude Publica. 2010;44(3):559-565. Crossref
17. Desta K, Woldeamanuel Y, Azazh A, et al. High gastrointestinal colonization rate with extended-spectrum β-lactamase-producing *Enterobacteriaceae* in hospitalized patients: emergence of carbapenemase-producing *K. pneumoniae* in Ethiopia. PLoS One. 2016;11(8):e0161685. Crossref
18. Teklu DS, Negeri AA, Legese MH, Bedada TL, Woldemariam HK, Tullu KD. Extended-spectrum beta-lactamase-production and multi-drug resistance among Enterobacteriaceae isolated in Addis Ababa, Ethiopia. Antimicrob Resist Infect Control. 2019; 8:39. Crossref
19. Moges F, Eshetie S, Abebe W, et al. High prevalence of extended-spectrum beta-lactamase-producing gram-negative pathogens from patients attending Felege Hiwot Comprehensive Specialized Hospital, Bahir Dar, Amhara region. PLoS One. 2019;14(4):e0215177. Crossref
20. Legese MH, Weldearegay MG, Asrat D. Extended-spectrum beta-lactamase- and carbapenemase-producing *Enterobacteriaceae* among Ethiopian children. Infect Drug Resist. 2017;10:27-34. Crossref
21. Engda T, Moges F, Gelaw A, Eshete S, Mekonnen F. Prevalence and antimicrobial susceptibility patterns of extended spectrum beta-lactamase producing *Entrobacteriaceae* in the University of Gondar Referral Hospital environments, northwest Ethiopia. BMC Res Notes. 2018;11:335. Crossref
22. Gashaw M, Berhane M, Bekele S, et al. Emergence of high drug resistant bacterial isolates from patients with health care associated infections at Jimma University medical center: a cross sectional study. Antimicrob Resist Infect Control. 2018;7:138. Crossref
23. Mulualem Y, Kasa T, Mekonnen Z, Suleman S. Occurrence of extended spectrum beta (beta)-lactamases in multi-drug resistant *Escherichia coli* isolated from a clinical setting in Jimma University Specialized Hospital, Jimma, and Southwest Ethiopia. East Afr J Public Health. 2012;9(2):58-61. PMID: 23139958.
24. Zeynudin A, Pritsch M, Schubert S, et al. Prevalence and antibiotic susceptibility pattern of CTX-M type extended-spectrum β-lactamases among clinical isolates of gram-negative bacilli in Jimma, Ethiopia. BMC Infect Dis.2018;18:524. Crossref
25. Eshetie S, Unakal C, Gelaw A, Ayelign B, Endris M, Moges F. Multidrug resistant and carbapenemase producing Enterobacteriaceae among patients with urinary tract infection at referral Hospital, Northwest Ethiopia. Antimicrob Resist Infect Control. 2015;4:12. Crossref
26. Beyene G, Nair S, Asrat D, Mengistu Y, Engers H, Wain J. Multidrug resistant Salmonella Concord is a major cause of salmonellosis in children in Ethiopia. J Infect DevCtries. 2011;5:023-033. Crossref
27. Abera B, Kibret M, Mulu W. Extended-spectrum beta (β)-lactamases and antibiogram in Enterobacteriaceae from clinical and drinking water sources from Bahir Dar City, Ethiopia. PLoS One. 2016;11(11):e0166519. Crossref
28. Seid J, Asrat D. Occurrence of extended spectrum beta-lactamse enzymes in clinical isolates of Klebsiella species from

Harar region, eastern Ethiopia. Acta Trop. 2005;95(2);143-148. Crossref
29. Abayneh M, Tesfaw G, Abdissa A. Isolation of extended-spectrum *β*-lactamase-(ESBL) - producing *E. coli* and *K. pneumoniae* from patients with community-onset urinary tract infections in Jimma University Specialized Hospital, Southwest Ethiopia. Can J Infect Dis Med Microbiol. 2018;2018:4846159. Crossref
30. Siraj SM, Ali S, Wondafrash B. Extended-spectrum-lactamase production and antimicrobial resistance in Klebsiellapneumoniae and Escherichia coli among inpatients and outpatients of Jimma University Specialized Hospital, South-west, Ethiopia. Afr J Microbiol Res. 2014;8(43):3687-3694.
31. Mulisa G, Selassie L, Jarso G, Shiferew T, Zewdu A. Prevalence of extended spectrum beta-lactamase producing Enterobacteriaceae: a cross sectional study at Adama Hospital, Adama, Ethiopia. J Emerg Infect DisPatho. 2016;1(1):102.
32. Bitew A. High prevalence of multi-drug resistance and extended spectrum beta-lactamase- production in non-fermenting gram-negative bacilli in Ethiopia. Infect Dis Res Treat. 2019;12:1-7.
33. Beyene D, Bitew A, Fantew S, Mihret A, Evans M. Multidrug-resistant profile and prevalence of extended spectrum β-lactamase and carbapenemase- production in fermentative gram-negative bacilli recovered from patients and specimens referred to National Reference Laboratory, Addis Ababa, Ethiopia. PLoS One. 2019;14(9):e0222911. Crossref
34. Sonda T, Kumburu H, van Zwetselaar M, et al. Meta-analysis of proportion estimates of extended-spectrum-beta-lactamase-producing *Enterobacteriaceae* in East Africa hospitals. Antimicrob Resist Infect Control.2016;5:18. Crossref
35. Abrar S, Hussain S, Khan RA, Ul Ain N, Haider H, Riaz S. Prevalence of extended-spectrum-β-lactamase-producing *Enterobacteriaceae*: first systematic meta-analysis report from Pakistan. Antimicrob Resist Infect Control. 2018;7:26. Crossref
36. Tansarli GS, Poulikakos P, Kapaskelis A, Falagas ME. Proportion of extended-spectrum b-lactamase (ESBL)-producing isolates among *Enterobacteriaceae* in Africa: evaluation of the evidence—systematic review. J Antimicrob Chemother. 2014;69:1177-1184. Crossref
37. Mansouri F, Sheibani H, Masroor MJ, Afsharian M. Extended-spectrum beta-lactamase (ESBL)-producing *Enterobacteriaceae* and urinary tract infections in pregnant/postpartum women: a systematic review and meta-analysis. Int J Clin Pract. 2019;37(12). Crossref
38. Zhang J, Zheng B, Zhao L, et al. Nationwide high prevalence of CTX-M and an increase of CTX-M-55 in *Escherichia coli* isolated from patients with community-onset infections in Chinese county hospitals. BMC Infect Dis. 2014;14:659-663.
39. Obeng-Nkrumah N, Twum-Danso K, Krogfelt K, Newman MJ. High levels of extended-spectrum beta-lactamases in a major teaching hospital in Ghana: the need for regular monitoring and evaluation of antibiotic resistance. Am J Trop Med Hyg. 2013;89:960-964.
40. Magoué CL, Melin P, Gangoué-Piéboji J, Okomo Assoumou M-C, Boreux R, De Mol P. Prevalence and spread of extended-spectrum β-lactamase-producing *Enterobacteriaceae* in Ngaoundere, Cameroon. Clin Microbiol Infect. 2013;19:416-420.
41. Girlich D, Bouihat N, Poirel L, Benouda A, Nordmann P. High rate of faecal carriage of extended-spectrum β-lactamase and OXA-48 carbapenemase-producing *Enterobacteriaceae* at a university hospital in Morocco. Clin Microbiol Infect. 2014;20:350-354.
42. Hoban DJ, Lascols C, Nicolle LE, et al. Antimicrobial susceptibility of *Enterobacteriaceae*, including molecular characterization of extended-spectrum beta-lactamase-producing species, in urinary tract isolates from hospitalized patients in North America and Europe: results from the SMART study. Diagn Microbiol Infect Dis. Elsevier Inc. 2012;74(1):62-67. Crossref
43. Yang Q, Xu YC, Kiratisin P, Dowzicky MJ. Antimicrobial activity among gram-positive and gram-negative organisms collected from the Asia-Pacific region as part of the Tigecycline Evaluation and Surveillance Trial: comparison of 2015 results with previous years. Diagn Microbiol Infect Dis. 2017;89:314-323.
44. Hawser SP, Bouchillon SK, Hoban DJ, Badal RE, Hsueh PR, Paterson DL. Emergence of high levels of extended-spectrum-beta-lactamase-producing gram-negative bacilli in the Asia-Pacifc region: data from the Study for Monitoring Antimicrobial Resistance Trends (SMART) program, 2007. Antimicrob Agents Chemother. 2009;53:3280-3284.
45. Lu PL, Liu YC, Toh HS, et al. Epidemiology and antimicrobial susceptibility profiles of Gram-negative bacteria causing urinary tract infections in the Asia-Pacific region: 2009-2010 results from the Study for Monitoring Antimicrobial Resistance Trends (SMART). Int J Antimicrob Agents. 2012;40:S37-S43.
46. Lewis JM, Lester R, Garner P, Feasey NA. Gut mucosal colonisation with extended-spectrum beta-lactamase producing *Enterobacteriaceae* in sub-Saharan Africa: a systematic review and meta-analysis [version 2; peer- review: 2 approved]: Wellcome Open Res. 2020;4:160. Crossref
47. Muhie OA. Antibiotic use and resistance pattern in Ethiopia: systematic review and meta-analysis. *Int J Microbiol*. 2019, Article ID 2489063, 8 pages. Crossref
48. Pavez M, Troncoso C, Irma Osses I, et al. High prevalence of CTX-M-1 group in ESBL-producing *Enterobacteriaceae* infection in intensive care units in southern Chile. *Braz J Infect Dis.* 2019;23(2):102-110.
49. Moges F, Endris M, Belyhun Y, Worku W. Isolation and characterization of multiple drug resistance bacterial pathogens from waste water in hospital and non-hospital environments, Northwest Ethiopia. *BMC Res Notes*. 2014;7:215. Published 2014 Apr 5. Crossref
50. Rodríguez-Baño J, Gutiérrez-Gutiérrez B, Machuca I, Pascual A. Treatment of infections caused by extended-spectrum-beta-lactamase-, AmpC-, and carbapenemase-producing *Enterobacteriaceae*. Clin Microbiol Rev. 2018;31:e00079-17. Crossref
51. Harris P, Paterson D, Rogers B. Facing the challenge of multidrug-resistant gram-negative bacilli in Australia. *MJA*. 2015;202(5). Crossref
52. Seboxa T, Amogne W, Abebe W, et al. High mortality from blood stream infection in Addis Ababa, Ethiopia, is due to antimicrobial resistance. PLoS One. 2015;10(12):e0144944. Crossref
53. Flokas M, Karanika S, Alevizakos M, Mylonakis E. Prevalence of ESBL-producing *Enterobacteriaceae* in pediatric blood-stream infections: a systematic review and meta-analysis. PLoS One. 2017;12(1). Crossref

DTI
ISSN 1177-3928
Drug Target Insights 2020; 14: 26-33
DOI: 10.33393/dti.2020.2103
ORIGINAL RESEARCH ARTICLE
Open Access

Targeting *Streptococcus pneumoniae* UDP-glucose pyrophosphorylase (UGPase): in vitro validation of a putative inhibitor

Monica Sharma[1], Swati Sharma[1], Pallab Ray[2], Anuradha Chakraborti[1]

[1]Molecular Genetics Laboratory, Department of Experimental Medicine and Biotechnology, Postgraduate Institute of Medical Education & Research (PGIMER), Chandigarh - India
[2]Bacteriology Laboratory, Department of Medical Microbiology, Postgraduate Institute of Medical Education & Research (PGIMER), Chandigarh - India

ABSTRACT

Background: Genome plasticity of *Streptococcus pneumoniae* is responsible for the reduced efficacy of various antibiotics and capsular polysaccharide-based vaccines. Therefore, targets independent of capsular types are sought to control the pneumococcal pathogenicity. UDP-glucose pyrophosphorylase (UGPase) is one such desired candidate being responsible for the synthesis of UDP-glucose, a sugar precursor in capsular biosynthesis and metabolic Leloir pathway. Being crucial to pneumococcal pathobiology, the effect of UGPase inhibition on virulence was evaluated in vitro.
Methods: A putative inhibitor, uridine diphosphate (UDP), was evaluated for effective inhibitory concentration in *S. pneumoniae* and A549 cells, its efficacy and toxicity. The effect of UDP on adherence and phagocytosis was measured in human respiratory epithelial (A549 and HEp-2) and macrophage (THP1 and J774.A.1) cell lines respectively.
Results: A differential effective inhibitory concentration of UDP for UGPase inhibition was observed in *S. pneumoniae* and A549 cells, that is, 5 and 100 μM respectively. UDP treatments lowered percent cytotoxicity in pneumococcal-infected monolayers and didn't exert adverse effects on viabilities. *S. pneumoniae* adherence to host cells decreased significantly with UDP treatments. UDP induced the secretion of interleukin (IL)-1β, tumor necrosis factor (TNF)-α, IL-6, and IL-8 and increased pneumococcal phagocytosis.
Conclusion: Our study shows UDP-mediated decrease in the virulence of *S. pneumoniae* and demonstrates UDP as an effective inhibitor of pneumococcal UGPase.

Keywords: Capsule, *galU*, Inhibitor, Pneumococcus, UDP, Virulence

Introduction

Streptococcus pneumoniae (pneumococcus) is an important healthcare-associated pathogen being responsible for various invasive pneumococcal diseases (IPDs), for example, bacteremia, pneumonia, septicemia, and meningitis, and non-IPDs, for example, acute otitis media and sinusitis (1). Pneumococcal infections are associated with significant morbidity and mortality globally, specifically in children younger than 5 years, elderly adults, and individuals with immune deficiencies. Global disease burden and mortality estimates have documented 341,029 deaths in children aged below 5 years; 494,340 deaths in the elderly (aged above 70 years), and total 1,189,937 deaths among all ages due to pneumococcal infections (2-4). This huge burden of pneumococcal diseases is fueled by the rise of new capsular serotypes and spread of antimicrobial-resistant clones (5). Introduction of the capsular polysaccharide (CPS)-based vaccines and pneumococcal conjugate vaccines had provided a little relief, but they still remain unsatisfactory due to limited serotype protection and replacement, restricted efficacy of vaccine at the mucosal surface, implementation issues, and high cost (6,7). Hence, formulation of alternative preventive measures independent of serotypes

Received: February 26, 2020
Accepted: July 30, 2020
Published online: October 7, 2020

Corresponding author:
Prof. Anuradha Chakraborti
Department of Experimental Medicine and Biotechnology
Postgraduate Institute of Medical Education & Research (PGIMER)
Chandigarh-160012, India
superoxide14@gmail.com

is inevitable for the better management of pneumococcal diseases.

Pneumococcal strains have been shown to synthesize a distinct serotype-specific polysaccharide capsule capable of dodging host immune components (8,9). The loss of capsule has been associated with rapid phagocytosis (10,11). Genetic dissection of the *cps/cap* gene cluster encoding for CPS had strongly advocated the involvement of other unlinked genes that are dispersed in chromosome in CPS synthesis (12,13). One of the genes, *galU*, encodes for enzyme uridine diphosphate (UDP)-glucose pyrophosphorylase (UGPase), and its role in the virulence of various gram-negatives and gram-positives is well studied (14-19). UGPase catalyzes the synthesis of UDP-glucose (UDP-glc), which is an important glycosyl donor for the modification and interconversion of sugars in metabolic and capsular pathways (17,19,20). The *galU* mutants of pneumococcus have been shown to be acapsular despite the presence of functional *cps* genes (14,19).

UGPase has been considered as a suitable target to control the pneumococcal virulence (17,21) as *galU* has been reported in all pneumococcal strains regardless of capsular types (14). Also, mammalian UGPases have been evolutionarily unrelated to their prokaryotic counterparts, suggesting that its putative inhibitors would not be inimical to the host (17,21,22). The effects of UGPase inhibition in the pathogenicity of pneumococcus have not been elucidated so far despite the availability of evidence of gene mutation studies (19). A study has screened few chemical inhibitors for the inhibition of UGPase activity in a calorimetric assay from purified extracts (23), but no study is available on inhibitor-mediated host-pathogen interaction. Therefore, for the selection of UGPase inhibitor, we modeled and analyzed the structure of *S. pneumoniae* UGPase using I-TASSER (Iterative-Threading ASSEmbly Refinement) server (http://zhang.bioinformatics.ku.edu/I-TASSER) to delineate its tertiary structure, active site residues, and properties. In this study, we have studied the effect of UGPase inhibition on the virulence of *S. pneumoniae* during host-pathogen interactions and validated a putative inhibitor of pneumococcal UGPase for its inhibition potentials and efficacy in vitro.

Materials and methods

This study was approved by the Institute Ethics Committee (IEC Memo no. 87770-PG11-ITRG/11384). Respiratory epithelial (A549 and HEp-2) and macrophage (J774.A.1 and THP1) cell lines were procured from the cell repository of National Centre for Cell Sciences (NCCS), Pune, India. *S. pneumoniae* reference strains D39 (NCTC 7466) and MTCC 655 (NCTC 7465) were procured from Microbial Type Culture Collection (MTCC), IMTECH, Chandigarh, India. A clinical blood isolate of serotype 19F was also used in the study as its occurrence has been reported frequently in IPDs. Clinical strain was isolated from the blood sample of a patient suffering from lower respiratory tract infection of *S. pneumoniae* only.

Cell culture

A549 and THP1 cell lines were cultured and maintained in RPMI 1640, while HEp-2 and J774.A.1 cell lines were cultured in Minimal Essential Medium (MEM) and Dulbecco's Modified Eagle's Medium (DMEM), respectively, at 37°C with 5% CO_2. All the media were supplemented with 10% (v/v) heat-inactivated fetal bovine serum (FBS), 0.15% (v/v) sodium bicarbonate, streptomycin (100 µg/mL), and penicillin (100 U/mL). Antibiotic-free media were prepared for experiments involving bacterial infection.

UDP as UGPase inhibitor

Effective concentration of UDP as inhibitor of UGPase was evaluated by UGPase assay (17) in both *S. pneumoniae* and A549 cells. Log phase culture of *S. pneumoniae* and confluent cell monolayers were treated with UDP at different concentrations for 1 hour at 37°C and 5% CO_2. A549 cells in phosphate-buffered saline (PBS) were lysed with three cycles of temperature-shock (5 minutes each). Bacterial pellets were sonicated (3 cycles; pulse 10 seconds ON, 30 seconds OFF) in ice bath. UGPase activity was assessed in total 1 mL reaction mixture with freshly prepared extracts (100 µL) at 25°C. Reaction mixture constituted 50 mM Tris-HCl buffer (pH 7.5), 16 mM $MgCl_2$, 0.6 mM β-nicotinamide adenine dinucleotide phosphate (NADP), 0.6 mM UDP-glucose, UDP-glucose dehydrogenase (0.7 U), and phosphoglucomutase (0.07 U). Reaction was initiated with the addition of sodium pyrophosphate (1.7 mM) and NADPH formation was determined by measuring the increase in absorbance at 340 nm. Blank consisted of reaction mixture without cell or bacterial extract.

Inhibitor toxicity to host cells

A549 cell monolayers were treated with different concentrations of UDP for 1 hour at 37°C and untreated cells were taken as reference. The effect of UDP on viability of cells was evaluated using MTT assay (24). Briefly, MTT solution (2.5 mg/mL; Sigma) was added to monolayers and incubated for 4 hours. Media containing MTT was discarded and dimethyl sulfoxide (DMSO, 200 µL) was added. Absorbance was recorded at 590 nm in microplate reader (Bio-Rad 680).

Expression of UGPase in host cells

A549 and HEp-2 monolayers were treated with UDP at effective inhibiting dose for 1 hour at 37°C, 5% CO_2 and untreated cells were taken as control. Total protein was extracted from cell pellet by sonication (3 minutes: pulse 30 seconds ON, 30 seconds OFF) in ice-chilled PBS and was quantitated. Samples were electrophoresed in 10% sodium dodecyl sulfate-polyacrylamide gel electrophoresis (SDS-PAGE) and separated proteins were transferred onto polyvinylidene difluoride (PVDF) membrane. Membranes were processed and incubated with anti-UGP2 antibody (1:2,000, Abcam) for 3 hours at 37°C followed by treatment with horseradish peroxidase (HRP)-conjugated secondary antibody (1:20,000) for 2 hours at 37°C. Pierce® ECL western blotting peroxidase substrate (ThermoScientific) was used for developing protein bands, which were quantitated with FluorChem M Protein-Simple (Bio-Techne). GAPDH as endogenous control was simultaneously blotted and analyzed. Expression of UGPase was normalized with the value of GAPDH in each sample.

Adherence assay

Efficacy of UDP to inhibit the adherence of *S. pneumoniae* during infection with A549 and HEp-2 monolayers was checked by flow cytometer (BD Biosciences) (25). Log phase cultures of pneumococcus were labeled with fluorescein isothiocyanate (FITC, 1.0 µg/µL) and infected onto monolayers at 100:1 multiplicity of infection (MOI: bacteria/cell) in the presence and absence of inhibitor at effective dose. Monolayers were incubated at 37°C at 5% CO_2 for 2 hours followed by trypsinization (0.05%) and fixation with ice-cold paraformaldehyde (2%). Samples were analyzed using FACScan flow cytometer using CellQuest 3.3 software (BD Biosciences). Mean fluorescence intensity (MFI) values were obtained from control samples (unlabeled host cells and bacteria). Adherence was calculated from the MFI of host cell with adherent pneumococci divided by MFI of labeled pneumococci. Effectiveness of inhibitor was evaluated from the adherence potential of *S. pneumoniae* to monolayers in the presence of inhibitor.

Phagocytosis assay

FITC-labeled pneumococci were loaded (MOI, 100:1) onto macrophage cells (THP1 and J774.A.1) in the presence and absence of UDP for 1 hour at 37°C in 5% CO_2. Cells were fixed with cold 2% paraformaldehyde. Briefly, cells were collected, centrifuged, washed as required, and were suspended in ice-cold PBS. Trypan blue (0.2%) was added to quench fluorescence of extracellularly attached pneumococci, just before analysis in flow cytometer (BD BioSciences). MFI of FITC-positive cells was calculated to assess the phagocytic activity in comparison to controls (unlabeled cells and bacteria).

For opsonophagocytic assay (OPA), bacterial cells (10^6 cfu/mL) were labeled with FITC (1 µg/µL) after inactivation at 95°C for 5 minutes. Nonviability was confirmed by overnight incubation of blood agar plates streaked with bacterial suspension (100 µL). Labeled bacteria were incubated with pooled human sera (10% of 1:2 diluted in PBS) for 30 minutes at 37°C, 150 rpm. Bacteria were further inoculated onto THP1 and J774.A.1 cells at MOI 100:1 for 1 hour at 37°C and 5% CO_2. Control tubes contained PBS or heat-inactivated (56°C for 45 minutes) pooled sera. The cells were obtained, washed, centrifuged, and fixed with cold 2% paraformaldehyde and analyzed in a flow cytometer (26).

Expression of postinfection cytokines

A549 monolayers were incubated with effective dose of UDP for 1 hour at 37°C, 5% CO_2. In another set, monolayers were treated with 10 µM MRS2578 for 30 minutes before incubation with UDP (27). Total ribonucleic acid (RNA) was extracted from trypsinized cell pellets using TRIzol reagent followed by complementary deoxyribonucleic acid (cDNA) synthesis using messenger RNA RevertAid™ First Strand cDNA Synthesis Kit (Thermo Scientific). Expression of various cytokines (interleukin [IL]-6, IL-1β, IL-8, tumor necrosis factor [TNF]-α) was analyzed using real-time polymerase chain reaction (PCR; Roche Lightcycler® 480) in reactions (10 µL) containing 50 ng cDNA, 0.5 µM primer, 1X SYBR mix, and deionized water. Gene-specific primers were designed using Primer-3Tool and PCRs were run in primer-specific cycling conditions and with appropriate negative controls for each reaction.

Statistical analysis

Each experiment was performed at least three times in duplicate or triplicate sets. GraphPad Prism 6.0 was used for statistical calculations. Student's t-test, or Mann-Whitney U-test or analysis of variance (ANOVA) was applied as appropriate. A p value less than 0.05 was considered to represent a significant association.

Results

Putative inhibitor of UGPase

The structure of *S. pneumoniae* UGPase was analyzed in silico using I-TASSER server (http://zhang.bioinformatics.ku.edu/I-TASSER; PhD Thesis). The tertiary structure, active site residues, and its substrate-binding properties were analyzed. The local conformational changes induced near the active site in response to binding of its natural substrate were analyzed. Using information of the active site pocket of UGPase and literature-based evidence (11,14,17,21-23), UDP was selected as a probable inhibitor of *S. pneumoniae* UGPase. In silico analysis showed that UDP binding did not result in alteration in local conformation of enzymatic active site. The effective inhibitory concentrations of UDP, its extent of inhibition, and probable toxicity to host cell lines were studied. The pneumococcal virulence and clearance of infection in response to UDP were explored in vitro.

Effect of UDP on UGPase activity

UGPase activity was evaluated at different UDP concentrations (0.05-100 µM) in A549 cells and *S. pneumoniae* D39 strain. Concentration-dependent dose response curve showed that UDP decreased UGPase activity in host A549 cells (Fig. 1A) as well as in pneumococcus (Fig. 1B). UDP-treated A549 cells showed a declined UGPase activity in comparison to untreated (0.0 µM) control cells (Fig. 1A). UGPase activity was not significantly decreased in the cells treated with 0.1-3 µM UDP. However, activity was significantly decreased at 5 µM ($p = 0.009$) and 100 µM ($p = 0.011$) UDP treatments. The inhibition of UGPase activity in A549 cells was 2.8 fold higher at 100 µM UDP treatment in comparison to 5 µM treatment.

In *S. pneumoniae* D39 strain, a significant decrease in UGPase activity was observed at 2 µM UDP ($p = 0.02$) treatment (Fig. 1B). At 5 µM UDP, threefold inhibition ($p = 0.01$) was observed in UGPase activity in comparison to 100 µM. Further, effect of UDP (at 5 and 100 µM) on UGPase activity was evaluated in invasive *S. pneumoniae* isolate (retrieved from blood sample), which showed a decrease in activity at 5 µM UDP ($p = 0.015$) (Fig. 1C). Comparative analysis of UDP treatment on blood isolate and reference D39 strain showed that 5 µM UDP treatments for 1 hour were effective to reduce the bacterial UGPase activity (Fig. 1C) by half than in its host counterpart (Fig. 1A).

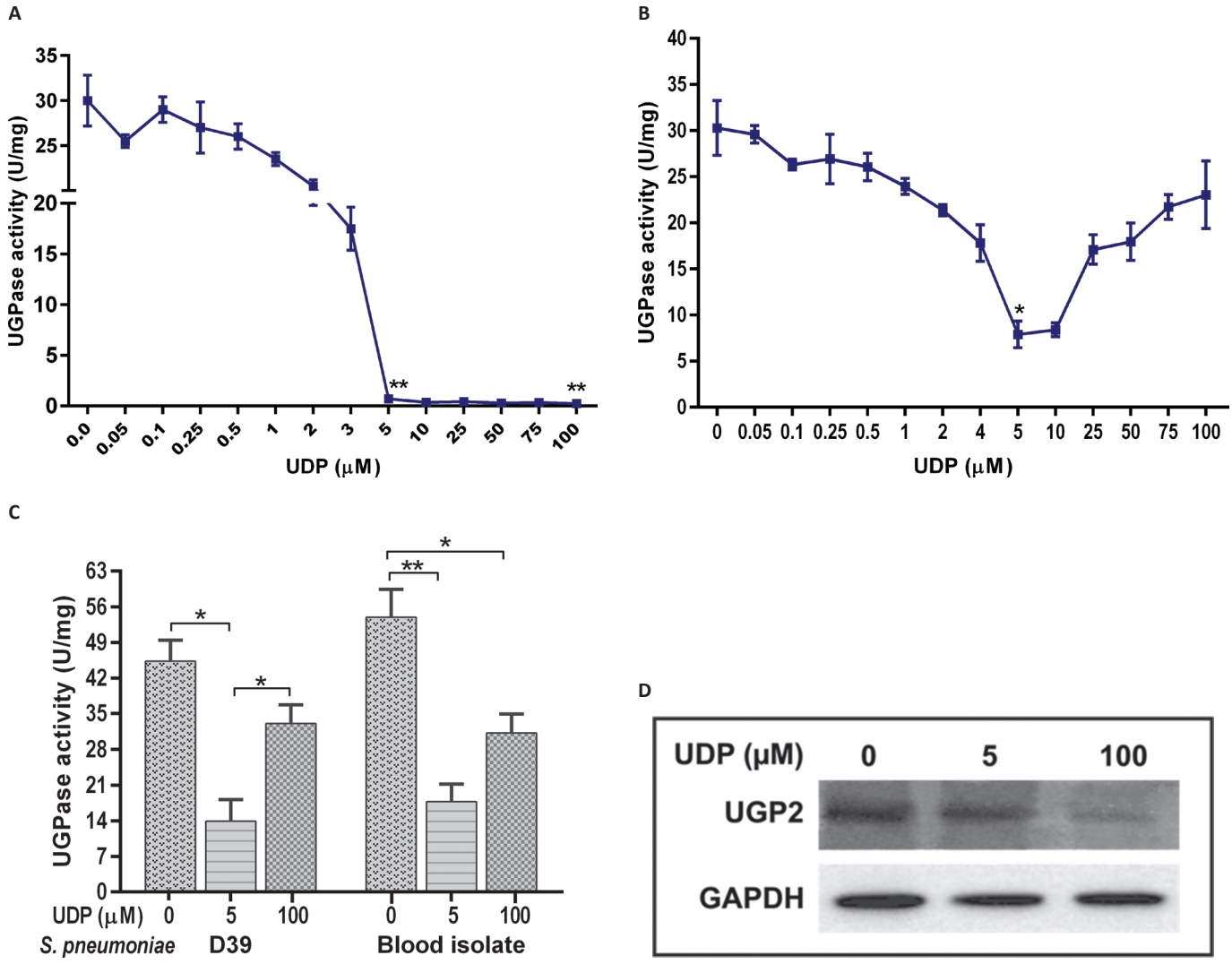

Fig. 1 - Uridine diphosphate (UDP)-glucose pyrophosphorylase **(**UGPase) activity in response to fractional treatment of UDP in **(A)** A549 cells, **(B)** *S. pneumoniae* D39 strain, **(C)** comparative analysis of *S. pneumoniae* UGPase activity in response to UDP treatments. The p values calculated in comparison to control (untreated). **(D)** Western blot analysis of UGP2 in A549 cell lysate, *p < 0.05, **p < 0.01.

Further analysis of UGPase expression in A549 cell lysate using human anti-UGP2 antibody reconfirmed the significant decrease (p = 0.03) at 100 μM UDP treatment in comparison to 5 μM treated and control (untreated) cells (Fig. 1D). However, we could not analyze the UGPase expression in *S. pneumoniae* due to unavailability of antibody against bacterial enzymes.

UDP treatment and A549 cell survival

The effect of UDP on A549 cell viability was evaluated in a dose-dependent manner in the absence (control) and presence of *S. pneumoniae* infection (Fig. 2). Uninfected (control) cells treated with UDP (0.5-100 μM) showed negligible changes in the percentage cell viability. However, A549 cells infected with pneumococci (D39 and blood isolate) showed a significant decrease in percent viability in the absence of UDP treatment (p = 0.001). Notably, the viability of infected A549 cells was elevated at higher UDP treatments (>10 μM) in a dose-dependent manner (Fig. 2A). Further, a comparative analysis of UDP treatments (0, 5, 100 μM) to A549 cells showed significantly improved viability at 100 μM treatment in D39 (p = 0.009) and blood isolate (p = 0.04) infected cells, while no change in cell viability was observed in uninfected (control) cells (Fig. 2B). Thus, UDP seems safer to explore for its potential as it did not exert any cytotoxic effect on A549 cells (Fig. 2), while it improved the percentage cell viability in the presence of bacterial infection.

Further, effect of UGPase inhibition on adherence and phagocytosis of *S. pneumoniae* (blood isolate and standard strains MTCC 655; a highly capsular strain and D39) was evaluated at effective 5 μM UDP concentration (Fig. 1).

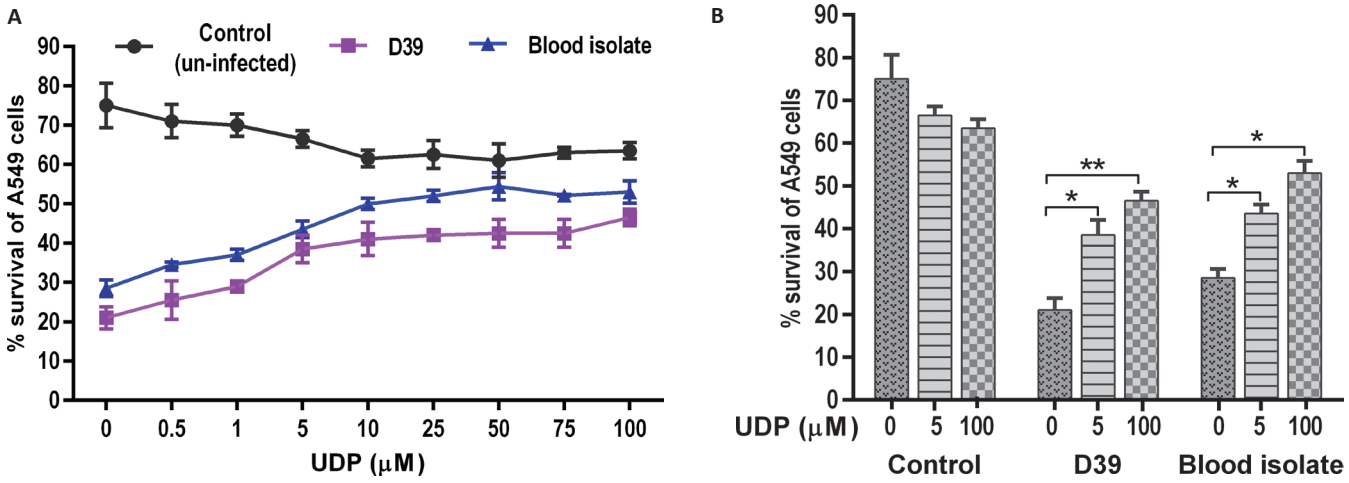

Fig. 2 - Effect of uridine diphosphate (UDP) treatment on A549 cell survival. **(A)** Treatment-response curve of cells infected with *S. pneumoniae*, **(B)** comparative analysis of UDP treated and untreated (0 μM) cells, control: uninfected A549 cells, *p < 0.05, **p < 0.01.

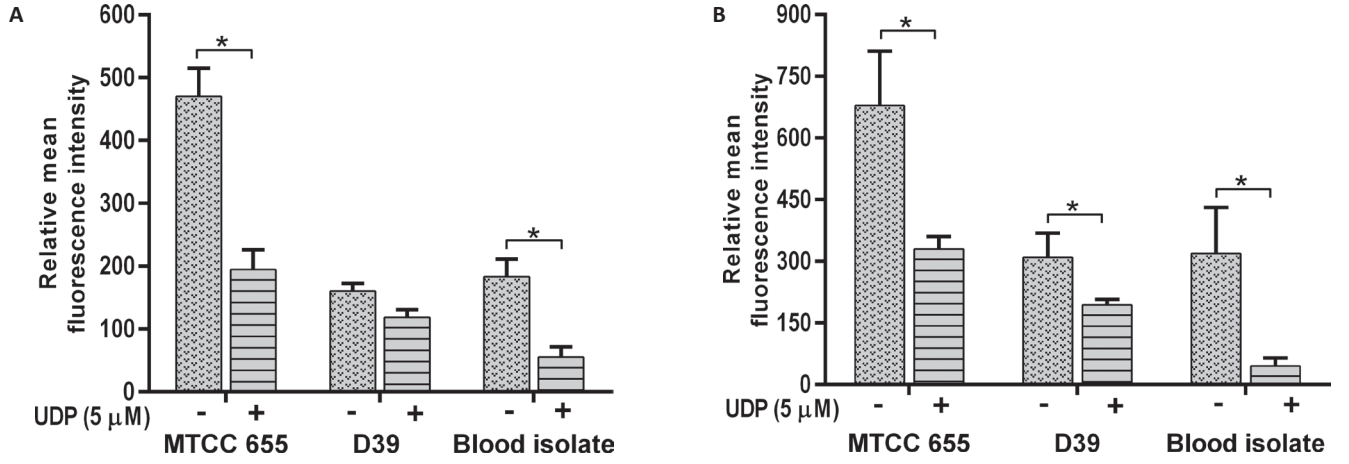

Fig. 3 - Effect of uridine diphosphate (UDP) treatment on adherence of *S. pneumoniae* by **(A)** A549 and **(B)** HEp-2 cells, *p < 0.05.

Effect of UDP on S. pneumoniae *adherence*

All *S. pneumoniae* strains showed a decrease in adherence to A549 (p = 0.018) and HEp-2 cells (p = 0.001) in the presence of 5 μM UDP (Fig. 3). Adherence of MTCC 655 and blood isolate was significantly (p<0.05) lowered in both the cell lines (Fig. 3A and B), while D39 showed a significant (p = 0.031) decrease in HEp-2 cells only (Fig. 3B). Adherence of blood isolate to A549 (p = 0.032) and HEp-2 (p = 0.014) cells declined by three- to fivefold.

Effect of UDP on phagocytosis of S. pneumoniae

The phagocytosis of *S. pneumoniae* was increased in the presence of UDP in both J774.A.1 (p = 0.01) and THP1 (p = 0.022) cells (Fig. 4A and B respectively). Phagocytosis of D39 strain was significantly higher than MTCC 655 strain (p = 0.033) in both the cell lines, which could be attributed to heavy encapsulation in the latter. UDP treatment also showed an increase in phagocytosis of blood isolate by J774.A.1 (p = 0.034) and THP1 cells (p = 0.041). Overall, UDP-dependent fold change in phagocytosis ranged from 1.4 to 1.9 for pneumococcal strains. It is well known that host immune cells use complement factors for the clearance of *S. pneumoniae*, and OPA of heat-inactivated *S. pneumoniae* was found to be enhanced in the presence of UDP in both the cell lines (Fig. 5A and B). Interestingly, J774.A.1 cells (Fig. 5A) showed marked increase in the OPA of blood isolate than MTCC 655 and D39 strains. Phagocytosis of MTCC 655 and D39 strains was higher in THP1 cells (Fig. 5B) in the presence of UDP (5 μM) and sera.

Real-time PCR analysis of cytokines

An attempt was made to evaluate the cytokine response in A549 cells in response to UDP treatment as previous studies have shown the activation of inflammatory pathway upon UDP stimulation from monocytes and microglial cells (28,29). Interestingly, UDP treatment (5 μM) induced the secretion of

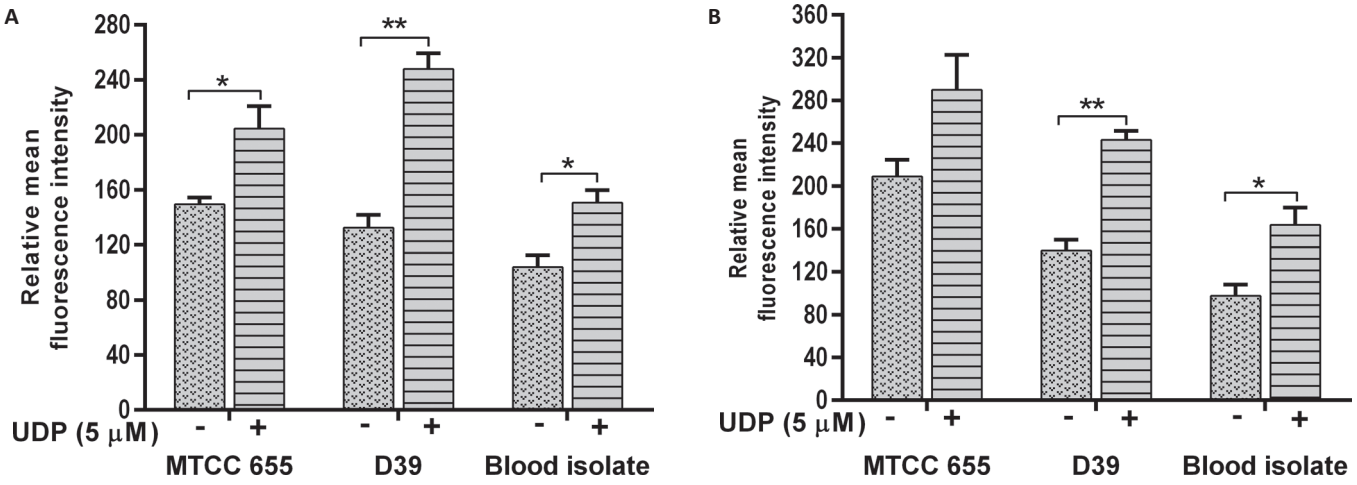

Fig. 4 - Effect of uridine diphosphate (UDP, 5 μM) on phagocytosis of *S. pneumoniae* by **(A)** J774.A.1 and **(B)** THP1 cells, *p < 0.05, **p < 0.01.

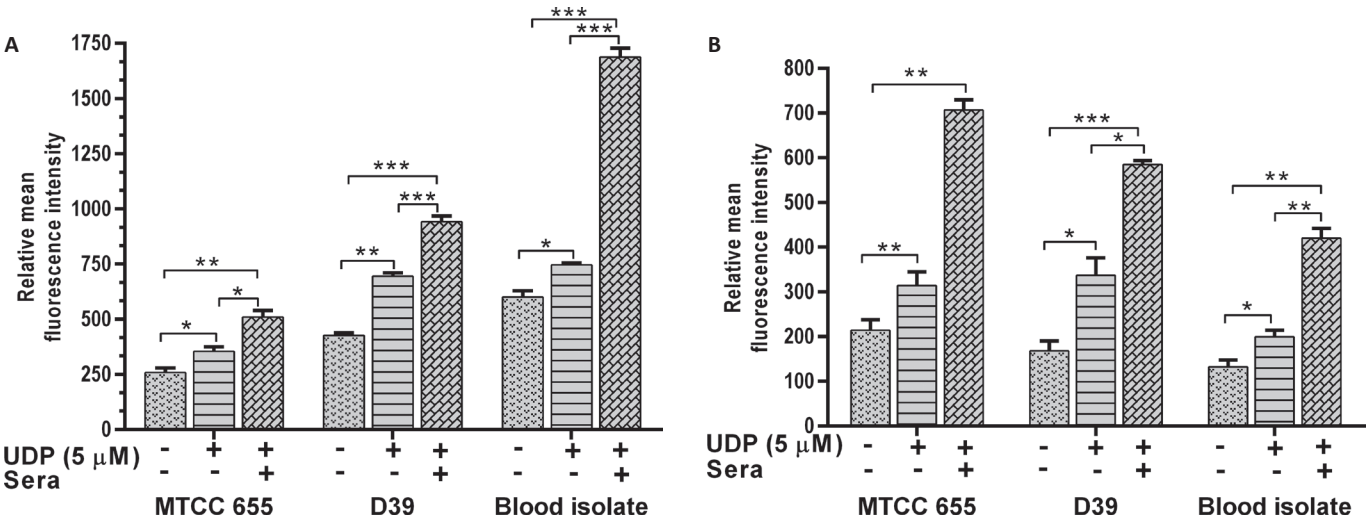

Fig. 5 - Effect of uridine diphosphate (UDP, 5 μM) on opsonophagocytosis of *S. pneumoniae* by **(A)** J774.A.1 and **(B)** THP1 cells, *p < 0.05, **p < 0.01, ***p < 0.001.

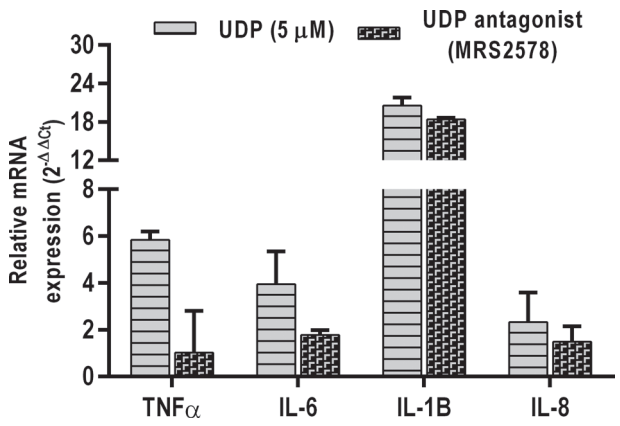

Fig. 6 - Relative messenger ribonucleic acid (mRNA) expression of cytokines induced in A549 cells, MRS2578: antagonist of uridine diphosphate (UDP).

IL-1β, TNF-α, IL-6, and IL-8 from the A549 alveolar epithelial cells (Fig. 6). An UDP antagonist MRS2578 (Sigma) effectively suppressed the expression of these cytokines in A549 cells. In agreement with these results, UDP is shown to bind its purinergic receptor P2Y6 on various cells and stimulate signaling cascade (30,31).

Conclusions

The paradox of infections caused by *S. pneumoniae* lies in the availability of preventive measures such as antibiotics and vaccines, but not effective prevention from the pneumococcal diseases, especially in low- to middle-income settings. The major reason for this paradox is the genome plasticity of pneumococcus and diverse nature of *cps* loci, which has precluded the absolute success of vaccines (11,12,32). Evidently, various virulence factors of pneumococci had been explored to understand its pathobiology and with broader

prospect to yield potential targets for preventive interventions (8-11,21). Elucidation of *cps* loci from different pneumococcal serotypes has established a crucial role of *galU*-encoded UGPase in capsule formation (14,17,18). UGPase-catalyzed reaction provides UDP-glucose (glc), a key sugar precursor to fulfill various capsular (CPS biosynthesis pathway) and metabolic (Leloir pathway) needs of pneumococcus (12-14,18,20,36-38). In this study, we explored the potential of UGPase in modulating *S. pneumoniae* pathogenicity by using UDP as an UGPase inhibitor.

UDP proved to be an effective inhibitor of pneumococcal UGPase and mediated a significant reduction in the in vitro virulence of pneumococci. The differential concentration-based enzyme activity inhibition maxima suggests the feasibility of selective inhibition of pneumococcal UGPase (5 µM UDP) without inimical effect on host. The decline in pneumococcal adherence to host cell lines also accentuates the efficacy of UDP as an inhibitor. A study by Zavala et al used nucleoside analogs, namely abacavir, decitabine, stavudine, and zidovudine, to show 42%-58% inhibition of UGPase, but did not elaborate on the use of high concentration (7.5 mM) of inhibitors, their toxic effects, and safety as antipneumococcal drug (23). Our study establishes the noncytotoxicity of UDP to host cells and boosted uptake of *S. pneumoniae* upon UDP stimulation by macrophage cell lines. Our findings are supported by previous studies on the clearance of *Escherichia coli* from peritonitis mouse model in response to direct UDP injection (33) and increased host defenses upon UDP binding to P2Y6 receptor (34-36). The crucial role of UDP as inflammatory inducer in brain injuries has been reported in microglia and astrocytes (28). Likewise, we have also found the activation of proinflammatory cytokines in alveolar epithelial cells in response to pneumococcal infection. The stimulation of cytokines by UDP emphasizes its protective functional nature, which might enhance its efficacy as a potent inhibitor.

The present study provides evidence to the UDP-mediated reduction in the virulence of *S. pneumoniae*. Being one of the intercellular messengers, UDP acts as a protective signaling molecule and activates P2Y6 receptors that are known to result in wide range of physiologic responses, such as induction of cytokines, chemokines, phagocytosis, and increase in concentration of extracellular nucleotides (33,35,37,38). The evidence of UDP meddling with host-pathogen interactions has opened the vast horizon to investigate its underlying mechanisms, which would definitely shed light on its potential utility in restraining the pneumococcal virulence. The present work is a little step forward in search of potential *S. pneumoniae* inhibitor independent of serotypes, though the inhibitory effect of UDP should be evaluated in vivo to ascertain its efficacy. Our study has been limited in evaluating the cytokine response and UDP-mediated behavior of P2Y6 receptors, which further need a detailed investigation. Mechanistic understanding of UDP-mediated UGPase inhibition and its in vivo validation would be crucial for translating the outcome of this study.

Author contributions

Monica Sharma performed the experiments, analyzed the data, and wrote the manuscript. Swati Sharma helped in manuscript editing. Anuradha Chakraborti and Monica Sharma designed the study. Pallab Ray provided the clinical isolates for the study. Anuradha Chakraborti and Pallab Ray reviewed the study and manuscript.

Disclosures

Financial support: The authors are grateful to the Indian Council of Medical Research (ICMR), New Delhi, India for financial support and providing Senior Research Fellowship (File no. 80/768/2012-ECD-1) to Ms. Monica Sharma and funding the project. Swati Sharma received research fellowship from Council of Scientific and Industrial Research (CSIR) New Delhi, India. Authors disclose no other external funding sources.
Conflict of interest: The authors declare no conflict of interest.

References

1. Musher DM. *Streptococcus pneumoniae*. In: Mandell GL, Bennett JE, Dolin R, eds. Mandell, Douglas, and Bennett's principles and practice of infectious diseases. 7th ed. Philadelphia, PA: Churchill Livingstone Elsevier 2010; 2623-2642.
2. Troeger C, Blacker B, Khalil IA, et al., SRM GBD 2016 Lower Respiratory Infections Collaborators. Estimates of the global, regional, and national morbidity, mortality, and aetiologies of lower respiratory infections in 195 countries, 1990-2016: a systematic analysis for the Global Burden of Disease Study 2016. Lancet Infect Dis. 2018;18:1191-1210.
3. Wahl B, O'Brien KL, Greenbaum A, et al. Burden of *Streptococcus pneumoniae* and *Haemophilus influenzae* type b disease in children in the era of conjugate vaccines: global, regional, and national estimates for 2000-15. Lancet Glob Health. 2018;6:e744-e757.
4. Wahl B, Sharan A, Deloria Knoll M, et al. National, regional, and state-level burden of *Streptococcus pneumoniae* and *Haemophilus influenzae* type b disease in children in India: modeled estimates for 2000-15. Lancet Glob Health. 2019;7:e735-e747.
5. Kim SH, Song JH, Chung DR, et al. Changing trends in antimicrobial resistance and serotypes of *Streptococcus pneumoniae* isolates in Asian countries: an Asian Network for Surveillance of Resistant Pathogens (ANSORP) study. Antimicrob Agents Chemother. 2012;56:1418-1426.
6. Azarian T, Grant LR, Arnold BJ, et al. The impact of serotype-specific vaccination on phylodynamic parameters of *Streptococcus pneumoniae* and the pneumococcal pan-genome. PLoS Pathog. 2018;14:e1006966.
7. McLaughlin JM, Jiang Q, Isturiz RE, et al. Effectiveness of 13-valent pneumococcal conjugate vaccine against hospitalization for community-acquired pneumonia in older US adults: a test-negative design. Clin Infect Dis. 2018;67:1498-1506.
8. Mitchell AM, Mitchell TJ. *Streptococcus pneumoniae*: virulence factors and variation. Clin Microbiol Infect. 2010;16:411-418.
9. Brooks LRK, Mias GI. *Streptococcus pneumoniae*'s virulence and host immunity: aging, diagnostics, and prevention. Front Immunol. 2018;9:1366.
10. Magee AD, Yother J. Requirement for capsule in colonization by *Streptococcus pneumoniae*. Infect Immun. 2001;69:3755-3761.
11. Shainheit MG, Mulé M, Camilli A. The core promoter of the capsule operon of *Streptococcus pneumoniae* is necessary for colonization and invasive disease. Infect Immun. 2014;82:694-705.
12. García E, Llull D, López R. Functional organization of the gene cluster involved in the synthesis of the pneumococcal capsule. Int Microbiol. 1999;2:169-176.
13. García E, Llull D, Muñoz R, Mollerach M, López R. Current trends in capsular polysaccharide biosynthesis of *Streptococcus pneumoniae*. Res Microbiol. 2000;151:429-435.

14. Mollerach M, López R, García E. Characterization of the galU gene of *Streptococcus pneumoniae* encoding a uridine diphosphoglucose pyrophosphorylase: a gene essential for capsular polysaccharide biosynthesis. J Exp Med. 1998;188:2047-2056.
15. Chang HY, Lee JH, Deng WL, Fu TF, Peng HL. Virulence and outer membrane properties of a galU mutant of *Klebsiella pneumoniae* CG43. Microb Pathog. 1996;20:255-261.
16. Priebe GP, Dean CR, Zaidi T, et al. The *galU* gene of *Pseudomonas aeruginosa* is required for corneal infection and efficient systemic spread following pneumonia but not for infection confined to the lung. Infect Immun. 2004;72:4224-4232.
17. Bonofiglio L, García E, Mollerach M. Biochemical characterization of the pneumococcal glucose 1-phosphate uridylyltransferase (GalU) essential for capsule biosynthesis. Curr Microbiol. 2005;51:217-221.
18. Bonofiglio L, García E, Mollerach M. The *galU* gene expression in *Streptococcus pneumoniae*. FEMS Microbiol Lett. 2012;332:47-53.
19. Cools F, Torfs E, Vanhoutte B, et al. *Streptococcus pneumoniae galU* gene mutation has a direct effect on biofilm growth, adherence and phagocytosis in vitro and pathogenicity in vivo. Pathog Dis. 2018;76.
20. Frey PA. The Leloir pathway: a mechanistic imperative for three enzymes to change the stereochemical configuration of a single carbon in galactose. FASEB J. 1996;10:461-470.
21. Alvaro Berbis M, Maria Sanchez-Puelles J, Javier Canada F, Jimenez-Barbero J. Structure and function of prokaryotic UDP-glucose pyrophosphorylase, a drug target candidate. Curr Med Chem. 2015;22:1687-1697.
22. Mollerach M, García E. The galU gene of Streptococcus pneumoniae that codes for a UDP-glucose pyrophosphorylase is highly polymorphic and suitable for molecular typing and phylogenetic studies. Gene. 2000;260:77-86.
23. Zavala A, Kovacec V, Levín G, et al. Screening assay for inhibitors of a recombinant *Streptococcus pneumoniae* UDP-glucose pyrophosphorylase. J Enzyme Inhib Med Chem. 2017;32:203-207.
24. Twentyman PR, Luscombe M. A study of some variables in a tetrazolium dye (MTT) based assay for cell growth and chemosensitivity. Br J Cancer. 1987;56:279-285.
25. Hara-Kaonga B, Pistole TG. A dual fluorescence flow cytometric analysis of bacterial adherence to mammalian host cells. J Microbiol Methods. 2007;69:37-43.
26. Hu BT, Yu X, Jones TR, et al. Approach to validating an opsonophagocytic assay for *Streptococcus pneumoniae*. Clin Diagn Lab Immunol. 2005;12:287-295.
27. Kim B, Jeong HK, Kim JH, Lee SY, Jou I, Joe EH. Uridine 5′-diphosphate induces chemokine expression in microglia and astrocytes through activation of the P2Y6 receptor. J Immunol. 2011;186:3701-3709.
28. Cox MA, Gomes B, Palmer K, et al. The pyrimidinergic P2Y6 receptor mediates a novel release of proinflammatory cytokines and chemokines in monocytic cells stimulated with UDP. Biochem Biophys Res Commun. 2005;330:467-473.
29. Grbic DM, Degagné É, Larrivée JF, et al. P2Y6 receptor contributes to neutrophil recruitment to inflamed intestinal mucosa by increasing CXC chemokine ligand 8 expression in an AP-1-dependent manner in epithelial cells. Inflamm Bowel Dis. 2012;18:1456-1469.
30. Ginsburg-Shmuel T, Haas M, Grbic D, et al. UDP made a highly promising stable, potent, and selective P2Y6-receptor agonist upon introduction of a boranophosphate moiety. Bioorg Med Chem. 2012;20:5483-5495.
31. Hao Y, Liang JF, Chow W, Cheung W, Ko W. P2Y6 receptor-mediated proinflammatory signaling in human bronchial epithelia. PLoS ONE. 2014;9:e106235.
32. Subramanian K, Henriques-Normark B, Normark S. Emerging concepts in the pathogenesis of the *Streptococcus pneumoniae*: from nasopharyngeal colonizer to intracellular pathogen. Cell Microbiol. 2019;2:e13077.
33. Zhang Z, Wang Z, Ren H, et al. P2Y6 agonist uridine 5′-diphosphate promotes host defense against bacterial infection via monocyte chemoattractant protein-1–mediated monocytes/macrophages recruitment. J Immunol. 2011;186:5376-5387.
34. Idzko M, Ferrari D, Eltzschig HK. Nucleotide signalling during inflammation. Nature. 2014;509:310-317.
35. Koizumi S, Shigemoto-Mogami Y, Nasu-Tada K, et al. UDP acting at P2Y6 receptors is a mediator of microglial phagocytosis. Nature. 2007;446:1091-1095.
36. Inoue K, Koizumi S, Kataoka A, Tozaki-Saitoh H, Tsuda M. P2Y(6)-evoked microglial phagocytosis. Int Rev Neurobiol. 2009;85:159-163.
37. Neher JJ, Neniskyte U, Hornik T, Brown GC. Inhibition of UDP/P2Y6 purinergic signaling prevents phagocytosis of viable neurons by activated microglia in vitro and in vivo. Glia. 2014;62:1463-1475.
38. Zierhut M, Dyckhoff S, Masouris I, et al. Role of purinergic signaling in experimental pneumococcal meningitis. Sci Rep. 2017;7:44625.

DTI
ISSN 1177-3928
Drug Target Insights 2020; 14: 34-47
DOI: 10.33393/dti.2020.2185
REVIEW
Open Access

Interaction of drugs with lipid raft membrane domains as a possible target

Hironori Tsuchiya[1], Maki Mizogami[2]

[1]Asahi University School of Dentistry, Mizuho, Gifu - Japan
[2]Department of Anesthesiology, Kizawa Memorial Hospital, Minokamo, Gifu - Japan

ABSTRACT

Introduction: Plasma membranes are not the homogeneous bilayers of uniformly distributed lipids but the lipid complex with laterally separated lipid raft membrane domains, which provide receptor, ion channel and enzyme proteins with a platform. The aim of this article is to review the mechanistic interaction of drugs with membrane lipid rafts and address the question whether drugs induce physicochemical changes in raft-constituting and raft-surrounding membranes.

Methods: Literature searches of PubMed/MEDLINE and Google Scholar databases from 2000 to 2020 were conducted to include articles published in English in internationally recognized journals. Collected articles were independently reviewed by title, abstract and text for relevance.

Results: The literature search indicated that pharmacologically diverse drugs interact with raft model membranes and cellular membrane lipid rafts. They could physicochemically modify functional protein-localizing membrane lipid rafts and the membranes surrounding such domains, affecting the raft organizational integrity with the resultant exhibition of pharmacological activity. Raft-acting drugs were characterized as ones to decrease membrane fluidity, induce liquid-ordered phase or order plasma membranes, leading to lipid raft formation; and ones to increase membrane fluidity, induce liquid-disordered phase or reduce phase transition temperature, leading to lipid raft disruption.

Conclusion: Targeting lipid raft membrane domains would open a new way for drug design and development. Since angiotensin-converting enzyme 2 receptors which are a cell-specific target of and responsible for the cellular entry of novel coronavirus are localized in lipid rafts, agents that specifically disrupt the relevant rafts may be a drug against coronavirus disease 2019.

Keywords: Drug target, Fluidity, Lipid raft, Membrane domain, Membrane interaction

Introduction

Since Singer and Nicolson proposed a fluid mosaic model, the concept of membrane organization has progressively changed, that is, plasma membranes are not the homogeneous bilayers of uniformly distributed lipids but the lipid complex with laterally separated membrane domains such as lipid rafts and caveolae (1). Lipid rafts are small (10-200 nm), heterogeneous, dynamic, and cholesterol- and sphingolipid-enriched membrane domains that are distinct from the rest of the membrane structures (2), whereas caveolae are a subset of lipid rafts and organizationally maintained by characteristic protein caveolins (3). Lipid rafts in a liquid-ordered (L_o) phase coexist with the bulk of membranes in a liquid-disordered (L_d) phase (4). Lipid raft membrane domains play an important role in cellular signal transduction and trafficking by compartmentalizing membranes and providing functional membrane proteins with a platform (4-7). Pharmacologically relevant receptors, ion channels and enzymes are localized or cluster in membrane lipid rafts and caveolae (8-11).

Given the localization of receptors, ion channels and enzymes in membrane lipid rafts, the mode of drug action is first interpretable in a simple manner of receptor/channel/enzyme and ligand interaction as known in the conventional mechanistic theory. The second possibility is that drugs may act on membrane lipids to affect the organizational integrity of lipid rafts, resulting in modulation of the activity of receptors, ion channels and enzymes embedded in membrane domains. It is of much interest to know whether drugs interact

Received: September 17, 2020
Accepted: November 11, 2020
Published online: December 22, 2020

Corresponding author:
Hironori Tsuchiya
Asahi University School of Dentistry
1851 Hozumi, Mizuho, Gifu 501-0296 - Japan
tsuchi-hiroki16@dent.asahi-u.ac.jp

preferentially with lipid rafts compared with non-raft overall membrane lipid bilayers and whether such interaction at a membrane lipid level is linked to pharmacological and cytotoxic effects of drugs. While cholesterol is essential to raft and caveola formation, the regulatory effects of membrane domains on receptors and ion channels were confirmed by depleting cholesterol in plasma membranes (12-15).

The purpose of the present study is to review the interaction of drugs with membrane lipid rafts and the membranes surrounding such domains by searching scientific articles from a mechanistic point of view in order to gain new insights into a drug target. Since various proteins embedded in membranes are functionally modulated by membrane fluidity, order and phase transition, the focus of our review is on addressing the question whether drugs modify the physicochemical properties of raft-constituting and raft-surrounding membranes to affect the formation, stability and integrity of lipid raft membrane domains.

Methods

The present review is based on articles that were retrieved from PubMed/MEDLINE and Google Scholar by searching databases from 2000 to 2020. The publications earlier than 2000 were exceptionally cited if they are essential to advancing the discussion. Research papers published in English in internationally recognized journals and online journals were preferred, but review articles were additionally used to deepen understanding of the concept of plasma membranes and the mode of drug action. For reviewing as diverse drugs as possible without confining to a specific class of drug, the literature searches were carried out using the following terms or combinations thereof: “lipid raft,” “caveola,” “membrane domain,” “membrane interaction,” “fluidity,” “receptor,” “channel” and “enzyme.” Collected articles were independently reviewed by title, abstract and text for relevance with preference to more recent publications.

Results and discussion

Drug and raft interaction methodology

Since the methodology of drug and membrane raft interaction is essential to facilitate readers’ understanding of individual studies, representative experiments are mentioned as follows.

In in vitro experiments, drugs are subjected to the reaction with raft model (raft-like) membranes or liposomes that mimic the lipid composition and property of lipid raft micro domains (16,17). Ternary lipid membranes are used as a raft model, which is frequently prepared with an equimolar mixture of 1-palmitoyl-2-oleoylphosphatidylcholine (POPC), sphingomyelin (SM) and cholesterol (18), in which cholesterol functions as a spacer between sphingolipid hydrocarbon chains and as a glue to keep the raft assembly together (19). Such raft model membranes have the advantage that the membrane effects of drugs can be determined more easily than in vivo experiments (20). Lipid rafts isolated from cells are also used experimentally. Since lipid rafts are relatively insoluble in cold non-ionic detergents, cells are treated with Triton X-100 and membrane lipid rafts are fractionated by sucrose density gradient centrifugation (SDGC) (21).

In in vivo experiments, human and animal subjects are treated with drugs, followed by SDGC to isolate cellular membrane lipid rafts. Cholesterol is not only a critical determinant for membrane fluidity but also an essential component to form the L_o membrane domains. Cellular cholesterol contents are manipulated by treating animals with cholesterol metabolic inhibitors, culturing cells in cholesterol-deficient media and using cholesterol-depleting agents. Methyl-β-cyclodextrin (MBC), to form a 2:1 complex with cholesterol (22), is most widely used for cholesterol depletion (23).

Drug-induced physicochemical or biophysical changes in raft model membranes and membrane lipid rafts are determined by fluorescence polarization (FP) or anisotropy (FA), differential scanning calorimetry (DSC), nuclear magnetic resonance (NMR) spectroscopy, neutron diffraction (ND), X-ray diffraction (XD) and their complementary combination.

General anesthetics

General anesthetics and their related sedatives, anxiolytics and adjuncts act on inhibitory γ-aminobutyric acid type A ($GABA_A$) receptors and excitatory *N*-methyl-D-aspartate (NMDA) receptors (24). Intravenous and inhalational anesthetics are a positive allosteric modulator or a direct activator of $GABA_A$ receptors to enhance their inhibitory functions, inducing general anesthesia, sedation, anxiolysis and convulsion cessation (25). Inhalational anesthetics are also a non-competitive antagonist of NMDA receptors to reduce neuronal excitation, producing analgesic, sedative and anesthesia-maintaining effects (26,27). These anesthesia-relevant $GABA_A$ receptors and NMDA receptors are associated with lipid raft membrane domains (28,29). Results of the literature search indicated that general anesthetics interact with membrane lipid rafts and membranes as shown in Table I.

Intravenous anesthetic propofol

FP experiments demonstrated that propofol structure-specifically interacts with binary liposomal membranes prepared with 80 mol% POPC and 20 mol% cholesterol (30) and quinary liposomal membranes prepared with 55 mol% phospholipids (POPC, SM, 1-palmitoyl-2-oleoylphosphatidylethanolamine (POPE) and 1-palmitoyl-2-oleoylphosphatidylserine (POPS)) and 45 mol% cholesterol (31), resulting in an increase of membrane fluidity at clinically relevant 0.125-10 μM. L_o and L_d phase equilibrium is present in giant plasma membrane vesicles (GPMVs) isolated from rat basophil leukemia cells, which are used as a model of membrane heterogeneity for lipid rafts. Gray et al treated GPMVs with propofol and its structural analogs to examine their effects on liquid-liquid transition by analyzing the lateral distribution of fluorescent probe DiI-C_{12} microscopically (32). Propofol reduced the critical transition temperature at 2.5-10 μM, but not 2,6-di-*tert*-butylphenol without the anesthetic activity at the same concentrations. Therefore, propofol is considered

TABLE I - Interaction of general anesthetics with lipid raft membrane domains and membranes

Drug class	Drug	Membrane	Induced membrane modification	Reference
Intravenous anesthetic	Propofol (0.125-1.0 μM)	Binary liposomal membranes (80 mol% POPC and 20 mol% cholesterol)	Increased membrane fluidity	30
Intravenous anesthetic	Propofol (10 μM)	Quinary liposomal membranes (55 mol% phospholipids (POPC, SM, POPE and POPS) and 45 mol% cholesterol)	Increased membrane fluidity	31
Intravenous anesthetic	Propofol (2.5-10 μM)	GPMVs isolated from rat basophil leukemia cells	Reduced the critical transition temperature structure-specifically	32
Intravenous anesthetic	Propofol (10 and 30 μM)	Human airway smooth muscle cell membranes	Reduced the intracellular Ca^{2+} concentration responses to 10 μM histamine, disrupted caveolae and decreased caveolin-1 expression	33
Inhalational anesthetic	Isoflurane (1 and 5 mM)	POPC/cholesterol liposomal membranes, erythrocyte ghosts and brain endothelial cell-mimetic membranes	Increased membrane fluidity	34
Inhalational anesthetic	Isoflurane (2.5-12 mM)	LUVs (62.5 mol% DPPC and 37.5 mol% cholesterol)	Weakened the sterol-phospholipid association in cholesterol-rich L_o phase membranes	35
Inhalational anesthetic	Halothane (1.5 mol%)	Multilayer membranes (DPPC and DLPC, 1:1 molar ratio)	Reduced the transition temperature by about 5°C	36
Inhalational anesthetic	Xenon (4.6-fold MAC) Nitrous oxide (4.6-fold MAC) Halothane (three- to fivefold MAC) Isoflurane (three- to fivefold MAC)	Raft model membranes (DOPC, SM and cholesterol, 1:1:0.2 molar ratio)	Increased the L_d phase Decreased the relative intensity of L_o to L_d phase	37
Barbiturate	Rats injected with sodium pentobarbital (50 mg/kg, i.p.)	Lipid rafts isolated from rat brains 15 minutes after drug injection	Reduced the transition temperature	38

DLPC = 1,2-dilauroylphosphatidylcholine; DOPC = 1,2-dioleoylphosphatidylcholine; DPPC = 1,2-dipalmitoylphosphatidylcholine; GPMV = giant plasma membrane vesicle; LUV = large unilamellar vesicle; MAC = minimum alveolar concentration; POPC = 1-palmitoyl-2-oleoylphosphatidylcholine; POPE = 1-palmitoyl-2-oleoylphosphatidylethanolamine; POPS = 1-palmitoyl-2-oleoylphosphatidylserine; SM = sphingomyelin.

to decrease the magnitude of membrane heterogeneity structure-specifically, affecting receptor and ion channel proteins sensitive to raft heterogeneity. While propofol is known to produce bronchodilatation, the airway relaxation involves a decrease of Ca^{2+} concentrations in airway smooth muscle cells that are regulated by caveolae. By exposing human airway smooth muscle cells to propofol at 10 and 30 μM, Grim et al found that propofol increases in membrane caveolae and reduces the intracellular Ca^{2+} concentration response to 10 μM histamine (33). They also suggested that propofol may induce caveolar disruption and caveolin-1 expression decrease.

Inhalational anesthetics

Patel et al investigated the membrane effects of isoflurane using different membrane systems such as POPC/cholesterol liposomal membranes, erythrocyte ghosts and brain endothelial cell-mimetic membranes (34). FA measurements indicated that isoflurane increases the membrane fluidity at 1 and 5 mM. Turkyilmaz et al prepared large unilamellar vesicles (LUVs) with 1,2-dipalmitoylphosphatidylcholine (DPPC) and cholesterol to be 2.5 mol% or 37.5 mol% cholesterol-containing DPPC membranes to verify the membrane effects of inhalational anesthetics (35). Isoflurane and halothane weakened and strengthened the sterol-phospholipid association in cholesterol-rich L_o phase membranes and in cholesterol-poor L_d phase membranes, respectively, at 2.5-12 mM. In ND and XD experiments of Weinrich et al, halothane was subjected to the reaction with multilayer membranes that were prepared with an equimolar mixture of DPPC and 1,2-dilauroylphosphatidylcholine (DLPC) to form distinct DPPC-rich ordered and DLPC-rich fluid phase (36). Halothane reduced the transition temperature by about 5°C at 1.5 mol% corresponding to about twice the minimum alveolar concentration (MAC) for human anesthesia, but not non-anesthetic

1,2-dichlorohexafluorocyclobutane even at fivefold MAC. Weinrich and Worcester determined the effects of different anesthetics on liquid phase distribution in raft model membranes prepared with 1,2-dioleoylphosphatidylcholine (DOPC), SM and cholesterol (1:1:0.2 molar ratio) by ND and XD analysis (37). Xenon and nitrous oxide increased the L_d phase at 4.6-fold MAC, and halothane and isoflurane decreased the relative intensity of L_o to L_d phase at three- to fivefold MAC.

Barbiturate

Pentobarbital is intravenously and intraperitoneally administered especially in veterinary anesthesia or sedation. Sierra-Valdez et al characterized the in vivo effects of pentobarbital on rat brain lipid rafts, which were isolated 15 min after injecting rats with sodium pentobarbital at 50 mg/kg intraperitoneally (38). DSC analysis revealed that pentobarbital reduces the transition temperature from L_o to L_d phase.

Membranous sodium channel blocker local anesthetics

Local anesthetics reversibly block voltage-gated sodium (Nav) channels that are responsible for the initiation and propagation of action potentials in excitable cells, inhibiting sensory and motor functions (39). Among nine distinct Nav channels (Nav1.1 to Nav1.9) cloned from mammals, Nav1.8 channel plays a crucial role in pain transmission and this isoform is implicated as a site of action for anesthetic and analgesic drugs. While Nav channels are present in caveolae-type and non-caveolae-type lipid rafts, Nav1.8 channel clustering in such membrane domains is essential to the propagation of action potentials in nociceptive axons (40,41). Nav1.8 channels are associated with lipid rafts in rat dorsal root ganglionic neurons, but cholesterol depletion induces dissociation between Nav1.8 channels and lipid rafts (42). Results of the literature search on the interaction of local anesthetics with membrane lipid rafts and membranes are shown in Table II.

Kamata et al incubated human erythrocytes with lidocaine at 18.4 mM and prepared erythrocyte ghosts, followed by SDGC fractionation and immunoblotting analysis for flotillin-1 (caveolae-associated integral membrane protein) that is assumed to stabilize lipid rafts (43). Lidocaine reversibly disrupted erythrocyte membrane lipid rafts and abolished flotillin-1 in lipid rafts together with depleting cholesterol. Bandeiras et al treated LUVs prepared with POPC, SM and cholesterol (1:1:1 molar ratio) with tetracaine and lidocaine, and then evaluated their membrane effects by DSC and phosphorus NMR spectroscopy (44). Tetracaine and lidocaine increased the fluidity of raft-like membranes at 25 and 69 mM,

TABLE II - Interaction of membranous sodium channel blocker local anesthetics with lipid raft membrane domains and membranes

Drug class	Drug	Membrane	Induced membrane modification	Reference
Local anesthetic	Lidocaine (18.4 mM)	Human erythrocyte membranes	Disrupted membrane rafts reversely and abolished flotillin-1 in lipid rafts	43
Local anesthetic	Tetracaine (25 mM) Lidocaine (69 mM)	LUVs (POPC, SM and cholesterol, 1:1:1 molar ratio)	Increased the fluidity of raft-like membranes	44
Local anesthetic	Dibucaine (0.05 and 0.2 mM)	Raft-like membranes (POPC, DPPC and cholesterol, 2:1:1 molar ratio)	Reduced the miscibility temperature of L_o and L_d phase separation	45
Local anesthetic	Lidocaine (10-20 mol%) Tetracaine (10-20 mol%)	Raft-like membranes (POPC, DPPC and cholesterol, 2:2:1 molar ratio)	Reduced the miscibility temperature of L_o and L_d phase separation and decreased the line tension at L_o/L_d phase boundary	46
Local anesthetic	Dibucaine (0.2 mM) Tetracaine (0.2 mM)	LUVs (POPC, SM and cholesterol, 16:43:41 molar ratio)	Increased the fluidity of L_o phase membranes, but not L_d phase membranes	47
Local anesthetic	Lidocaine (50-200 μM) Bupivacaine (50-200 μM) Ropivacaine (50-200 μM) Prilocaine (50-200 μM)	SUVs (DOPC, POPE, SM, CB and cholesterol, 16.7:16.7:16.7:16.7:33.3; DOPC, SM and cholesterol, 33.3:33.3:33.3; and DOPC, POPE, POPS, SM and cholesterol, 5:5:10:40:40 molar ratio)	Increased the membrane fluidity with the relative potency being bupivacaine > ropivacaine > lidocaine > prilocaine More effective in interacting with the reference biomimetic membranes than the raft model membranes	49
Local anesthetic	Bupivacaine enantiomers (5-50 μM)	SUVs (POPC, POPE, POPS, POPI, SM, cardiolipin and cholesterol, 25:16:3:3:3:10:40 molar ratio)	Increased the fluidity of biomimetic membranes with the relative potency being *R*(+)-bupivacaine > racemic bupivacaine > *S*(–)-bupivacaine	50

CB = cerebroside; DOPC = 1,2-dioleoylphosphatidylcholine; DPPC = 1,2-dipalmitoylphosphatidylcholine; LUV = large unilamellar vesicle; POPC = 1-palmitoyl-2-oleoylphosphatidylcholine; POPE = 1-palmitoyl-2-oleoylphosphatidylethanolamine; POPI = 1-palmitoyl-2-oleoylphosphatidylinositol; POPS = 1-palmitoyl-2-oleoylphosphatidylserine; SM = sphingomyelin; SUV = small unilamellar vesicle.

respectively. Yoshida et al prepared lipid bilayer membranes with DOPC, DPPC and cholesterol (2:1:1 molar ratio) to be laterally separated into L_o and L_d phase together with labeling the membranes with fluorescent probe rhodamine DHPE (dihexadecanoyl-*sn*-glycero-3-phosphoethanolamine) (45). After treating the membrane preparations with dibucaine at 0.05 and 0.2 mM, they observed the raft-like membrane domains by fluorescence microscopy at 20-40°C to determine changes in miscibility temperature of the L_o and L_d phase separation and in line tension at the L_o/L_d phase boundary. Dibucaine reduced the miscibility temperature, which was accompanied by the line tension decrease. Dibucaine also made the L_o domains smaller at 25°C, although most membranes were present without such raft-like domains at above 25°C. In a similar microscopic experiment using liposomes prepared with DOPC, DPPC and cholesterol (2:2:1 molar ratio), lidocaine and tetracaine reduced the miscibility temperature of ternary membranes at 10-20 mol% relative to liposomal lipids, but not binary membranes without cholesterol (46). Both local anesthetics also decreased the line tension at the L_o/L_d phase boundary. Kinoshita et al performed FA experiments to reveal the effects of local anesthetics on raft-like L_o/non-raft L_d phase membranes by using LUVs that were prepared with DOPC, SM and cholesterol (16:43:41 and 65:16:19 in molar ratio for L_o phase and L_d phase, respectively) (47). Dibucaine disordered the lipid packing or increased the fluidity of L_o phase membranes at 0.2 mM more potently than tetracaine, whereas dibucaine and tetracaine showed no significant effects on L_d phase membranes. However, these studies (43-47) used drug concentrations much higher than clinically and experimentally relevant ones (48) and the tested dibucaine and tetracaine are not widely used in clinical anesthesia.

Tsuchiya et al prepared small unilamellar vesicles (SUVs) with DOPC, POPE, SM, cerebroside (CB) and cholesterol (16.7:16.7:16.7:16.7:33.3 molar ratio); DOPC, SM and cholesterol (33.3:33.3:33.3 molar ratio); and DOPC, POPE, POPS, SM and cholesterol (5:5:10:40:40 molar ratio) for raft model membranes, and POPC, POPE, POPS, 1-palmitoyl-2-oleoylphosphatidylinositol (POPI), SM, cardiolipin and cholesterol (25:16:3:3:3:10:40 molar ratio) for reference biomimetic membranes (49,50). They treated these membrane preparations with lidocaine, bupivacaine, ropivacaine and prilocaine at anesthetic and cardiotoxic concentrations, followed by FP measurements. All the tested anesthetics interacted with raft model and biomimetic membranes to increase the membrane fluidity at 50-200 μM with the relative potency being bupivacaine > ropivacaine > lidocaine > prilocaine (49). They were more effective in interacting with the reference membranes than the raft membranes. Biomimetic membranes showed different interactivity with the relative potency being *R*(+)-bupivacaine > racemic bupivacaine > *S*(–)-bupivacaine at 5-50 μM, being consistent with the rank order of their anesthetic and cardiotoxic effects (50). However, raft model membranes did not exhibit significant enantioselectivity as the reference biomimetic membranes. These results may suggest that lipid rafts are less likely to contribute at least to the enantioselective effects of local anesthetics.

Membranous receptor- and enzyme-acting drugs

Results of the literature search on the interaction of receptor-acting adrenergic and opioid drugs and enzyme-acting anti-inflammatory drugs with membrane lipid rafts and membranes are shown in Table III.

Beta-adrenergic blockers

Beta-blockers are perioperatively used to reduce the risk of myocardial ischemia, arrhythmia and cardiac morbidity during anesthesia. Lipid raft/caveola domains encompass β_2-adrenergic receptors, but not β_1-adrenergic receptors for signal transduction (12,51). Mizogami et al prepared SUVs with POPC, SM, POPE, CB and cholesterol (1:1:1:1:2 molar ratio) to compare the membrane effects between different β-blockers at 0.2 and 1 mM by measuring FP (52). Nonselective propranolol most potently increased the fluidity of raft model membranes, followed by alprenolol and oxprenolol, but not β_1-selective atenolol, metoprolol and esmolol. In a similar FP study using SUVs prepared with 33.3 mol% cholesterol and 66.7 mol% phospholipids consisting of equimolar DOPC, SM, POPE and CB, nonselective propranolol and alprenolol increased the fluidity of raft model membranes at 20-200 μM, whereas β_1-selective landiolol and esmolol were not effective even at 200 μM (53). Nonselective β-blockers could reduce the activity of β_2-adrenergic receptors by fluidizing the membrane lipid rafts together with antagonizing β_1-adrenergic receptors by interacting with β_1-adrenergic receptor proteins, producing nonselective blockade of β-adrenergic receptors. In contrast, selective β_1-blockers do not affect β_2-adrenergic receptors through interaction with lipid rafts, thereby enhancing the selectivity for β_1-adrenergic receptors.

Beta-blockers, particularly β_1-selective agents, have been used for treating hypertension (54). Although the altered vascular signaling processes are implicated in hypertension, whether lipid rafts/caveolae are responsible for such pathogenic events remains unclear (55), so no significant interaction between antihypertensive drugs and lipid rafts was found in the literature.

Alpha-adrenergic agonists

Alpha$_2$-agonists with the sedative, analgesic, anesthetic-sparing and sympatholytic activity are used as an adjuvant for anesthesia. Mizogami and Tsuchiya performed FP experiments to investigate their effects on SUVs that were prepared with 33.3 mol% cholesterol and 66.7 mol% phospholipids (consisting of equimolar DOPC, SM, POPE and CB) to be raft model membranes and with cholesterol and phospholipids of different compositions to be neuro-mimetic and cardiomyocyte-mimetic membranes (56). Dexmedetomidine interacted with the non-raft membranes to increase their fluidity most potently at 5-200 μM, followed by levomedetomidine and clonidine. However, these α_2-agonists exerted much weaker effects on the raft model membranes so that dexmedetomidine and levomedetomidine did not show large difference in membrane interactivity despite being significantly different in sedative activity between medetomidine enantiomers.

TABLE III - Interaction of membranous receptor- and enzyme-acting drugs with lipid raft membrane domains and membranes

Drug class	Drug	Membrane	Induced membrane modification	Reference
Adrenergic receptor-acting drug	Nonselective β-blockers (0.2 and 1 mM) Selective β_1-blockers (0.2 and 1 mM)	SUVs (POPC, SM, POPE, CB and cholesterol, 1:1:1:1:2 molar ratio)	Nonselective propranolol most potently increased the membrane fluidity, followed by alprenolol and oxprenolol, but not β_1-selective atenolol, metoprolol and esmolol	52
Adrenergic receptor-acting drug	Nonselective β-blockers (20-200 μM) Selective β_1-blockers (20-200 μM)	SUVs (33.3 mol% cholesterol and 66.7 mol% phospholipids of equimolar DOPC, SM, POPE and CB)	Nonselective propranolol and alprenolol increased the membrane fluidity, but not β_1-selective landiolol and esmolol	53
Adrenergic receptor-acting drug	Alpha$_2$-agonists (5-200 μM)	SUVs (33.3 mol% cholesterol and 66.7 mol% phospholipids (DOPC, SM, POPE and CB))	Dexmedetomidine increased the fluidity of non-raft membranes most potently, followed by levomedetomidine and clonidine, although the effects on raft model membranes were much weaker without showing large difference between medetomidine enantiomers	56
Opioid receptor-acting drug	Rats injected with morphine (25 mg/kg, i.p.)	Hippocampus and caudate membranes	Increased the membrane fluidity	59
	Rats injected with naloxone (2 mg/kg, i.p.)	Hippocampus and caudate membranes	Decreased the membrane fluidity	
	Morphine (10 nM and 10 μM)	Rat brain membrane preparations	Increased the membrane fluidity	
	Naloxone (1 nM)	Rat brain membrane preparations	Reversed the membrane-fluidizing effects of 10 nM morphine	
Opioid receptor-acting drug	Codeine (0.1 M) ***N***-Methylcodeine (0.1 M)	DPPC MLVs	Reduced the phase transition temperature	60
Opioid receptor-acting drug	Etorphine (10 nM)	Human embryonic kidney cells expressing μ-receptors	Translated μ-receptors from lipid rafts to non-raft regions	61
	Mice injected with etorphine (5 μg/kg, s.c.)	Hippocampi isolated after drug injection		
Cyclooxygenase-acting anti-inflammatory drug	Aspirin (3 mM)	DPPC bilayer membranes containing 32.5 mol% cholesterol	Increased the membrane fluidity Disrupted the membrane organization and prevented raft formation	63
Cyclooxygenase-acting anti-inflammatory drug	Aspirin (10 mol%)	MLVs (70 mol% DMPC and 30 mol% cholesterol)	Bound to raft-like L_o phase domains and disturbed their organization	64
Cyclooxygenase-acting anti-inflammatory drug	Indomethacin (5 μM) Naproxen (25 μM) Aspirin (50 μM) Ibuprofen (150 μM)	Baby hamster kidney cells	Affected the organization of raft-like ordered lipid and protein membrane nanoclusters	65

CB = cerebroside; DMPC = 1,2-dimyristoylphosphatidylcholine; DOPC = 1,2-dioleoylphosphatidylcholine; DPPC = 1,2-dipalmitoylphosphatidylcholine; MLV = multilamellar vesicle; POPC = 1-palmitoyl-2-oleoylphosphatidylcholine; POPE = 1-palmitoyl-2-oleoylphosphatidylethanolamine; SM = sphingomyelin; SUV = small unilamellar vesicle.

The mechanistic relevance of lipid rafts to the enantioselective effects of α_2-agonists is inconclusive as Morris et al reported that α_1-adrenergic receptors, but not α_2-adrenergic receptors, occupy membrane lipid rafts (57).

Opioid analgesics

Morphine and its related drugs act on inhibitory opioid receptors of μ, κ and δ subtypes expressed in nociceptive neuronal circuits. Mu-receptors responsible for the effects of opioid analgesics and antagonists are located within lipid raft/caveola membrane domains (58).

Heron et al performed in vivo experiments to inject rats with opioids intraperitoneally and in vitro experiments to subject membranes prepared from rat brains to the reaction with opioids, followed by FP measurements (59). Morphine increased the fluidity of hippocampus and caudate membranes from rats injected at 25 mg/kg (i.p.) and the fluidity of the membrane preparations at 10 nM and 10 μM**.** In contrast, opioid antagonist naloxone decreased the membrane fluidity of the same brain regions at 2 mg/kg (i.p.) and reversed the in vitro membrane-fluidizing effect of 10 nM morphine at 1 nM. Budai et al evaluated the effects of different opioids on DPPC multilamellar vesicles (MLVs) by DSC and electron paramagnetic resonance (EPR) spectroscopy (60). Codeine and *N*-methylcodeine reduced the phase transition temperature of DPPC membranes at 0.1 M. Zheng et al treated HEK (human embryonic kidney) 293 cells expressing μ-receptors with or subcutaneously injected mice with opioid agonists (61). SDGC cell fractions and hippocampus isolates demonstrated that etorphine of 10 nM and 5 μg/kg (s.c.) translocate μ-receptors from lipid rafts to non-raft regions as well as cholesterol-depleting MBC.

Anti-inflammatory drugs

Non-steroidal anti-inflammatory drugs are considered to exert therapeutic and adverse effects by inhibiting cyclooxygenase (COX)-2 and COX-1, respectively. COX-2 is localized in lipid raft/caveola membrane domains and associated with caveolin-1 (62).

Alsop et al studied the effects of aspirin on different DPPC/cholesterol bilayer membrane systems by Langmuir-Blodgett, DSC and ND experiments (63). Aspirin (3 mM) increased the membrane fluidity of DPPC membranes containing 32.5 mol% cholesterol, disrupted the membrane organization and prevented the formation of L_o phase lipid rafts. In the following neutron scattering experiments and molecular dynamics simulations, they prepared MLVs with 70 mol% 1,2-dimyristoylphosphatidylcholine (DMPC) and 30 mol% cholesterol to study the membrane effect of aspirin (64). Aspirin bound to raft-like L_o phase domains and disrupted their organization at 10 mol%. Zhou et al reported that 5 μM indomethacin, 25 μM naproxen, 50 μM aspirin and 150 μM ibuprofen acted on BHK (baby hamster kidney) cells to affect the organization of raft-like ordered lipid and protein membrane nanoclusters by interacting with plasma membranes (65).

Anticancer drugs

In addition to conventional mechanistic effects, anticancer drugs exhibit apoptosis-inducing activity. Lipid rafts contribute to induction of the apoptosis selective for cancer cells (66). Alkylphospholipids, platinum(II) complex and antibiotics are presumed to act on lipid rafts as a membrane gateway to induce apoptosis (67). Alves et al recently published an excellent review on the biophysics of cancer cells and the relevance of drug and membrane interaction to cancer therapy (68). Results of the literature search on the interaction of anticancer drugs with membrane lipid rafts and membranes are shown in Table IV.

Alkylphospholipids

Ausili et al treated MLVs prepared with POPC, SM and cholesterol (1:1:1 molar ratio) with edelfosine at 10-20 mol% relative to membrane lipids, followed by DSC, XD and NMR analysis (69). Edelfosine altered the raft organization and induced the appearance of a sharp phase transition at 20 mol%, suggesting a fluidity increase in membrane lipid rafts. When incubating with human acute T-cell leukemia (Jurkat T) cells, edelfosine colocalized in lipid rafts at concentrations higher than 20 mol%. 10-(Octyloxy) decyl-2-(trimethylammonium) ethyl phosphate (ODPC) with the cytotoxic activity against cancer cell lines inhibits the proliferation of leukemia cells by inducing apoptosis. Gomide et al prepared giant unilamellar vesicles (GUVs) with DOPC, SM and cholesterol (1:1:1 molar ratio) to examine the effects of perifosine and ODPC on lipid rafts (70). In fluorescence microscopic observations, perifosine and ODPC disrupted membrane raft domains in GUVs so that the domains disappeared in less than 1 min after treatment at 100 μM. Castro et al treated MLVs or unilamellar vesicles (ULVs) prepared with POPC, *N*-palmitoyl-SM and cholesterol (1:1:1 molar ratio) with anticancer alkylphospholipids, followed by FA measurements (71). Edelfosine and miltefosine were demonstrated to increase the fluidity of raft model membranes at 5-10 mol% relative to membrane lipids. Wnętrzak et al studied the effects of synthetic phospholipid analog erucylphosphocholine on raft-mimic Langmuir monolayers composed of SM and cholesterol (2:1 molar ratio) (72). Erucylphosphocholine increased the membrane raft fluidity at higher than 0.3 mol% relative to membrane lipids and weakened the interaction between cholesterol and SM. In a thermodynamic study using the same Langmuir monolayers, anticancer 2-hydroxyoleic acid increased the membrane fluidity of raft-mimic monolayers at higher than 0.1 mol% relative to membrane lipids (73).

Cisplatin

Cisplatin acts on plasma membranes to trigger the Fas death receptor pathway at a membrane level (74). Lacour et al treated human colon carcinoma (HT29) cells (7×10^5 cells) with cisplatin at 5 μg/mL for 0.25-4 hours (75). The cells were subjected to 12-DSA (12-doxylstearic acid) spin labeling followed by EPR spectroscopic analysis or cell lysis with Triton X-100 followed by SDGC fractionation and immunoblot

TABLE IV - Interaction of anticancer drugs with lipid raft membrane domains and membranes

Drug class	Drug	Membrane	Induced membrane modification	Reference
Alkylphospholipid	Edelfosine (≥20 mol%)	MLVs (POPC, SM and cholesterol, 1:1:1, molar ratio)	Increased the fluidity of lipid rafts	69
		Human acute T-cell leukemia cells	Colocalized in membrane lipid rafts	
Alkylphospholipid	Perifosine (100 μM) ODPC (100 μM)	GUVs (DOPC, SM and cholesterol, 1:1:1 molar ratio)	Disrupted membrane raft domains	70
Alkylphospholipid	Edelfosine (5-10 mol%) Miltefosine (5-10 mol%)	MLVs or ULVs (POPC, ***N***-palmitoyl-SM and cholesterol, 1:1:1 molar ratio)	Increased the fluidity of raft model membranes	71
Alkylphospholipid	Erucylphosphocholine (≥0.3 mol%)	Raft-mimic Langmuir monolayers (SM and cholesterol, 2:1 molar ratio)	Increased the membrane raft fluidity and weakened the interaction between cholesterol and SM	72
Alkylphospholipid	2-Hydroxyoleic acid (≥0.1 mol%)	Raft-mimic Langmuir monolayers (SM and cholesterol, 2:1 molar ratio)	Increased the membrane raft fluidity	73
Platinum(II) complex	Cisplatin (5 μg/mL)	Human colon carcinoma cells	Increased the membrane fluidity, which was inhibited by 10 μg/mL nystatin pretreatment Translocated CD95 into lipid rafts, which was prevented by 10 μg/mL nystatin pretreatment	75
Platinum(II) complex	Cisplatin (25 μM)	Human colon carcinoma cells	Increased the membrane raft fluidity and induced apoptosis, which was inhibited by cholesterol (30 μg/mL) and monosialoganglioside-1 (80 μM)	76
Antibiotic	Azithromycin (132 μM)	SUVs (DOPC, SM and cholesterol, 1:1:1 molar ratio)	Increased the fluidity of raft-like membranes	77
Antibiotic	Daunorubicin (40-75 μM)	LUVs (DMPC, SM and cholesterol, 7:1.5:1.5 molar ratio)	Decreased the fluidity of raft-like membranes	78
Antibiotic	Doxorubicin (40-75 μM)	LUVs (DMPC and SM, 8:2 molar ratio or DMPC, SM and cholesterol, 7:1.5:1.5 molar ratio)	Increased the fluidity of binary membranes, but not ternary membranes	79

DMPC = 1,2-dimyristoylphosphatidylcholine; DOPC = 1,2-dioleoylphosphatidylcholine; GUV = giant unilamellar vesicle; LUV = large unilamellar vesicle; MLV = multilamellar vesicle; ODPC = 10-(octyloxy) decyl-2-(trimethylammonium) ethyl phosphate; POPC = 1-palmitoyl-2-oleoylphosphatidylcholine; SM = sphingomyelin; SUV = small unilamellar vesicle; ULV = unilamellar vesicle.

analysis. Cisplatin increased the fluidity of plasma membranes as soon as 0.25 hours after the treatment, although its membrane effect was inhibited by pretreating with cholesterol sequestering nystatin at 10 μg/mL. The cell exposure to cisplatin for 4 hours induced the translocation of CD95 (cluster of differentiation 95 known as Fas receptor) into lipid rafts, which was prevented by nystatin pretreated at 10 μg/mL. Rebillard et al treated human colon carcinoma (HT29) cells growing in the exponential phase with cisplatin at 25 μM for 1-72 hours (76). They isolated lipid rafts by SDGC and performed EPR spectroscopic analysis after 12-DSA spin labeling. Cisplatin treatment for 1 hour increased membrane raft fluidity and that for 72 hours induced apoptosis. Such effects were inhibited by membrane-stabilizing cholesterol (30 μg/mL) and monosialoganglioside-1 (80 μM).

Anticancer antibiotics

Berquand et al treated SUVs prepared with DOPC, SM and cholesterol (1:1:1 molar ratio) with macrolide antibiotic azithromycin (77). FP analysis revealed that azithromycin increases the fluidity of a hydrophobic region of raft-like membranes at 132 μM. In FA experiments of Alves et al (78), anthracycline antibiotic daunorubicin (40-75 μM) decreased the fluidity of raft-like membranes of LUVs prepared with DMPC, SM and cholesterol (7:1.5:1.5 molar ratio), while this antibiotic was more effective in decreasing the membrane fluidity of LUVs prepared without cholesterol. Alves et al also investigated the effects of doxorubicin on LUVs prepared with DMPC and SM (8:2 molar ratio) or with DMPC, SM and cholesterol (7:1.5:1.5 molar ratio) by measuring FA (79). Doxorubicin increased the fluidity of binary membranes at 40-75 μM, but not raft-like ternary membranes containing cholesterol.

Phytochemicals

A variety of phytochemicals (bioactive components in plants) such as flavonoids exhibit a broad spectrum of pharmacological activity including antioxidant, antitumor,

anti-inflammatory, analgesic, antimicrobial, cardioprotective, anti-allergic and antiplatelet ones. Many of them with the amphiphilic structure share the property to interact with artificial and biological membranes. The membrane interactivity of phytochemicals was recently reviewed by Tsuchiya (80), especially the interaction of flavonoids with lipid rafts by Tarahovsky et al (81) and their induced changes in membrane fluidity by Selvaraj et al (82). Results of the literature search on the interaction of phytochemicals with membrane lipid rafts and membranes are shown in Table V.

TABLE V - Interaction of phytochemicals with lipid raft membrane domains and membranes

Drug class	Drug	Membrane	Induced membrane modification	Reference
Flavonoid	Quercetin (10 μM) EGCG (10 μM) Cyanidin (10 μM)	SUVs (phospholipids (POPC and SM) and cholesterol by varying the composition 55-80 mol% and 20-45 mol%)	Quercetin decreased the membrane fluidity most potently, followed by cyanidin and EGCG	84
Flavonoid	Quercetin (30 μM)	Human colon cancer cells (HT-29, SW-620 and Caco-2)	Enhanced TRAIL efficacy to induce apoptosis by accumulating death receptors in membrane lipid rafts	85
Flavonoid	Quercetin (10 and 100 μM) Luteolin (10 and 100 μM)	Mouse macrophages	Suppressed the accumulation of lipid rafts to inhibit TNF-α production	86
Flavonoid	Quercetin (2-16 μM)	SUVs (DMPC plus 20 or 33 mol% cholesterol)	Increased the fluidity of raft model membranes	87
Flavonoid	EGCG (5-100 μM)	SUVs (5 mol% cholesterol and 95 mol% POPC or DOPC)	Decreased the fluidity of binary membranes	88
Flavonoid	EGCG (5-20 μg/mL)	Human colon carcinoma cells	Reduced the membrane resistance to Triton X-100 by decreasing ordered membrane domains	89
Flavonoid	EGCG (5 μM)	Human prostate cancer cells	Inhibited $DiIC_{16}$ accumulation in lipid ordered domains and disrupted lipid rafts	90
Flavonoid	EGCG (5-20 μM)	Human multiple myeloma cells	Induced lipid raft clustering and apoptotic cell death	91
Flavonoid	Dimeric procyanidin (0.05-1 μg/mL)	Human acute T-cell leukemia cells	Increased the membrane fluidity	92
Flavonoid	Hexameric procyanidin (10 μM)	Human colon cancer cells	Decreased the membrane fluidity, although the membrane interactivity was lost by MBC (2.5 mM) Prevented the lipid raft disruption induced by MBC or deoxycholate	93
Stilbenoid	Resveratrol (10-80 μM)	LUVs (egg phosphatidylcholine, SM and cholesterol, 1:1:1 molar ratio)	Formed the ordered membrane domains and enhanced the membrane resistance to Triton X-100	94
Anthraquinonoid	Emodin (1-5 mol%) Aloin (1-5 mol%)	MLVs composed of DMPC	Reduced the phase transition temperature	95
Anthraquinonoid	Emodin (10-50 μg/mL)	Human umbilical vein endothelial cells	Disrupted lipid rafts	96
Terpenoid	Ginsenosides Rb2, Rc, Rd, Re, Rf, Rg1, Rg2 and Rh2 (50 μM)	HeLa cells	Increased the membrane fluidity Reduced the raft-marker protein concentration in lipid rafts	98
Terpenoid	Saikosaponin A (3-12 μM)	Mouse macrophages	Inhibited LPS-induced cytokine expression and Toll-like receptor localization in lipid rafts, and reduced membrane cholesterol levels	99

DMPC = 1,2-dimyristoylphosphatidylcholine; DOPC = 1,2-dioleoylphosphatidylcholine; EGCG = (–)-epigallocatechin-3-gallate; LPS = lipopolysaccharide; LUV = large unilamellar vesicle; MBC = methyl-β-cyclodextrin; MLV = multilamellar vesicle; POPC = 1-palmitoyl-2-oleoylphosphatidylcholine; SM = sphingomyelin; SUV = small unilamellar vesicle; TNF = tumor necrosis factor; TRAIL = TNF-related apoptosis-inducing ligand.

Flavonoids

Considering the distribution and accumulation in lipid bilayers, representative flavonoid quercetin and (–)-epigallocatechin-3-gallate (EGCG) possibly alter membrane fluidity and order, making or breaking raft-like domains (83). Tsuchiya and Mizogami compared the effects of different flavonoids on SUVs that were prepared with phospholipids (POPC and SM) and cholesterol by varying their compositions 55-80 mol% and 20-45 mol%, respectively (84). FP data indicated that quercetin interacts preferentially with the hydrophobic region of membranes to decrease the fluidity at 10 μM most potently, followed by cyanidin and EGCG. Psahoulia et al investigated the mechanism underlying an apoptosis-enhancing effect of quercetin by treating human colon cancer cells (HT-29, SW-620 and Caco-2) with quercetin at 30 μM (85). While tumor necrosis factor (TNF)-related apoptosis-inducing ligand (TRAIL) contributes to apoptosis induction, quercetin enhanced the TRAIL efficacy to induce apoptosis by accumulating death receptors in membrane lipid rafts. In a cell culture study of Kaneko et al, quercetin and luteolin suppressed the accumulation of lipid rafts at 10 and 100 μM to inhibit TNF-α production in mouse macrophages (86). They also suggested that these flavonoids change membrane fluidity. Ionescu et al prepared SUVs with DMPC plus 20 or 33 mol% cholesterol to form the L_o phase and examine the membrane effect of quercetin (87). FP measurements showed that quercetin increases the fluidity of raft model membranes at 2-16 μM.

Tsuchiya treated SUVs consisting of 5 mol% cholesterol and 95 mol% POPC or DOPC with several catechins, followed by FP measurements (88). Of the tested catechins, EGCG most potently interacted with binary membranes to decrease their fluidity at 5-100 μM. Adachi et al stained human colon carcinoma (HT29) cells with fluorescent $DiIC_{16}$ (1,1'-dihexadecyl-3,3,3',3'-tetramethylindocarbocyanine perchlorate) that is preferentially incorporated into the ordered membranes, and then treated the cells with EGCG at 5-20 μg/mL to analyze its membrane effects by fluorescent confocal microscopy (89). EGCG reduced the membrane resistance to Triton X-100 at as little as 5 μg/mL, possibly by decreasing the content of ordered membrane domains. Duhon et al exposed human prostate cancer (DU145) cells to $DiIC_{16}$ in the presence or absence of 5 μM EGCG, followed by fluorescence microscopic analysis (90). EGCG inhibited the accumulation of $DiIC_{16}$ in lipid-ordered domains and disrupted lipid rafts. Tsukamoto et al treated human multiple myeloma (U266) cells with EGCG at 5-20 μM for 3 hours and at 10 μM for 1-3 hours (91). Fluorescence resonance energy transfer and fluorescence microscopic assays indicated that EGCG dose- and time-dependently induces lipid raft clustering and apoptotic cell death.

Procyanidins contained in fruits and vegetables are oligomeric flavonoids with the anticancer activity. Verstraeten et al treated human acute T-cell leukemia (Jurkat T) cells (6×10^4 cells) with cocoa procyanidins and measured FP (92). Dimeric procyanidin increased the fluidity of plasma membranes in a concentration-dependent manner at 0.05-1 μg/mL. In the following experiment, they incubated human colon cancer (Caco-2) cells with 10 μM hexameric procyanidin in the absence or presence of 2.5 mM MBC (93). In contrast to dimeric procyanidin, hexameric procyanidin decreased the fluidity of plasma membranes, although its membrane interactivity was lost by cholesterol-depleting MBC. This procyanidin also prevented lipid raft disruption induced by MBC or deoxycholate (cholesterol depletion/redistribution).

Stilbenoids

Resveratrol present in grape skins and seeds has anticancer, antioxidant and cardioprotective property. Neves et al treated LUVs prepared with egg phosphatidylcholine, SM and cholesterol (1:1:1 molar ratio) with 10-80 μM resveratrol to investigate the effects on raft model membranes by three different methods (94). Resveratrol induced the phase separation and formed the ordered membrane domains at concentrations higher than 10 μM. Such effects were more pronounced in the presence of cholesterol and SM. Resveratrol was also effective at 80 μM in enhancing the membrane resistance to Triton X-100.

Anthraquinonoids

Pharmacological effects of aloe are attributed to anthraquinonoid component emodin and aloin (barbaloin). DSC experiments of Alves et al demonstrated that emodin interacts with MLVs composed of DMPC to reduce the phase transition temperature at 1-5 mol% more potently than aloin (95). Meng et al investigated the mechanism underlying a vascular anti-inflammatory effect of aloe by treating human umbilical vein endothelial cells grown to approximately 90% confluence with emodin (96). Emodin (10-50 μg/mL) inhibited the expression of proinflammatory cytokines and chemokines induced by 0.1 μg/mL lipopolysaccharide (LPS). Similar to cholesterol-depleting MBC (5-12.5 mM), emodin (10-50 μg/mL) disrupted lipid rafts that are relevant to the cell activation by LPS. Lipid raft disruption associated with integrin signaling pathway is also responsible for the inhibitory effects of emodin on tumor cell adhesion and spreading (97).

Terpenoids

Triterpenoid glycosides from *Panax ginseng* and triterpenoid saponin derivatives from *Radix bupleuri* have anti-inflammatory and anticancer activity. Yi et al treated HeLa cells with different ginsenosides at 50 μM and stained the cells with carboxy Laurdan, followed by fluorescence microscopy and generalized polarization imaging (98). Ginsenosides Rb2, Rc, Rd, Re, Rf, Rg1, Rg2 and Rh2 increased the fluidity of plasma membranes as well as cholesterol-depleting MBC (10 mM). When fractionating the HeLa cells by SDGC, ginsenoside Rh2 and MBC reduced the concentration of raft-marker proteins in the raft fraction, indicating that they disrupt lipid rafts. These effects of ginsenoside Rh2 were reversed by cholesterol overloading (20 μg/mL). In a cell culture study of Wei et al (99), 3-12 μM saikosaponin A inhibited the expression of cytokines in primary mouse macrophages stimulated by 0.1 μg/mL LPS. Such inhibitory effects were attenuated by replenishment of 84 μg/mL cholesterol, while 3-12 μM saikosaponin A reduced cholesterol levels in macrophage membranes. Saikosaponin A (3-12 μM) and MBC (10 mM) also inhibited the LPS-induced

localization in lipid rafts of Toll-like receptors that play a crucial role in the innate immune system.

Conclusions

Results of the literature search indicate that different classes of drugs interact with raft model membranes and cellular membrane lipid rafts in addition to interacting directly with membrane receptors, ion channels and enzymes. They could physicochemically modify membrane lipid rafts to be a platform for functional proteins and the membranes surrounding such raft domains, affecting the organizational integrity of lipid rafts with the subsequent alteration of receptor, channel and enzyme activity, thereby producing pharmacological effects. With respect to the induced membrane modification, raft-acting drugs are characterized as ones to decrease membrane fluidity, induce L_o phase or order plasma membranes, leading to lipid raft formation; and ones to increase membrane fluidity, induce L_d phase or reduce phase transition temperature, leading to lipid raft disruption. Targeting lipid raft membrane domains would open a new way for drug design and development.

Given the critical role of lipid rafts/caveolae in cellular signal transduction, odontology may be the promising field to which a raft-targeting concept is applied. Anticancer drugs interact with membrane lipid rafts to affect their physicochemical property and organizational integrity in association with apoptosis induction. Lipid raft membrane domains are responsible for cancer cell adhesion and migration, and the levels of cholesterol-rich lipid rafts are elevated in cancer cells compared with normal counterparts (100,101). While phytochemicals interact with membrane lipid rafts and regulate raft formation (83,85), such interactivity is responsible for their diverse bioactivities including apoptosis induction. Among raft-targeting compounds, alkylphospholipids and flavonoids could be a novel type of anticancer drug.

Since an outbreak of atypical pneumonia was first reported in Wuhan (China) in December 2019, novel coronavirus or severe acute respiratory syndrome coronavirus 2 (SARS-CoV-2) infections have spread worldwide, causing a global pandemic of coronavirus disease 2019 (COVID-19). SARS-CoV-2 spike proteins have a strong binding affinity to human angiotensin-converting enzyme 2 (ACE2) (102). Host cell ACE2 receptors, which are a cell-specific target of and responsible for the cellular entry of SARS-CoV-2, are localized in lipid rafts (103). Cholesterol-rich membrane domains are essential for the spike proteins to interact with ACE2 receptors efficiently (104) and cellular cholesterol levels are closely associated with COVID-19 lethality (105). Agents that specifically disrupt ACE2-localizing lipid rafts and deplete raft cholesterol may be a drug to reduce SARS-CoV-2 infectivity and COVID-19 severity.

Abbreviations

L_o, liquid-ordered; L_d, liquid-disordered; POPC, 1-palmitoyl-2-oleoylphosphatidylcholine; SM, sphingomyelin; SDGC, sucrose density gradient centrifugation; MBC, methyl-β-cyclodextrin; FP, fluorescence polarization; FA, fluorescence anisotropy; DSC, differential scanning calorimetry; NMR, nuclear magnetic resonance; ND, neutron diffraction; XD, X-ray diffraction; $GABA_A$, γ-aminobutyric acid type A; NMDA, *N*-methyl-D-aspartate; POPE, 1-palmitoyl-2-oleoylphosphatidylethanolamine; POPS, 1-palmitoyl-2-oleoylphosphatidylserine; GPMV, giant plasma membrane vesicle; LUV, large unilamellar vesicle; DPPC, 1,2-dipalmitoylphosphatidylcholine; DLPC, 1,2-dilauroylphosphatidylcholine; MAC, minimum alveolar concentration; DOPC, 1,2-dioleoylphosphatidylcholine; Nav, voltage-gated sodium; SUV, small unilamellar vesicle; CB, cerebroside; POPI, 1-palmitoyl-2-oleoylphosphatidylinositol; MLV, multilamellar vesicle; EPR, electron paramagnetic resonance; COX, cyclooxygenase; DMPC, 1,2-dimyristoylphosphatidylcholine; ODPC, 10-(octyloxy) decyl-2-(trimethylammonium) ethyl phosphate; GUV, giant unilamellar vesicle; ULV, unilamellar vesicle; EGCG, (–)-epigallocatechin-3-gallate; TNF, tumor necrosis factor; TRAIL, TNF-related apoptosis-inducing ligand; LPS, lipopolysaccharide; SARS-CoV-2, severe acute respiratory syndrome coronavirus 2; COVID-19, coronavirus disease 2019; ACE2, angiotensin-converting enzyme 2.

Author contributions

HT designed and conducted the present study and prepared the first draft of the manuscript. HT and MM did literature search, information analysis and manuscript preparation. Both authors reviewed and approved the final manuscript.

Disclosures

Conflict of interest: Authors disclose no potential conflicts of interest.

Financial support: This study was supported by JSPS KAKENHI grant number 20K10152 and JSPS KAKENHI grant number 17K11924.

References

1. Kusumi A, Fujiwara TK, Chadda R, et al. Dynamic organizing principles of the plasma membrane that regulate signal transduction: commemorating the fortieth anniversary of Singer and Nicolson's fluid-mosaic model. *Annu Rev Cell Dev Biol*. 2012;28(1):215-250. CrossRef Medline
2. Pike LJ. Rafts defined: a report on the Keystone Symposium on Lipid Rafts and Cell Function. *J Lipid Res*. 2006;47(7):1597-1598. CrossRef Medline
3. Hanzal-Bayer MF, Hancock JF. Lipid rafts and membrane traffic. *FEBS Lett*. 2007;581(11):2098-2104. CrossRef Medline
4. McMullen T, Lewis R, McElhany R. Cholesterol-phospholipid interactions, the liquid-ordered phase and lipid rafts in model and biological membranes. *Curr Opin Colloid Interface Sci*. 2004;8(6):459-468. CrossRef
5. Simons K, Toomre D. Lipid rafts and signal transduction. *Nat Rev Mol Cell Biol*. 2000;1(1):31-39. CrossRef Medline
6. Laude AJ, Prior IA. Plasma membrane microdomains: organization, function and trafficking. *Mol Membr Biol*. 2004;21(3):193-205. CrossRef Medline
7. George KS, Wu S. Lipid raft: A floating island of death or survival. *Toxicol Appl Pharmacol*. 2012;259(3):311-319. CrossRef Medline
8. O'Connell KM, Martens JR, Tamkun MM. Localization of ion channels to lipid Raft domains within the cardiovascular system. *Trends Cardiovasc Med*. 2004;14(2):37-42. CrossRef Medline

9. Maguy A, Hebert TE, Nattel S. Involvement of lipid rafts and caveolae in cardiac ion channel function. *Cardiovasc Res*. 2006;69(4):798-807. CrossRef Medline
10. Dalskov SM, Immerdal L, Niels-Christiansen LL, Hansen GH, Schousboe A, Danielsen EM. Lipid raft localization of $GABA_A$ receptor and Na^+, K^+-ATPase in discrete microdomain clusters in rat cerebellar granule cells. *Neurochem Int*. 2005;46(6):489-499. CrossRef Medline
11. Patel HH, Murray F, Insel PA. G-protein-coupled receptor-signaling components in membrane raft and caveolae microdomains. *Handb Exp Pharmacol*. 2008;186(186):167-184. CrossRef Medline
12. Xiang Y, Rybin VO, Steinberg SF, Kobilka B. Caveolar localization dictates physiologic signaling of β_2-adrenoceptors in neonatal cardiac myocytes. *J Biol Chem*. 2002;277(37):34280-34286. CrossRef Medline
13. Pottosin II, Valencia-Cruz G, Bonales-Alatorre E, Shabala SN, Dobrovinskaya OR. Methyl-β-cyclodextrin reversibly alters the gating of lipid rafts-associated Kv1.3 channels in Jurkat T lymphocytes. *Pflugers Arch*. 2007;454(2):235-244. CrossRef Medline
14. Levitt ES, Clark MJ, Jenkins PM, Martens JR, Traynor JR. Differential effect of membrane cholesterol removal on μ- and δ-opioid receptors: a parallel comparison of acute and chronic signaling to adenylyl cyclase. *J Biol Chem*. 2009;284(33):22108-22122. CrossRef Medline
15. Ding XQ, Fitzgerald JB, Matveev AV, McClellan ME, Elliott MH. Functional activity of photoreceptor cyclic nucleotide-gated channels is dependent on the integrity of cholesterol- and sphingolipid-enriched membrane domains. *Biochemistry*. 2008;47(12):3677-3687. CrossRef Medline
16. Gandhavadi M, Allende D, Vidal A, Simon SA, McIntosh TJ. Structure, composition, and peptide binding properties of detergent soluble bilayers and detergent resistant rafts. *Biophys J*. 2002;82(3):1469-1482. CrossRef Medline
17. Koumanov KS, Tessier C, Momchilova AB, Rainteau D, Wolf C, Quinn PJ. Comparative lipid analysis and structure of detergent-resistant membrane raft fractions isolated from human and ruminant erythrocytes. *Arch Biochem Biophys*. 2005;434(1):150-158. CrossRef Medline
18. Holland GP, McIntyre SK, Alam TM. Distinguishing individual lipid headgroup mobility and phase transitions in raft-forming lipid mixtures with ^{31}P MAS NMR. *Biophys J*. 2006;90(11):4248-4260. CrossRef Medline
19. Simons K, Ehehalt R. Cholesterol, lipid rafts, and disease. *J Clin Invest*. 2002;110(5):597-603. CrossRef Medline
20. Jacobson K, Mouritsen OG, Anderson RG. Lipid rafts: at a crossroad between cell biology and physics. *Nat Cell Biol*. 2007;9(1):7-14. CrossRef Medline
21. Boesze-Battaglia K. Isolation of membrane rafts and signaling complexes. *Methods Mol Biol*. 2006;332:169-179. CrossRef Medline
22. Loftsson T, Magnúsdóttir A, Másson M, Sigurjónsdóttir JF. Self-association and cyclodextrin solubilization of drugs. *J Pharm Sci*. 2002;91(11):2307-2316. CrossRef Medline
23. Mahammad S, Parmryd I. Cholesterol depletion using methyl-β-cyclodextrin. *Methods Mol Biol*. 2015;1232:91-102. CrossRef Medline
24. Chau PL. New insights into the molecular mechanisms of general anaesthetics. *Br J Pharmacol*. 2010;161(2):288-307. CrossRef Medline
25. Olsen RW, Li GD. $GABA_A$ receptors as molecular targets of general anesthetics: identification of binding sites provides clues to allosteric modulation. *Can J Anaesth*. 2011;58(2):206-215. CrossRef Medline
26. Yamakura T, Harris RA. Effects of gaseous anesthetics nitrous oxide and xenon on ligand-gated ion channels. Comparison with isoflurane and ethanol. *Anesthesiology*. 2000;93(4):1095-1101. CrossRef Medline
27. Daniell LC. Effect of anesthetic and convulsant barbiturates on N-methyl-*D*-aspartate receptor-mediated calcium flux in brain membrane vesicles. *Pharmacology*. 1994;49(5):296-307. CrossRef Medline
28. Li X, Serwanski DR, Miralles CP, Bahr BA, De Blas AL. Two pools of Triton X-100-insoluble $GABA_A$ receptors are present in the brain, one associated to lipid rafts and another one to the postsynaptic GABAergic complex. *J Neurochem*. 2007;102(4):1329-1345. CrossRef Medline
29. Parat MO. Could endothelial caveolae be the target of general anaesthetics? *Br J Anaesth*. 2006;96(5):547-550. CrossRef Medline
30. Tsuchiya H. Structure-specific membrane-fluidizing effect of propofol. *Clin Exp Pharmacol Physiol*. 2001;28(4):292-299. CrossRef Medline
31. Tsuchiya H, Ueno T, Tanaka T, Matsuura N, Mizogami M. Comparative study on determination of antioxidant and membrane activities of propofol and its related compounds. *Eur J Pharm Sci*. 2010;39(1-3):97-102. CrossRef Medline
32. Gray E, Karslake J, Machta BB, Veatch SL. Liquid general anesthetics lower critical temperatures in plasma membrane vesicles. *Biophys J*. 2013;105(12):2751-2759. CrossRef Medline
33. Grim KJ, Abcejo AJ, Barnes A, et al. Caveolae and propofol effects on airway smooth muscle. *Br J Anaesth*. 2012;109(3):444-453. CrossRef Medline
34. Patel J, Chowdhury EA, Noorani B, Bickel U, Huang J. Isoflurane increases cell membrane fluidity significantly at clinical concentrations. *Biochim Biophys Acta Biomembr*. 2020;1862(2):183140. CrossRef Medline
35. Turkyilmaz S, Almeida PF, Regen SL. Effects of isoflurane, halothane, and chloroform on the interactions and lateral organization of lipids in the liquid-ordered phase. *Langmuir*. 2011;27(23):14380-14385. CrossRef Medline
36. Weinrich M, Nanda H, Worcester DL, Majkrzak CF, Maranville BB, Bezrukov SM. Halothane changes the domain structure of a binary lipid membrane. *Langmuir*. 2012;28(10):4723-4728. CrossRef Medline
37. Weinrich M, Worcester DL. Xenon and other volatile anesthetics change domain structure in model lipid raft membranes. *J Phys Chem B*. 2013;117(50):16141-16147. CrossRef Medline
38. Sierra-Valdez FJ, Ruiz-Suárez JC, Delint-Ramirez I. Pentobarbital modifies the lipid raft-protein interaction: A first clue about the anesthesia mechanism on NMDA and $GABA_A$ receptors. *Biochim Biophys Acta*. 2016;1858(11):2603-2610. CrossRef Medline
39. Fozzard HA, Lee PJ, Lipkind GM. Mechanism of local anesthetic drug action on voltage-gated sodium channels. *Curr Pharm Des*. 2005;11(21):2671-2686. CrossRef Medline
40. Pristerá A, Okuse K. Building excitable membranes: lipid rafts and multiple controls on trafficking of electrogenic molecules. *Neuroscientist*. 2012;18(1):70-81. CrossRef Medline
41. Bao L. Trafficking regulates the subcellular distribution of voltage-gated sodium channels in primary sensory neurons. *Mol Pain*. 2015;11:61. CrossRef Medline
42. Pristerà A, Baker MD, Okuse K. Association between tetrodotoxin resistant channels and lipid rafts regulates sensory neuron excitability. *PLoS One*. 2012;7(8):e40079. CrossRef Medline
43. Kamata K, Manno S, Ozaki M, Takakuwa Y. Functional evidence for presence of lipid rafts in erythrocyte membranes: Gsα in rafts is essential for signal transduction. *Am J Hematol*. 2008;83(5):371-375. CrossRef Medline
44. Bandeiras C, Serro AP, Luzyanin K, Fernandes A, Saramago B. Anesthetics interacting with lipid rafts. *Eur J Pharm Sci*. 2013;48(1-2):153-165. CrossRef Medline

45. Yoshida K, Takashima A, Nishio I. Effect of dibucaine hydrochloride on raft-like lipid domains in model membrane system. *MedChemComm*. 2015;6(8):1444-1451. CrossRef
46. Sugahara K, Shimokawa N, Takagi M. Thermal stability of phase-separated domains in multicomponent lipid membranes with local anesthetics. *Membranes (Basel)*. 2017;7(3):33. CrossRef Medline
47. Kinoshita M, Chitose T, Matsumori N. Mechanism of local anesthetic-induced disruption of raft-like ordered membrane domains. *Biochim Biophys Acta, Gen Subj*. 2019;1863(9):1381-1389. CrossRef Medline
48. Groban L, Deal DD, Vernon JC, James RL, Butterworth J. Cardiac resuscitation after incremental overdosage with lidocaine, bupivacaine, levobupivacaine, and ropivacaine in anesthetized dogs. *Anesth Analg*. 2001;92(1):37-43. CrossRef Medline
49. Tsuchiya H, Ueno T, Mizogami M, Takakura K. Do local anesthetics interact preferentially with membrane lipid rafts? Comparative interactivities with raft-like membranes. *J Anesth*. 2010;24(4):639-642. CrossRef Medline
50. Tsuchiya H, Mizogami M. R(+)-, Rac-, and S(-)-bupivacaine stereostructure-specifically interact with membrane lipids at cardiotoxically relevant concentrations. *Anesth Analg*. 2012;114(2):310-312. CrossRef Medline
51. Pontier SM, Percherancier Y, Galandrin S, Breit A, Galés C, Bouvier M. Cholesterol-dependent separation of the β_2-adrenergic receptor from its partners determines signaling efficacy: insight into nanoscale organization of signal transduction. *J Biol Chem*. 2008;283(36):24659-24672. CrossRef Medline
52. Mizogami M, Takakura K, Tsuchiya H. The interactivities with lipid membranes differentially characterize selective and non-selective β_1-blockers. *Eur J Anaesthesiol*. 2010;27(9):829-834. CrossRef Medline
53. Tsuchiya H, Mizogami M. Characteristic interactivity of landiolol, an ultra-short-acting highly selective β_1-blocker, with biomimetic membranes: comparisons with β_1-selective esmolol and non-selective propranolol and alprenolol. *Front Pharmacol*. 2013;4:150. CrossRef Medline
54. Prichard BN, Cruickshank JM, Graham BR. Beta-adrenergic blocking drugs in the treatment of hypertension. *Blood Press*. 2001;10(5-6):366-386. CrossRef Medline
55. Callera GE, Montezano AC, Yogi A, Tostes RC, Touyz RM. Vascular signaling through cholesterol-rich domains: implications in hypertension. *Curr Opin Nephrol Hypertens*. 2007;16(2):90-104. CrossRef Medline
56. Mizogami M, Tsuchiya H. Membrane interactivity of anesthetic adjuvant dexmedetomidine discriminable from clonidine and enantiomeric levomedetomidine. *J Adv Med Med Res*. 2019;29:1-15. CrossRef
57. Morris DP, Lei B, Wu YX, Michelotti GA, Schwinn DA. The α_{1a}-adrenergic receptor occupies membrane rafts with its G protein effectors but internalizes via clathrin-coated pits. *J Biol Chem*. 2008;283(5):2973-2985. CrossRef Medline
58. Huang P, Xu W, Yoon SI, et al. Agonist treatment did not affect association of mu opioid receptors with lipid rafts and cholesterol reduction had opposite effects on the receptor-mediated signaling in rat brain and CHO cells. *Brain Res*. 2007;1184:46-56. CrossRef Medline
59. Heron DS, Shinitzky M, Zamir N, Samuel D. Adaptive modulations of brain membrane lipid fluidity in drug addiction and denervation supersensitivity. *Biochem Pharmacol*. 1982;31(14):2435-2438. CrossRef Medline
60. Budai M, Szabó Z, Szogyi M, Gróf P. Molecular interactions between DPPC and morphine derivatives: a DSC and EPR study. *Int J Pharm.* 2003;250:239–250. CrossRef
61. Zheng H, Chu J, Qiu Y, Loh HH, Law PY. Agonist-selective signaling is determined by the receptor location within the membrane domains. *Proc Natl Acad Sci USA*. 2008;105(27):9421-9426. CrossRef Medline
62. Liou JY, Deng WG, Gilroy DW, Shyue SK, Wu KK. Colocalization and interaction of cyclooxygenase-2 with caveolin-1 in human fibroblasts. *J Biol Chem*. 2001;276(37):34975-34982. CrossRef Medline
63. Alsop RJ, Toppozini L, Marquardt D, Kučerka N, Harroun TA, Rheinstädter MC. Aspirin inhibits formation of cholesterol rafts in fluid lipid membranes. *Biochim Biophys Acta*. 2015;1848(3):805-812. CrossRef Medline
64. Alsop RJ, Himbert S, Dhaliwal A, Schmalzl K, Rheinstädter MC. Aspirin locally disrupts the liquid-ordered phase. *R Soc Open Sci*. 2018;5(2):171710. CrossRef Medline
65. Zhou Y, Cho KJ, Plowman SJ, Hancock JF. Nonsteroidal anti-inflammatory drugs alter the spatiotemporal organization of Ras proteins on the plasma membrane. *J Biol Chem*. 2012;287(20):16586-16595. CrossRef Medline
66. Alves ACS, Dias RA, Kagami LP, et al. Beyond the "lock and key" paradigm: targeting lipid rafts to induce the selective apoptosis of cancer cells. *Curr Med Chem*. 2018;25(18):2082-2104. CrossRef Medline
67. van der Luit AH, Vink SR, Klarenbeek JB, et al. A new class of anticancer alkylphospholipids uses lipid rafts as membrane gateways to induce apoptosis in lymphoma cells. *Mol Cancer Ther*. 2007;6(8):2337-2345. CrossRef Medline
68. Alves AC, Ribeiro D, Nunes C, Reis S. Biophysics in cancer: the relevance of drug-membrane interaction studies. *Biochim Biophys Acta*. 2016;1858(9):2231-2244. CrossRef Medline
69. Ausili A, Torrecillas A, Aranda FJ, et al. Edelfosine is incorporated into rafts and alters their organization. *J Phys Chem B*. 2008;112(37):11643-11654. CrossRef Medline
70. Gomide AB, Thomé CH, dos Santos GA, et al. Disrupting membrane raft domains by alkylphospholipids. *Biochim Biophys Acta*. 2013;1828(5):1384-1389. CrossRef Medline
71. Castro BM, Fedorov A, Hornillos V, et al. Edelfosine and miltefosine effects on lipid raft properties: membrane biophysics in cell death by antitumor lipids. *J Phys Chem B*. 2013;117(26):7929-7940. CrossRef Medline
72. Wnętrzak A, Łątka K, Makyła-Juzak K, Zemla J, Dynarowicz-Łątka P. The influence of an antitumor lipid - erucylphosphocholine - on artificial lipid raft system modeled as Langmuir monolayer. *Mol Membr Biol*. 2015;32(5-8):189-197. CrossRef Medline
73. Węder K, Mach M, Hąc-Wydro K, Wydro P. Studies on the interactions of anticancer drug - Minerval - with membrane lipids in binary and ternary Langmuir monolayers. *Biochim Biophys Acta Biomembr*. 2018;1860(11):2329-2336. CrossRef Medline
74. Rebillard A, Lagadic-Gossmann D, Dimanche-Boitrel MT. Cisplatin cytotoxicity: DNA and plasma membrane targets. *Curr Med Chem*. 2008;15(26):2656-2663. CrossRef Medline
75. Lacour S, Hammann A, Grazide S, et al. Cisplatin-induced CD95 redistribution into membrane lipid rafts of HT29 human colon cancer cells. *Cancer Res*. 2004;64(10):3593-3598. CrossRef Medline
76. Rebillard A, Tekpli X, Meurette O, et al. Cisplatin-induced apoptosis involves membrane fluidification via inhibition of NHE1 in human colon cancer cells. *Cancer Res*. 2007;67(16):7865-7874. CrossRef Medline
77. Berquand A, Fa N, Dufrêne YF, Mingeot-Leclercq MP. Interaction of the macrolide antibiotic azithromycin with lipid bilayers: effect on membrane organization, fluidity, and permeability. *Pharm Res*. 2005;22(3):465-475. CrossRef Medline
78. Alves AC, Ribeiro D, Horta M, Lima JLFC, Nunes C, Reis S. A biophysical approach to daunorubicin interaction with model membranes: relevance for the drug's biological activity. *J R Soc Interface*. 2017;14(133):20170408. CrossRef Medline
79. Alves AC, Magarkar A, Horta M, et al. Influence of doxorubicin on model cell membrane properties: insights from *in vitro* and *in silico* studies. *Sci Rep*. 2017;7(1):6343. CrossRef Medline

80. Tsuchiya H. Membrane interactions of phytochemicals as their molecular mechanism applicable to the discovery of drug leads from plants. *Molecules*. 2015;20(10):18923-18966. CrossRef Medline
81. Tarahovsky YS, Kim YA, Yagolnik EA, Muzafarov EN. Flavonoid-membrane interactions: involvement of flavonoid-metal complexes in raft signaling. *Biochim Biophys Acta*. 2014;1838(5):1235-1246. CrossRef Medline
82. Selvaraj S, Krishnaswamy S, Devashya V, Sethuraman S, Krishnan UM. Influence of membrane lipid composition on flavonoid-membrane interactions: implications on their biological activity. *Prog Lipid Res*. 2015;58:1-13. CrossRef Medline
83. Tarahovsky YS, Muzafarov EN, Kim YA. Rafts making and rafts braking: how plant flavonoids may control membrane heterogeneity. *Mol Cell Biochem*. 2008;314(1-2):65-71. CrossRef Medline
84. Tsuchiya H, Mizogami M. Plant components exhibit pharmacological activities and drug interactions by acting on lipid membranes. *Pharmacog Commun.* 2012;2:58–71. Online
85. Psahoulia FH, Drosopoulos KG, Doubravska L, Andera L, Pintzas A. Quercetin enhances TRAIL-mediated apoptosis in colon cancer cells by inducing the accumulation of death receptors in lipid rafts. *Mol Cancer Ther*. 2007;6(9):2591-2599. CrossRef Medline
86. Kaneko M, Takimoto H, Sugiyama T, Seki Y, Kawaguchi K, Kumazawa Y. Suppressive effects of the flavonoids quercetin and luteolin on the accumulation of lipid rafts after signal transduction via receptors. *Immunopharmacol Immunotoxicol*. 2008;30(4):867-882. CrossRef Medline
87. Ionescu D, Margină D, Ilie M, Iftime A, Ganea C. Quercetin and epigallocatechin-3-gallate effect on the anisotropy of model membranes with cholesterol. *Food Chem Toxicol*. 2013;61:94-100. CrossRef Medline
88. Tsuchiya H. Stereospecificity in membrane effects of catechins. *Chem Biol Interact*. 2001;134(1):41-54. CrossRef Medline
89. Adachi S, Nagao T, Ingolfsson HI, et al. The inhibitory effect of (-)-epigallocatechin gallate on activation of the epidermal growth factor receptor is associated with altered lipid order in HT29 colon cancer cells. *Cancer Res*. 2007;67(13):6493-6501. CrossRef Medline
90. Duhon D, Bigelow RL, Coleman DT, et al. The polyphenol epigallocatechin-3-gallate affects lipid rafts to block activation of the c-Met receptor in prostate cancer cells. *Mol Carcinog*. 2010;49(8):739-749. CrossRef Medline
91. Tsukamoto S, Hirotsu K, Kumazoe M, et al. Green tea polyphenol EGCG induces lipid-raft clustering and apoptotic cell death by activating protein kinase Cδ and acid sphingomyelinase through a 67 kDa laminin receptor in multiple myeloma cells. *Biochem J*. 2012;443(2):525-534. CrossRef Medline
92. Verstraeten SV, Oteiza PI, Fraga CG. Membrane effects of cocoa procyanidins in liposomes and Jurkat T cells. *Biol Res*. 2004;37(2):293-300. CrossRef Medline
93. Verstraeten SV, Jaggers GK, Fraga CG, Oteiza PI. Procyanidins can interact with Caco-2 cell membrane lipid rafts: involvement of cholesterol. *Biochim Biophys Acta*. 2013;1828(11):2646-2653. CrossRef Medline
94. Neves AR, Nunes C, Reis S. Resveratrol induces ordered domains formation in biomembranes: implication for its pleiotropic action. *Biochim Biophys Acta*. 2016;1858(1):12-18. CrossRef Medline
95. Alves DS, Pérez-Fons L, Estepa A, Micol V. Membrane-related effects underlying the biological activity of the anthraquinones emodin and barbaloin. *Biochem Pharmacol*. 2004;68(3):549-561. CrossRef Medline
96. Meng G, Liu Y, Lou C, Yang H. Emodin suppresses lipopolysaccharide-induced pro-inflammatory responses and NF-κB activation by disrupting lipid rafts in CD14-negative endothelial cells. *Br J Pharmacol*. 2010;161(7):1628-1644. CrossRef Medline
97. Huang Q, Shen HM, Shui G, Wenk MR, Ong CN. Emodin inhibits tumor cell adhesion through disruption of the membrane lipid raft-associated integrin signaling pathway. *Cancer Res*. 2006;66(11):5807-5815. CrossRef Medline
98. Yi JS, Choo HJ, Cho BR, et al. Ginsenoside Rh2 induces ligand-independent Fas activation via lipid raft disruption. *Biochem Biophys Res Commun*. 2009;385(2):154-159. CrossRef Medline
99. Wei Z, Wang J, Shi M, Liu W, Yang Z, Fu Y. Saikosaponin a inhibits LPS-induced inflammatory response by inducing liver X receptor alpha activation in primary mouse macrophages. *Oncotarget*. 2016;7(31):48995-49007. CrossRef Medline
100. Murai T. The role of lipid rafts in cancer cell adhesion and migration. *Int J Cell Biol*. 2012;2012:763283. CrossRef Medline
101. Li YC, Park MJ, Ye SK, Kim CW, Kim YN. Elevated levels of cholesterol-rich lipid rafts in cancer cells are correlated with apoptosis sensitivity induced by cholesterol-depleting agents. *Am J Pathol*. 2006;168(4):1107-1118. CrossRef Medline
102. Zhang H, Penninger JM, Li Y, Zhong N, Slutsky AS. Angiotensin-converting enzyme 2 (ACE2) as a SARS-CoV-2 receptor: molecular mechanisms and potential therapeutic target. *Intensive Care Med*. 2020;46(4):586-590. CrossRef Medline
103. Lu Y, Liu DX, Tam JP. Lipid rafts are involved in SARS-CoV entry into Vero E6 cells. *Biochem Biophys Res Commun*. 2008;369(2):344-349. CrossRef Medline
104. Glende J, Schwegmann-Wessels C, Al-Falah M, et al. Importance of cholesterol-rich membrane microdomains in the interaction of the S protein of SARS-coronavirus with the cellular receptor angiotensin-converting enzyme 2. *Virology*. 2008;381(2):215-221. CrossRef Medline
105. Wang H, Yuan Z, Pavel MA, Hobson R, Hansen SB. The role of high cholesterol in age-related COVID19 lethality. *bioRxiv.* 2020.05.09.086249. CrossRef

Drug Target Insights

www.aboutscience.eu

ISSN 1177-3928

ABOUTSCIENCE